NONINVASIVE ASSESSMENT OF NEUROCHEMICAL BIOMARKERS IN HUMANS WITH AMYOTROPHIC LATERAL SCLEROSIS: CORRELATES OF CLINICAL HETEROGENEITY

A dissertation submitted to the faculty of the University of Minnesota

by

Ian Cheong

in partial fulfillment of the requirements for the degree of Doctor of Philosophy

Thesis advisor: Gülin Öz, Ph.D.

June 2018

ACKNOWLEDGEMENTS

I am grateful to my thesis advisor and mentor Gülin for supporting my intellectual development, teaching me persistence in research, and instilling a drive to continually improve myself.

I am also thankful for the guidance and educational support given to me by Drs. David Walk, Lynn Eberly, Janet Dubinsky, Brent Clark, and Yasushi Nakagawa.

Finally, I am thankful to everyone who volunteered for my thesis project and who have also inspired me to help find solutions to ALS.

THESIS OBJECTIVES

The highly fatal and rapidly progressive nature of the neuromuscular disease amyotrophic lateral sclerosis (ALS) has motivated intense efforts to discover therapeutic solutions. However, the disease's clinical and genetic heterogeneity as well as its seemingly multifactorial etiology have complicated the search for effective drug targets. Also contributing to the failures in drug development is the lack of robust outcome measures that are sensitive to treatment effect over the short-term. Traditional clinical trial endpoints, such as survival and disability scores, require large sample sizes and long study duration due to heterogeneity in clinical progression.

By definition, biomarkers are more reflective of underlying disease mechanisms and may change quickly in response to changes in disease state. Thus, using these markers as primary or secondary endpoints can lead to shorter trials with greater statistical power and expedite the screening of promising therapies for ALS. In addition, some biomarkers may aid in ALS diagnosis and facilitate earlier treatment. Others may predict disease outcome and be used to reduce heterogeneity within the studied sample.

Proton magnetic resonance spectroscopy (^{1}H-MRS) biomarkers are non-invasively measured and are relevant to disease processes that affect neuronal health in ALS, such as neuroinflammation, oxidative stress, and excitotoxicity. While many cross-sectional ^{1}H-MRS studies in ALS have identified metabolic differences in the brain between patients and healthy controls, the small number of longitudinal ^{1}H-MRS studies have not consistently demonstrated metabolic changes over time. These inconsistent findings are likely due to disease heterogeneity and variability in measurement precision.

This thesis research focuses on utilizing state-of-the-art ^{1}H-MRS technology developed in the last several years for a thorough examination of the biomarker potential of ^{1}H-MRS in ALS. The aims of this work are the following:

1. *To assess the test-retest reproducibility of the ^{1}H-MRS method with a highly optimized pulse sequence and protocol at 7 tesla.*
   This is an important step to determine the measurement precision of the technique and thereby its sensitivity to change. Determining the reproducibility is a prerequisite in order to consider the use of ^{1}H-MRS as a biomarker of progression and treatment response.
2. *To identify candidate biomarkers that aid in diagnosis.*
   By assessing an early-stage ALS cohort, metabolic abnormalities that are associated with relatively early symptoms may be identified using ^{1}H-MRS. The diagnostic sensitivity and specificity of ^{1}H-MRS measures will be assessed by using the baseline data from a longitudinal study design.
3. *To identify candidate biomarkers of disease prognosis.*
   Markers that can predict clinical outcomes will have a major impact in therapeutic trial design, in particular, the enabling of robust patient stratification. ^{1}H-MRS measures at baseline will be evaluated for their ability to predict survival, functional decline, and study withdrawal due to disease progression.
4. *To identify candidate biomarkers of disease progression through longitudinal evaluation of ^{1}H-MRS metabolites in patients with ALS.*
   Reliably quantified metabolites will be assessed over time and compared with measures of clinical progression. Metabolites that are likely relevant to ALS pathogenesis include *N*-acetylaspartate, *myo*-inositol, glutamate, glutathione, and γ-aminobutyric acid.

TABLE OF CONTENTS

List of Tables

List of Figures

1

Amyotrophic Lateral Sclerosis

1.1 The Affected Population

Among the rare motor neuron diseases, amyotrophic lateral sclerosis (ALS) is the most common and also the most fatal, with a median of survival of just 2 to 4 years after symptom onset. Typical ALS onset occurs in late adulthood between ages 45 and 74, although the disease can affect younger populations (~10% of cases before 45 and ~1% of cases before 25) [1]. In 10% of cases, the disease is inherited through an ALS-causing genetic mutation and is termed familial ALS. The other 90% of “sporadic” cases have no family history of ALS but may have genetic defects that are either known or remain to be identified.

Population-based studies have demonstrated regional variability in ALS frequency, complicating the estimation of global ALS burden. The prevalence in North America is ~3-4 per 100,000 and the incidence is ~2 per 100,000. In European countries, these numbers may be slightly higher, while in Asian countries they may be slightly lower [2]. Comparisons of incidence rates between sexes suggest that ALS affects men somewhat more than women.

Overall, slight improvement in survival rates over the last 20 years suggest advances in symptomatic care. However, the brutal progression of ALS has remained unchanged due

to a clear lack of robust disease-modifying therapies. Numerous large-scale clinical trials since the 1980's have produced only two approvals by the United States Food and Drug Administration (FDA) of modestly effective drugs (riluzole, edaravone). The need for biomarkers to accelerate therapeutic development is pressing.

1.2 Historical Background

The discovery of ALS is credited to neurologist Jean-Martin Charcot (1825-1893), who was the first to describe both the clinical manifestations of the disease and their neuropathologic correlates. Charcot named the disease after observing the combination of muscle atrophy and spinal cord lesions, including anterior horn degeneration and lateral column sclerosis. Controversially even to this day, Charcot also believed that the disease propagates in an anterograde direction from the lateral columns to the anterior horn gray matter.

1.3 A Disorder of the Brain

ALS is a neuromuscular disease driven by the degeneration of motor neurons of the brain and spinal cord. While progressive muscle atrophy and paralysis are clearly visible in ALS, the neurological component of ALS is much more challenging to evaluate. The disease typically does not cause macroscopic changes in neuroanatomy that can be identified by conventional imaging. Instead, electrophysiologic testing or advanced imaging techniques are currently the most sensitive methods to detect motor neuron defects *in vivo*. Thus, our understanding of CNS involvement in ALS has mostly relied on histological examinations of post-mortem neural tissue in humans and animal models. For many years since the time of Charcot, the spinal cord has been extensively studied in ALS because it generally shows the most striking anatomical changes. With new evidence of cerebral degeneration in ALS revealed by modern molecular and neuroimaging techniques, greater focus is being placed on the brain's role as a primary instigator of the disease's pathogenesis.

1.3.1 Neuropathology

Early histopathologic studies prior to the 1990's demonstrated selective degeneration of the large pyramidal cells of Betz, a type of corticospinal motor neuron or upper motor neuron (UMN) within motor cortex layer Vb. With conventional staining methods, reduced numbers of these cells were frequently reported along with degenerative changes in their morphology [3, 4]. Betz cells synapse directly with lower motor neurons (LMNs) of the spinal anterior horn and provide high-velocity motor control of the limbs. Despite their functional importance, these cells are few in number, making up only 10% of the pyramidal cells in layer Vb [5].

In these early studies, clusters of reactive astroglia were also frequently found surrounding Betz cells. Reactive astrogliosis was also seen in other layers of the motor cortex [6].

More recent studies have identified degenerative changes in other cell types within the motor cortex. Activated microglia have been observed in cortical layer V, although they appear to be more prominent within the subjacent white matter [7, 8]. The pyramidal cells of layer III and non-Betz neurons of layer V are also smaller in patients with ALS compared to non-ALS controls [9, 10]. Non-Betz layer V pyramidal neurons are critical for voluntary motor function, as many of them synapse onto interneurons of the spinal intermediate gray zone and indirectly influence LMNs. Reduced numbers of parvalbumin-positive cortical inhibitory interneurons have also been reported, supporting the theory of motor cortex hyperexcitability in ALS. In addition, demyelinated lesions are present in motor cortex layers and accompanied by increased numbers of reactive oligodendrocyte precursor cells [11]. Finally, and perhaps most remarkably, abnormal intraneuronal inclusions have been identified as a neuropathologic hallmark of ALS that extends beyond the motor cortex. Immunoreactivity studies have shown that nearly all of sporadic cases possess cytoplasmic aggregates of mislocalized, phosphorylated TAR DNA binding protein 43-kDa (TDP-43), which has a nuclear role as a transcription factor under normal conditions. Prominent TDP-43 pathology is present within the neurons of motor cortex layers II, III, V, and VI, including Betz cells [12]. TDP-43 aggregates are also found within corticospinal axons and oligodendrocytes of the subjacent white matter.

Familial ALS cases display cytoplasmic inclusions that have a different composition. In familial ALS associated with mutations in superoxide dismutase 1 (SOD1), aggregates contain misfolded SOD1 protein without TDP-43 as a component [13]. In familial ALS associated with mutations in the chromosome 9 open reading frame 72 (C9orf72) gene, TDP-43 aggregates are present as well as characteristic TDP-43-negative inclusions composed of dipeptide repeats [14]. C9orf72-associated ALS is also characterized by nuclear RNA foci, which are the accumulated transcripts of a hexanucleotide repeat expansion in the mutated gene [15]. Other types of inclusions in ALS include small eosinophilic Bunina bodies and accumulated neurofilament proteins in the soma and proximal axons [16].

Signs of white matter degeneration in ALS have been observed at all levels of the corticospinal tract, including the precentral gyrus, internal capsule, cerebral peduncles, pontine pyramidal fascicles, and lateral columns [17]. There is also evidence that the extrapyramidal motor system is involved. In particular, degenerating fibers are present in the reticular formation of the midbrain, pons, and medulla. The reticular nuclei also show TDP-43 pathology [12]. These nuclei and their associated axon bundles make up an important motor center that relays signals from the premotor and motor cortices to control muscle tone and maintain posture during movement (“indirect” corticospinal pathway). The degree to which pathology in this center contributes to the ALS motor phenotype has not been fully explored. However, our current knowledge about the functions of the reticulospinal pathway indicate that its impairment is likely a mechanism of clinical spasticity and hypertonia in ALS [18].

The pathological changes in the brainstem motor nuclei and spinal anterior horn are often of equal or greater severity than those observed in cortical UMNs. Reactive gliosis accompanies the degeneration and loss of LMNs. Cytoplasmic protein inclusions (e.g., aggregated TDP-43) are also present with LMNs, including the neurons comprising the motor nuclei of the pons (cranial nerves V and VII) and the medulla (X and XII).

1.3.2 Disease Mechanisms

Strong evidence exists for the involvement of multiple pathological mechanisms in ALS. These mechanisms include oxidative stress, excitotoxicity, neuroinflammation, protein aggregation, and disrupted axonal and nucleo-cytoplasmic transport.

Early studies highlighted possible derangements in glutamate neurotransmission. Defects in astrocytic glutamate transporter proteins were identified in motor cortex and spinal cord tissue of patients, suggesting reduced glutamate reuptake [19]. Increased glutamate levels have also been measured in patient CSF and plasma. These findings and supportive evidence from animal models of ALS have led to the hypothesis that motor neuron death may be driven by excessive glutamate stimulation. This theory is further supported by the understanding that riluzole, which is mildly neuroprotective in ALS, has an anti-excitotoxic mechanism of action [20]. Overall, the literature on this topic suggests that glutamate-mediated excitoxicity may be most relevant at early stages in ALS. Neurophysiologic studies using transcranial magnetic stimulation (TMS) have indicated that the threshold for cortical motor neuron excitation is reduced in early symptomatic and presymptomatic ALS and increases with advancing disease [21].

Oxidative stress is another major disease mechanism in ALS and arises from an inability to neutralize harmful oxidants produced through aerobic respiration. The literature on oxidative cell damage in ALS is extensive in both humans and animal models, most notably mice with SOD1 genetic mutations [22]. Post-mortem tissue studies have demonstrated increases in markers of protein, DNA, and lipid oxidation in the motor cortex and spinal cord of patients [23, 24]. The recently FDA-approved drug edaravone is also a free radical scavenger, confirming a role for oxidative stress in ALS pathogenesis [25]. Ultimately, oxidative stress in ALS probably arises from mitochondrial dysfunction, in which the leakage of electrons from the respiratory chain leads to increases in partially reduced oxygen [26]. Thus, mitochondria are likely among the major organelles to suffer oxidative damage in ALS, and their functions in cellular energetics and metabolite production may be critically impaired. Ultrastructural studies have demonstrated abnormal mitochondrial morphology in the motor neurons of patients [27]. Defects in the

respiratory chain protein complexes and increased frequency of mitochondrial DNA mutations have also been reported [28].

Glial cells provide critical trophic and metabolic support to neurons. Thus, the health of motor neurons in ALS may be influenced by alterations in the surrounding glial cell types. Astrocytes are responsible for glutamate uptake and recycling after synaptic activity, and these functions are altered in ALS [19]. Microglia also proliferate and, along with astrocytes, release pro-inflammatory molecules that may be neurotoxic [29]. The loss of oligodendrocytic myelination and metabolic support may also impact motor neurons [11].

The trafficking of cellular components is severely impaired in motor neurons in ALS. The aggregation of cytoskeletal neurofilaments block axonal transport, preventing mitochondrial movement across the length of the cell [30]. Recent studies also highlight defects in the trafficking of RNA and proteins between the nucleus and cytoplasm, which may cause the cytoplasmic accumulation of nuclear proteins such as TDP-43 [31].

Lastly, we do not fully understand how protein aggregates contribute to disease development and spread in ALS. A prevailing theory is that TDP-43 pathology may spread from cell to cell through a prion-like mechanism, wherein the protein aggregation self-perpetuates and is transmitted to neighboring cells. Supporting this possibility, studies have identified a prion-like domain on TDP-43 [32]. Other ALS-associated inclusion proteins such as SOD1 and fused-in-sarcoma (FUS) also demonstrate the potential for prion-like propagation [33].

Many of these disease processes are obviously interrelated. For example, excessive stimulation of glutamate receptors can lead to greater free radical generation through the influx of calcium. Oxidative stress can also have widespread effects, causing DNA damage and protein aggregation. Currently, the sequence of these events in the development of ALS is unclear. Furthermore, other neurodegenerative diseases (e.g. Parkinson’s, Huntington’s) show similar signs of these disease mechanisms, which indicates that they are non-specific and likely downstream of some initial insult. However, quantitative measures of these processes may be strong indicators of the extent

of pathologic burden in ALS. Specifically, their ability to detect changes in disease burden due to treatment or natural progression would have a massive impact on the development and evaluation of effective drugs.

1.4 The Clinical Presentation

1.4.1 Classical ALS

The typical or "classical" form of ALS is rapidly progressive (~2 to 4 year survival after symptom onset) and is characterized by the presence of both LMN and UMN signs on neuromuscular exam. The disease usually begins in a distinct region of the face, arms, or legs and spreads over time to involve the rest of the body. Death eventually occurs due to paralysis of the muscles of respiration. Clinical LMN signs include weakness, muscle wasting, and involuntary muscle twitching (fasciculations) due to denervation. Clinical UMN signs are physiologically complex and are due to lesions in either the corticospinal or extrapyramidal motor tracts that cause a loss of reflex inhibition. Hyperexcitable muscle stretch reflexes underlie the spasticity seen on exam, which is increased muscle contraction (tone) with increased speed of movement. Spasticity causes the slowness of repetitive limb and tongue movements and may be accompanied by involuntary rhythmic muscle contractions induced by stretching called clonus. Spasticity affecting the muscles of speech produces a characteristic dysarthria indicated by slow, strained speech with imprecise articulation of consonants. Exaggerated deep tendon reflexes are also observed along with other release signs such as plantar toe extension and pronounced masseteric and finger flexor reflexes. Compulsive laughter or crying, also referred to as pseudobulbar affect, is also a UMN sign and may arise from a disruption of the cortico-pontine-cerebellar pathway [34].

Proper diagnosis of ALS follows the guidelines given by the revised El Escorial Criteria. With this criteria, patients are classified according to the degree of diagnostic certainty. Generally, a person with possible ALS may display UMN and LMN signs at only one CNS level (cranial, cervical, thoracic, or lumbosacral), while a person with probable or definite ALS may display signs at two or more levels. In addition to the clinical exam

findings, the classification system also incorporates evidence of LMN dysfunction obtained by electrophysiology.

Although the combination of clinical UMN and LMN signs is almost pathognomonic for ALS, robust diagnostic markers are still necessary. The subtleness of symptom onset often leads to a long diagnostic delay and thus a delay in potential therapeutic benefit. Additionally, ALS must be distinguished from several rare mimic disorders using electrophysiology, neuroimaging, and genetic tests. Multifocal motor neuropathy and Kennedy's disease, which present with only LMN signs, are most frequently misdiagnosed as ALS.

1.4.2 Motor Phenotype Heterogeneity

The phenotypic variability in ALS is substantial and has called into question whether it can be explained by a single fundamental mechanism. Patients with ALS display differing degrees of UMN and LMN involvement, with some who may be more UMN-predominant and others more LMN-predominant. The site of onset is also variable, with most patients being limb-onset (~75%) and the rest being bulbar-onset. Bulbar-onset ALS has notably greater frequency among females than males. A minority of patients also have a slower rate of progression (~20%), for whom survival may extend past 4 years.

Assuming that there is a common fundamental mechanism, different forms of ALS may exist along a clinical spectrum. Pure UMN involvement may present at one extreme in the form of primary lateral sclerosis (PLS), while pure LMN involvement may present at the other end as progressive muscular atrophy (PMA). In both variants, the disease usually remains isolated to either the UMN or LMN level and displays a better prognosis than classical ALS. If they do exist on a continuum with classical ALS, it is unclear what prevents the variants from converting to an aggressive phenotype.

Due to the considerable clinical heterogeneity, consistent patterns in disease progression have been difficult to identify. Oftentimes, the body region that is initially affected displays both UMN and LMN signs that become worse before the disease spreads to other regions. Thus, the disease may always be maximal in the area that it begins. This has led to the proposal that ALS starts focally by affecting the UMNs and LMNs in a

random body region and spreads to contiguous neuroanatomic regions [35]. Due to their different somatotopic organizations, adjacent spread within the motor cortex affects different body parts compared to adjacent spread within the spinal cord and brainstem. This may explain why LMN signs tend to propagate to the contralateral side, while UMN signs may propagate to other ipsilateral regions. Thus, neuroanatomic differences between the subdivisions of the CNS may contribute to heterogeneity in regional progression.

1.4.3 Cognitive Phenotype

An estimated fifty percent of patients with ALS have significant cognitive-behavioral problems [36]. The deficits that are commonly observed overlap strongly with those seen in fronto-temporal dementia (FTD). Thus, patients may have impairments in frontal executive functions, language, working memory, and social cognition. Cognitively-impaired patients may also show atrophy in fronto-temporal areas on brain MRI and neuropathologic changes such as TDP-43 aggregates in these areas on *post-mortem* exam.

A major genetic link between ALS and FTD was discovered in 2011 as a hexanucleotide repeat expansion in the C9orf72 gene [15, 37], which encodes a protein that is likely important for normal inflammatory cell function. This mutation accounts for a particularly large proportion of familial cases of ALS and FTD, with a smaller prevalence among sporadic cases. Like ALS, FTD also features prominent TDP-43 pathology in the CNS [38]. These findings, along with the observation that patients with FTD occasionally develop motor neuron disease, suggest that these two diseases potentially exist along a continuum.

Due to problems with executive functioning, patients may exhibit disinhibition, apathy, poor planning, and perseverating behavior. Language deficits typically include naming difficulty, impaired word and sentence comprehension, and grammatical errors. As part of their severe cognitive impairment, patients with combined ALS-FTD have poor insight on their own condition and are especially challenging to manage. These patients generally progress more rapidly than those with pure motor phenotypes.

1.4.4 Clinical Assessments

Although survival is still the gold-standard outcome measure, the ALS Functional Rating Scale–Revised (ALSFRS-R) is frequently used as an endpoint for therapeutic evaluation in clinical trials. It is a measure of disability in 12 items of daily living: (1) speech, (2) salivation, 3) swallowing, (4) writing, (5) feeding, (6) dressing, (7) turning, (8) walking, (9) climbing, (10) dyspnea, (11) orthopnea, and (12) ventilatory support [39]. Each item is rated from 0 to 4 yielding a total score out of 48, with lower scores indicating greater disability. Region-specific disability scores can be obtained by summing the scores on appropriate items. For example, upper limb disability is typically scored using only items 4, 5, and 6.

The ALSFRS-R has high intra- and inter-rater reliability and is currently used in early and late phase clinical trials. Therapeutic efficacy is determined by assessing change in the rate of ALSFRS-R decline. Due to variability in individual progression rates, ALSFRS-R typically needs to be observed in large samples for at least 6 months. Thus, the smaller and shorter trials (phase II) based on this outcome measure are frequently underpowered, and candidates that go on to larger phase III trials are at high risk of failure. An additional concern is that ALSFRS-R decline may not be linear, as plateaus and even reversals are common [40, 41]. The reliance on disability scores over time is also prone to withdrawal bias, as longer study durations cause declining participation from patients with advanced disability and overrepresentation of those with more slowly progressive disease. Finally, ALSFRS-R is a subjective measure due to its self-reporting questionnaire format, and some of its questions focus on symptoms that may respond to symptomatic treatments.

Formal disease staging systems have been recently developed to aid in classifying patients according to their degree of disease advancement. The King's staging criteria is popular and based on the number of CNS regions that display weakness [42]. Classifications range from Stage 1 (one region with weakness) to Stage 4 (need for gastrostomy or ventilatory support) and are determined by clinical exam and history. King's stages can also be derived from ALSFRS-R scores with 92% accuracy [43].

Neurologists have also created various systems to quantify clinical UMN burden. Most of these are based on hyperreflexia and spasticity grading. Others incorporate finger- and foot-tapping speed, which are slow in ALS. In the Penn UMN scale, signs of hyperreflexia, clonus, and spasticity are scored in each body region (limbs, face, trunk) and totaled for a score out of 33 [7]. This system may give too much weight to reflexes from the same limb, which tend to be affected together in ALS. But more generally, clinical UMN signs are not a reliable surrogate for UMN pathology. Particularly at advanced clinical stages, areflexia is commonly observed due to prominent LMN disease in spite of possible UMN degeneration.

The Edinburgh Cognitive-Behavioral ALS Screen (ECAS) is regularly used in ALS clinics to test for disease-associated cognitive-behavioral impairments [44]. The ECAS assesses executive function and language but also tests memory and visuospatial functions, which are less commonly affected in ALS. In addition, a behavioral questionnaire is completed by the patient's caregiver, which screens for behavioral changes associated with FTD.

1.5 The Ideal Biomarker

Since the 1980's, over 60 molecules have been evaluated in randomized controlled clinical trials for the treatment of ALS. Of all the candidates, only riluzole (1995) and edaravone (2017) have received FDA approval. The many clinical trial failures are a result of the complex underlying biology of ALS but are also due to issues with trial design. Trials have relied upon traditional clinical endpoints such as survival, function, and limb and respiratory muscle strength. These outcome measures require a rather prolonged period of assessment to capture changes due to treatment. Thus, while they may be adequate for phase III trials with large enrollment and long follow-up, the measures may miss treatment effects in the smaller and shorter phase II trials. Biomarkers that can detect a biologic response to treatment over shorter timeframes can be used during the early phases to greatly power and expedite the selection of the most promising candidates for further evaluation.

We need biomarkers that reflect both the natural history of disease progression and the biological effect of treatment (pharmacodynamic). The most sensitive measures should be closely linked to underlying pathological mechanisms in ALS, such as those described in section 1.3. In particular, by reflecting change in disease mechanisms, biomarkers can identify the treatments with mild-to-substantial disease-modifying effects.

In addition to progression and pharmacodynamic biomarkers, prognostic biomarkers can identify patients who are at risk of a particular outcome (e.g. fast versus slow progression). Phenotypic heterogeneity in ALS makes it likely that therapies may be beneficial for some disease subgroups and not others. Prognostic biomarkers would be especially useful for stratifying patients at the beginning of trial randomization.

Diagnostic biomarkers would also have an important impact in ALS. Since the diagnosis of ALS is oftentimes delayed from symptom onset, markers that can help identify the disease earlier will allow prompt administering of treatments and earlier-stage patient enrollment in clinical and research studies.

The ideal biomarker for ALS is an objective measure with the following characteristics:

1) Low intra-subject variability (high-retest reproducibility) in healthy stable individuals in order to detect subtle pathological changes over time or changes due to treatment effect,
2) Low inter-subject variability among different clinical phenotypes in order to achieve robust patient stratification,
3) High specificity to a particular spatial location in the body,
4) High sensitivity and specificity to the measured pathologic process(es), and
5) Minimal invasiveness and ease of measurement.

^{1}H-MRS biomarkers can fulfill many of these qualities. They have molecular-level sensitivity and specificity and show high test-retest reproducibility (described in Chapter 3). They are also non-invasively obtained from specific locations in the body.

2

^{1}H Magnetic Resonance Spectroscopy

2.1 Introduction

Proton magnetic resonance spectroscopy (^{1}H-MRS) can be used to measure metabolite concentrations in brain regions *in vivo*. Although other half-spin nuclei (e.g., ^{13}C, ^{31}P, and ^{19}F) are also MR-visible, ^{1}H-MRS is most commonly performed due to its higher sensitivity and because it can use the same hardware as conventional MRI. The development of ultra-high field technology has improved the sensitivity or signal-to-ratio (SNR) of ^{1}H-MRS, enabling the analysis of smaller volumes of interest and the reliable quantification of more metabolites.

In disease applications, the ability of ^{1}H-MRS to detect changes in metabolite concentrations has great value. Metabolic changes due to disease processes can occur both during and before overt cell loss, making ^{1}H-MRS a potentially sensitive technique for studying early to advanced disease stages. Furthermore, as some metabolites have known cellular functions (e.g. glutathione, GABA) as well as high cellular specificity (e.g. *N*-acetylaspartate), ^{1}H-MRS signal changes are usually interpreted with greater clarity compared to other neuroimaging techniques. The likely relevance of ^{1}H-MRS metabolites in disease biology makes them promising biomarker candidates as well as potential tools for understanding natural disease progression. Consistently, ^{1}H-MRS has revealed metabolic derangements in the brain in numerous neurologic conditions. A

review of prior applications of this technique in ALS will be given later in the chapter. Subsequent chapters will focus on novel applications of ultra-high field ^{1}H-MRS to capture pathologic changes in ALS and identify biomarker candidates.

2.2 Basic Principles

^{1}H-MRS is a technique based on nuclear magnetic resonance (NMR) theory. The ability to detect metabolites individually is a result of exploiting differences in the molecular structure surrounding protons in each metabolite.

Due to their intrinsic angular momentum, protons in an external magnetic field B_0 will precess according to a frequency described by the Larmor equation $\omega_0 = \gamma B_0$, where γ is the gyromagnetic ratio of ^{1}H (approximately 42.6 MHz/T). Thus, at 1.5, 3.0, and 7.0 T, the resonance frequencies of ^{1}H will be approximately 63.9, 127.8, and 298.2 MHz, respectively. However, differences in the resonance frequency occur because protons are shielded from the external field B_0 by small magnetic fields that are generated by surrounding electrons. The degree of shielding is unique and constant for various proton-containing functional groups and is the basis for the "shift" in resonance frequency called the chemical shift. The chemical shift for a proton is relative to a reference frequency and also increases proportionally with field strength. Therefore, to standardize the frequency scale, the chemical shift δ is described in parts per million (ppm) of the reference frequency:

$$\delta \text{ (ppm)} = \frac{(\omega - \omega_{ref})*10^{6}}{\omega_{0}},$$

where ω_{ref} is typically the resonance frequency of methyl protons in tetramethylsilane (TMS). However, since TMS is not present in the human body, the ppm scale for *in vivo* ^{1}H-MRS studies is usually generated by using the *N*-acetylaspartate methyl singlet as a reference and setting its resonance frequency at 2.02 ppm.

Protons within molecules are also affected by neighboring nuclei. Known as *J*-coupling, magnetic interactions occur between nuclei indirectly through their bonding electrons and cause the splitting of resonances into multiplets. This has important consequences for the

in vivo spectrum because the splitting leads to broader and less intense signals, which are more difficult to detect (e.g. glutamate, GABA). Additionally, the signal intensity and spectral lineshape of *J*-coupled resonances undergo modulation depending on choice of pulse sequence echo time (TE).

An example of an *in vivo* proton MR spectrum acquired from the human brain is shown in Figure 2.1. The area under each resonance is proportional to the number of protons with that particular resonance frequency and thus the metabolite concentration.

To generate a spectrum of resonance frequencies, the MR signal is acquired as a function of time before it is converted into the frequency domain. For a simple pulse-and-acquire experiment, this process is summarized in the following steps:

1) Proton spins aligned in the direction of B_0 produce a net magnetization (z-axis). This magnetization is flipped 90° into the transverse plane (x-y) by applying a radiofrequency (RF) excitation pulse B_1 at the Larmor frequency.
2) The system returns to equilibrium according to two time constants. The recovery of magnetization in the z-axis is described by the longitudinal relaxation constant T_1. The magnetization in the x-y plane decays according to the transverse relaxation constant T_2^*, as spins lose their phase coherence due to B_0 and local magnetic field inhomogeneities. The T_2^* decay induces a signal in a receiver coil, which is known as the free induction decay (FID).
3) The FID contains time domain information for the resonating protons of every metabolite. A Fourier transformation of the FID gives signal intensity on a frequency scale.

Importantly, in many current ^{1}H-MRS techniques, the FID is not collected after a single pulse, but rather multiple RF pulses are applied to generate an echo. The most well-known is the spin echo [45], which can be generated by applying a 180° RF pulse after 90° nutation to refocus dephasing spins on the transverse plane [46]. In spin-echo experiments, only the dephasing due to B_0 inhomogeneity (T_2* effects) is refocused, and thus the T_2 decay caused by spin-spin interactions is mainly observed.

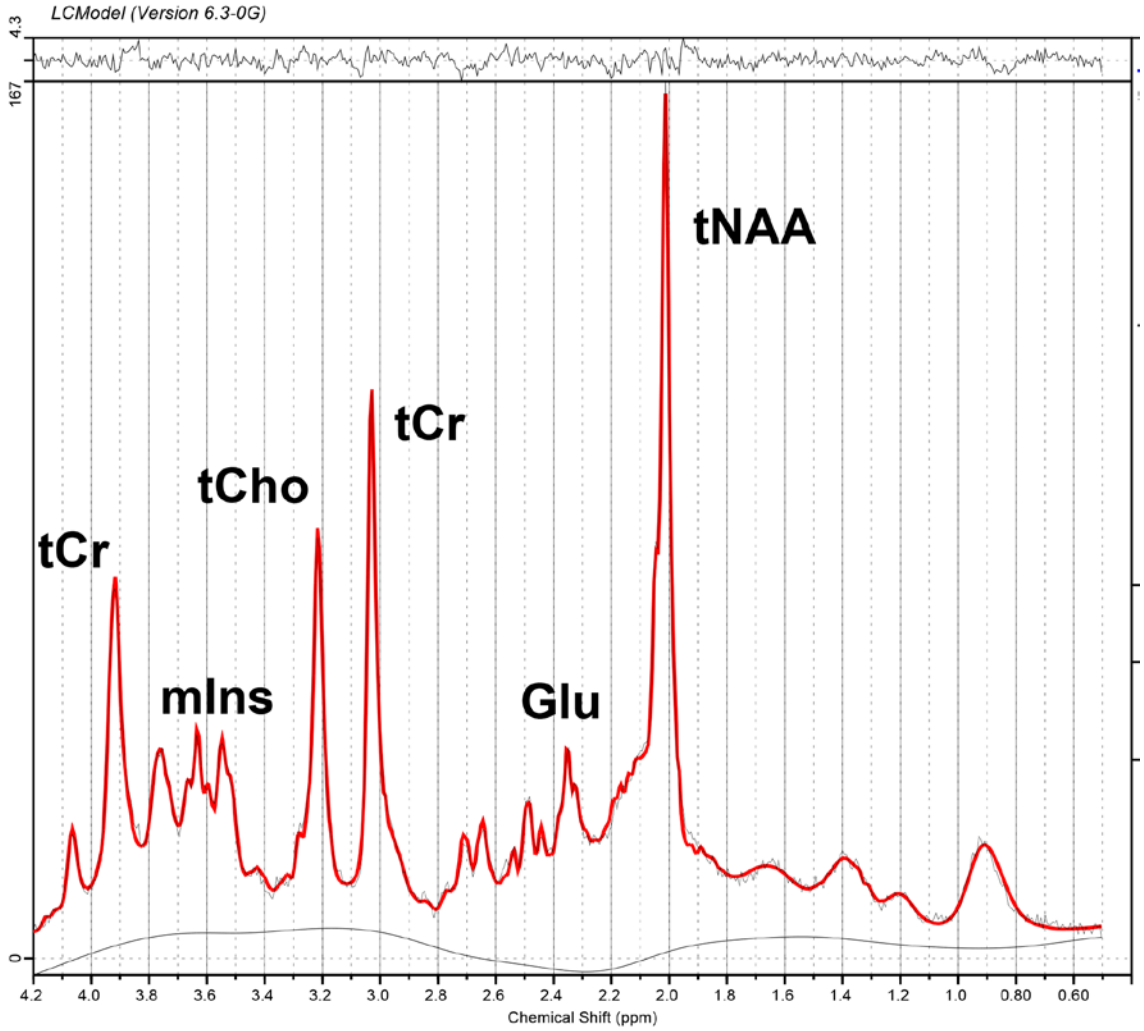

Figure 2.1 A typical frequency-domain ^{1}H MR spectrum acquired at 7 tesla from the motor cortex of a healthy human. An estimation of the spectral peaks (in red) is displayed over the raw spectrum and was generated with fitting software (LCModel). The ^{1}H resonances of abundant metabolites are labeled: glutamate (Glu), *myo*-inositol (mIns), total choline (tCho), total creatine (tCr), and total *N*-acetylaspartate (tNAA).

2.3 The Technique

2.3.1 Single-voxel Methods

Spatial localization in ^{1}H-MRS relies on the detection of an echo signal after slice-selective excitation of a 3D rectangular volume. Slice selection is achieved by applying frequency-selective RF pulses in combination with field gradients.

Classic examples of localization sequences include the point-resolved spectroscopy sequence (PRESS) and the stimulated echo acquisition mode (STEAM). In PRESS, a slice-selective 90° pulse is followed by two 180° refocusing pulses applied orthogonally to produce a spin echo. In STEAM, three slice-selective 90° pulses applied in each direction generate a stimulated echo [47]. The stimulated echo intrinsically has only half the signal intensity of a spin echo. However, STEAM has notable advantages over PRESS, including sharper slice selection, shorter minimum echo time, and the higher achievable bandwidths of 90° pulses. These characteristics make STEAM more applicable at ultra-high field strengths, where metabolite T_2s are considerably shorter and chemical shift displacement error is worse than at lower fields. Chemical shift displacement error refers to the mismapping of metabolite resonances with different chemical shifts to voxels that are spatially shifted and is more pronounced at high fields due to increased spectral dispersion. Larger pulse bandwidths are important for reducing this artifact.

At high field strengths ($B_0 \geq 3$ T), inhomogeneity in the RF transmit field B_1 can also cause nonuniform excitation of the voxel and thus reduced SNR. Localization by adiabatic selective refocusing (LASER) can help address this with adiabatic pulses, which excite proper flip angles despite inhomogeneous B_1 as long as an RF power threshold is met. Additionally, the pairs of slice-selective adiabatic 180° pulses in LASER achieve excellent slice selection, have large bandwidth, and produce a full-intensity spin echo [48]. The drawbacks to LASER are its high RF power requirements and relatively long minimum TE due to having more pulses. A shorter version of LASER called semi-LASER is not fully adiabatic but has a shorter minimum TE and requires less power [49].

Localization sequences for ^{1}H-MRS do not achieve perfect boundaries and may excite regions outside of the intended volume. In particular, voxel selection near edges of the brain can result in unwanted lipid signals from the scalp. Therefore, outer volume suppression (OVS) pulses are typically run before the slice-selective pulses to saturate the lipid signal.

Water is highly concentrated in the brain (~39-44 M in tissue). In contrast, metabolite concentrations are several orders of magnitude lower at 1-10 mM. Thus, a strategy for the suppression of the large water resonance is necessary and incorporated into ^{1}H-MRS pulse sequences. The VAPOR scheme is a popular method for saturating the water signal by using 8 frequency-selective pulses applied consecutively with variable RF power and timing [50]. This method allows effective water suppression in the setting of inhomogeneous B_1 fields.

Adjustments are also necessary to correct for nonuniformity in the external field B_0. Tissue has an intrinsic magnetic susceptibility that causes local deviations in B_0. These local field inhomogeneities are especially strong near interfaces between tissue and air (e.g. frontal sinuses, ear canals) and need to be minimized to avoid broad linewidths and low spectral resolution. In B_0 shimming, the variations in the field are mapped, and small corrective magnetic fields are applied through shim coils to achieve uniformity over a target area. Efficient, high quality, and fully automated shimming can currently be achieved with FASTMAP, which maps B_0 along projections to determine first- and second-order shim correction terms [51]. Since B_0 inhomogeneity increases with field strength, strong second-order shims are needed in addition to linear shims at field strengths 3 T and higher.

2.3.2 Single-voxel versus Multi-voxel Spectroscopy

In single-voxel ^{1}H-MRS, each acquisition is performed on a single region of tissue where pathology is known or expected. Limited scanner time, particularly in the clinical setting, will therefore allow the analysis of only a few regions during a single session. On the other hand, multi-voxel techniques (MRSI) can be applied to the whole brain and enable the interrogation of multiple regions simultaneously. An advantage to this approach is

that no prior knowledge is required regarding where the disease occurs. In addition, the spatial resolution of MRSI can identify regional differences in spectral pattern, which may be informative of disease spread.

To encode spatial information, MRSI applies gradients that alter the phase in each direction. The number of phase-encoding steps in each direction determine the spatial resolution and therefore the scan time. Therefore, large volume 3D acquisitions with high spatial resolution will typically require long scan times. A major challenge in the development of MRSI is the reduction of scan time for clinical applicability.

Aside from the lack of spatial encoding, single-voxel MRS currently has clear technical advantages over MRSI [52]. MRSI requires homogeneous B_0 and B_1 fields over a large volume, which is difficult to achieve especially at higher field strengths. In contrast, effective corrections for field inhomogeneities can be performed locally for single-voxel techniques. MRSI's larger brain coverage can also lead to incomplete lipid and water suppression.

Consequently, spectra are often acquired at long TEs with MRSI to minimize the resulting artifacts, and the SNR is typically lower with fewer visible metabolites. Finally, the voxel boundaries are generally less well-defined with MRSI than with single-voxel MRS.

2.3.3 Pros and Cons of Ultra-high Field ^{1}H-*MRS*

The emergence of ultra-high field (≥ 7 T) MR technology has enhanced the utility of ^{1}H-MRS as an investigative tool in brain disease research. In particular, the increased field strength is associated with increases in SNR, which creates important advantages. Firstly, the minimum allowable voxel size is decreased, and thus smaller regions in the brain can be analyzed. Secondly, a given SNR can be achieved with fewer spectral averages, thus shortening the overall scan time. At ultra-high fields, increases in spectral dispersion also lead to improved quantification precision and the separation of overlapping resonances such as glutamate (Glu) and glutamine (Gln).

However, ^{1}H-MRS methodology has also become more complex to address several challenges associated with ultra-high field scanning. In particular, magnetic field inhomogeneities (both B_0 and B_1) become more severe at these higher field strengths. RF shimming methods need to be applied locally in regions that experience signal loss due to increased B_1 inhomogeneity. And as described before, strong higher-order shims are needed to reduce local B_0 variation.

In addition to field variations, ultra-high fields are also associated with shorter metabolite T_2 relaxation times and greater signal modulation for *J*-coupled resonances. Consequently, pulse sequences that can reach ultra-short TEs (< 10 ms) such as STEAM are employed to minimize signal loss. Semi-LASER is also used despite somewhat longer TEs (< 50 ms) because T_2 relaxation times are lengthened and *J*-modulation is partially minimized by the train of adiabatic 180° refocusing pulses [53, 54]. Importantly, both STEAM and semi-LASER also utilize high bandwidth pulses, which are required at ultra-high fields to minimize greater chemical shift displacement errors caused by increased spectral dispersion.

Perhaps the greatest question surrounding ultra-high field ^{1}H-MRS is whether it provides value beyond the methods that are presently available for clinical MR systems. Ultra-high field scanners are currently utilized only in the research setting, and the specific advantages that make ultra-high field ^{1}H-MRS beneficial for patients still need to be demonstrated and established.

2.3.4 Spectral post-processing

During acquisition, subject motion can cause drifts in the frequency and phase of the measured spectrum. In addition, eddy currents that arise from the switching of field gradients produce transient magnetic fields that distort spectral lineshapes. These typical artifacts are corrected after data acquisition by using automated methods.

Eddy current correction is frequently performed in the time domain (prior to Fourier transformation). Typically, an unsuppressed water signal is acquired with the same

parameters as the metabolite spectrum, with all gradients executed. A phase correction term is derived from this water signal and then applied to measured spectrum.

If the SNR is sufficient, frequency and phase fluctuations are also corrected on single scans. In one approach, a particular scan (such as the first average) is used as a reference to which the other scans are registered. The phase and frequency adjustments for each scan are then determined using a common peak such as the creatine signal.

After the post-processing corrections, multiple scans are averaged to increase SNR. The SNR of the summed spectrum is proportional to the square root of the number of averages.

2.3.5 Quantification

In metabolite quantification, the areas of the metabolite peaks are estimated by applying a fitting algorithm to the measured *in vivo* spectrum. The most popular fitting software is LCModel [55], which is fully automated and analyzes data in the frequency domain. With LCModel, the measured spectrum is analyzed as a linear combination of known metabolite spectra (basis spectra). These basis spectra can be measured from metabolite solutions *in vitro* or simulated using density matrix calculations. During fitting, the amplitudes, phases, frequencies, and linewidths of the basis spectra are adjusted to achieve the closest approximation to the measured spectrum, and the coefficient of each adjusted function represents the estimated metabolite concentration. Each concentration estimate is also provided with a Cramér-Rao Lower Bounds (CRLB) value, which expresses the minimum error associated with model fitting. In ^{1}H-MRS studies, CRLB values have often been treated as estimates of measurement reliability. An example of an LCModel fit is displayed in Figure 2.1.

The quantification of short-TE, ultra-high field spectra is complicated by the appearance of broad macromolecule signals that crowd the baseline. If not accounted for, this causes fitting problems and inaccurate quantification. Thus, a macromolecule spectrum is normally measured (through a metabolite-nulling experiment) and included in the set of basis spectra [56].

Absolute concentrations

Absolute metabolite quantification is performed by scaling the metabolite peak areas using a reference signal of known concentration. The reference signal is commonly an unsuppressed water signal from the selected voxel. The water concentration within the voxel is not known exactly but the assumed value is usually between 40-45 M depending on tissue composition (72% and 82% water content for white and gray matter, respectively). Alternatively, an external reference signal can be acquired at a different time but from the same voxel location as the human head in a phantom containing a known metabolite concentration. This approach requires corrections for coil loading and phantom temperature and does not account for local magnetic field inhomogeneities.

For accurate quantification, corrections for signal losses due to T_2 relaxation need to be applied. T_1 corrections may be neglected if sufficiently long repetition times are used. For water-scaling, the T_2 of water within tissue can be determined by fitting a series of unsuppressed water signals measured at different TEs with a biexponential decay function while using a known value for the T_2 of CSF. The T_2 of metabolites should be determined for the specific pulse sequence and field strength, unless the TE is short enough such that decay is negligible. Ultimately, the accuracy of absolute quantification depends on the validity of the T_2 assumptions, which are more difficult to make in the context of pathology wherein T_2s are known to change.

Even if placed directly in brain parenchyma, a voxel will generally contain some percentage of CSF. When not accounted for, CSF contamination will result in underestimated metabolite concentrations in tissue. This is particularly important in studies of disease conditions marked by prominent tissue atrophy that causes increased CSF volume. The CSF percentage within a voxel can be estimated by applying a segmentation algorithm on a structural image (e.g., T_1-weighted) or by fitting a biexponential decay curve as described above.

Metabolite Ratios

For an easier analysis without T_2 assumptions and %CSF corrections, studies often choose to report metabolite ratios instead of absolute concentrations. Ratios are usually

referenced to total creatine (tCr) concentrations, which are stable in healthy conditions and in several diseases. However, in some pathologies, cellular energy metabolism may be affected and tCr levels may change. Thus, disease-related changes in ratios to tCr are more difficult to interpret as they can indicate changes in the metabolite-of-interest, tCr, or both.

2.4 Disease Markers

2.4.1 Limits for Detection

In order to be visible by ^{1}H-MRS, metabolites must be sufficiently abundant in tissue (millimolar concentration) and also contain mobile protons associated with longer T_2 relaxation times. Thus, most neurotransmitters and other chemical messengers cannot be detected by the technique due to low abundance. Large, immobile macromolecules such as nucleic acids and most proteins are also invisible. Instead, ^{1}H-MRS mainly detects low molecular weight hydrocarbons with resonating protons in the 1-5 ppm range.

2.4.2 N-acetylaspartate

The strongest signal in the ^{1}H MR spectrum of normal human brain is a singlet belonging to the methyl group of *N*-acetylaspartate (NAA). NAA is one of the most abundant molecules in the brain (~12 mM globally) [57] but has much lower concentration in non-neural tissues (< 50 μM) [58]. In the early 1990's, immunohistochemical studies in rodent brain showed that NAA is predominantly localized to neuronal cell types, with especially high concentrations in cortical pyramidal neurons [59, 60]. NAA expression was observed diffusely in cell bodies, dendritic processes, and axons, including those of major white matter tracts. NAA was also found within immature oligodendrocytes and related progenitor cells [61], which are important for myelin synthesis during early development. In adults, it is unclear how much these relatively small cell populations contribute to the overall NAA signal.

The neuronal specificity of NAA and the discovery of its reduction in many neurological conditions suggest that it may indicate changes in neuronal density. However, in studies

of various brain illnesses, changes in NAA were reversed by treatment or recovery time. Therefore, NAA is likely sensitive to reversible neuronal dysfunction in addition to permanent cell loss. Some examples of reversible cell changes that may influence NAA levels include altered mitochondrial NAA metabolism and morphological changes such as dendritic or cell body shrinkage.

NAA is currently an established marker of neuronal integrity despite general uncertainty about its major cellular function. There is strong evidence that the synthesis of NAA occurs in the mitochondria as well as the endoplasmic reticulum. In particular, NAA production seems to depend on mitochondrial respiration and may influence neuronal energy metabolism through the citric acid cycle [62]. As another possibility, NAA may be a storage form for acetyl groups that are needed for oligodendrocytic myelin synthesis. Oligodendrocytes likely use membrane transporters to import extracellular NAA, after which it is catabolized with the enzyme aspartoacylase. The extracellular presence of NAA (~100 μM) also indicates that it is regularly released from neurons, perhaps for the purpose of maintaining osmotic balance. Finally, NAA is a substrate in the synthesis of NAAG, a structurally related peptide that also displays a prominent neuronal-specific distribution in the brain. NAAG colocalizes with many other neurotransmitters and may have an important role in modulating their release. Notably, the genes for the proteins involved in NAA synthesis have been recently identified [63, 64], which may help efforts to better understand NAA's biological function.

Like many other neurological diseases, ^{1}H-MRS studies in ALS have demonstrated reduced levels of NAA in the brain. However, increased NAA levels have been detected in the CSF of patients with ALS [65], which could arise from increased osmoregulatory activity or upregulated catabolism of extracellular NAAG.

In most ^{1}H-MRS studies of neurological conditions, NAA has been reported with NAAG as a sum called total NAA (tNAA) because their resonances are difficult to separate from each other at low field strengths. The methyl proton resonances of NAAG may account for up to 25% of the tNAA signal. Thus, changes in tNAA may be driven by changes in one or both of these molecules [66].

2.4.3 Myo-inositol

Myo-inositol (mIns) is a six-carbon cyclic ring sugar alcohol that is abundant within brain tissue (~4-8 mM, mostly intracellular). The *myo*- configuration is the most common isomeric form of inositol (90%). Small concentrations of *myo*-inositol are also present in CSF and plasma.

The spin system of mIns shows strong *J*-coupling, with two prominent multiplets at 3.52 and 3.61 ppm [67]. Thus, to minimize signal loss due to *J*-modulation, mIns is usually best observed using short TE. The measured mIns signal may also include minor contributions from related phosphoinositols and glycine.

Myo-inositol is a potential glial cell marker. The earliest evidence supporting this is from two cell culture studies that compared its levels between neuronal and glial cell types. One study observed that the uptake of extracellular radiolabeled mIns was much larger in glial cells than in neurons [68]. The other study observed high mIns concentrations in glia but not in neurons using ^{1}H-NMR [69]. Since then, elevated mIns levels have been reported for several neurological conditions associated with gliosis, including ALS, and hence have been interpreted as indicating glial proliferation.

However, caution must be taken to avoid treating mIns as a glial-specific marker. Studies have demonstrated high mIns concentrations in some neuronal populations [70]. In addition, elevated mIns levels have been observed in the absence of gliosis assessed histologically. Thus, we must be aware that changes in mIns may be non-specific to glial pathology and may reflect other disease-related changes. In particular, the levels of mIns may be strongly influenced by changes in cellular osmotic state due to its function as an osmolyte. Cellular swelling that occurs during glial activation may therefore be associated with increased mIns; however, this change could be mitigated by compensatory mechanisms to maintain osmotic balance [71]. Additionally, mIns is known to have a broad role as the main precursor to the molecular components of the phosphatidylinositol cycle. This cycle is important for many critical cell signaling events and the generation of membrane phospholipids [72].

2.4.4 Glutamate and glutamine

Glutamate (Glu) is a ubiquitous amino acid with a high intracellular concentration in the brain (~5-10 mM). It is the most abundant neurotransmitter in the brain but also serves a critical role as a building block for many cellular molecules, including proteins and other metabolites and neurotransmitters. Glu may also be a major source of energy in addition to glucose [73]. These functions may explain why large intracellular Glu pools are maintained, particularly within neurons.

Extracellular Glu release causes the excitation of post-synaptic neurons. Excessive Glu-mediated neuronal excitation is one of the proposed mechanisms underlying motor neuron loss in ALS. The basal concentration of extracellular Glu is small at ~1-5 μM and is tightly maintained through reuptake mechanisms. Increasing and prolonging this concentration at ~100 μM is enough to cause rapid cell necrosis [74]. Thus, any possible changes in extracellular Glu levels in ALS are likely too small to be detected by ^{1}H-MRS. Instead, ^{1}H-MRS may be more sensitive to major instabilities in intracellular Glu, which can be reduced secondary to neuronal degeneration or altered by abnormalities in any of Glu's metabolic pathways. Reduced levels of Glu have been observed in post-mortem brain tissue in ALS [75]. Conversely, studies of extracellular fluids (CSF and plasma) in patients with ALS have shown elevated levels of Glu [65, 76].

The Glu spectrum has *J*-coupled resonances that overlap substantially with resonances of other metabolites, particularly glutamine (Gln). Consequently, ultra-high fields are necessary to resolve and quantify Glu reliably. At lower fields, Glu is typically reported with Gln as a sum called Glx due to insufficient spectral resolution. The interpretation of changes in Glx can be difficult as Glu and Gln are connected through the Glu-Gln cycle, which leads to speculation about how one metabolite may influence the other's concentration. Increased Glx has often been interpreted as an increase in the biosynthesis of both molecules, presumably due to a higher Glu-Gln cycle turnover rate driven by excessive glutamatergic neurotransmission. However, Glu and Gln do not always

fluctuate jointly. In particular, Glx is not a robust measure in conditions where Glu and Gln levels may change in opposite directions [77].

Most of Gln in brain tissue (2-4 mM) is synthesized within astrocytes using Glu as a precursor. Thus, at ultra-high fields, the measurement of Gln may be a rough astrocytic marker. Additionally, however, Gln may be an indirect marker of extracellular Glu levels. Astroglial Gln is predominantly synthesized using neuronal Glu acquired through reuptake from the extracellular space. Thus, increased Gln by itself could reflect increased glutamatergic neurotransmission. ^{1}H-MRS studies in ALS mouse models have demonstrated longitudinal increases in Gln levels in multiple brain regions as well as higher levels compared to wildtype [78].

2.4.5 Gamma-aminobutyric acid

Although most neurons in the brain are glutamatergic, there are also considerable numbers of inhibitory neurons (~20% in cortex) that use the neurotransmitter γ-aminobutyric acid (GABA). The status of GABAergic neurons is relevant to ALS, as increased cortical excitability at early disease stages is likely associated with decreased cortical inhibition [79].

In the *in vivo* spectrum, GABA is a weakly represented molecule (~1 mM) with *J*-coupled resonances that are obscured by the contributions of more abundant metabolites. The most widely applied method for measuring GABA is a ^{1}H-MRS editing technique that selectively changes the phase of an obscured signal without affecting the overlying signals. Also known as *J*-difference editing, a frequency-selective pulse applied at the GABA resonance of 1.90 ppm will refocus the *J*-modulation of its coupled spin at 3.02 ppm [80]. Subtracting a typical *J*-modulated spectrum from this edited spectrum has two consequences: 1) elimination of the overlying creatine signal at 3.04 ppm; 2) a positive, in-phase GABA signal at 3.02 ppm.

2.4.6 Glutathione

Glutathione is the primary antioxidant in the brain. In its reduced form (GSH), the thiol group enables direct scavenging of oxygen radicals and participates in enzyme-catalyzed reduction of harmful peroxides. The ratio of GSH to its oxidized form GSSG is also important in maintaining the cell's redox balance. Depletion of intracellular GSH pools is associated with cell injury via oxidative damage in *in vivo* and *in vitro* models. Thus, changes in GSH levels may be an indicator of increased oxidative stress burden, which is a known pathological feature of ALS. Post-mortem studies in ALS have also identified reduced GSH peroxidase activity in the brain, demonstrating the potential relevance of this metabolite to the disease's neuropathology.

GSH is mostly intracellular, with concentrations in the brain ranging from 1 to 3 mM [81]. The GSH spectrum is a small contribution with substantial resonance overlap. To measure the signal, *J*-difference editing techniques may be applied that exploit the coupling between spins at 2.95 and 4.96 ppm [82]. In this approach, overlapping resonances near the region of 2.95 ppm (e.g. Cr and GABA) are eliminated by subtraction. Alternatively, GSH can be quantified at ultra-high fields without spectral editing [83].

2.5 Prior Investigations in ALS

The first MR spectroscopic study in ALS was conducted using long-echo PRESS ^{1}H-MRSI at 1.5 T and discovered lower tNAA to tCr ratio (tNAA/tCr) in cortical areas in patients compared to healthy controls [84]. The reductions were especially significant in the motor cortex, a finding that has been confirmed in numerous studies since. In the last 20 years, ^{1}H-MRS has revealed metabolic abnormalities in several different CNS regions in ALS, both motor and extra-motor. The abnormalities are not only in tNAA, but also in other metabolites such as Glu and mIns that are best observed with optimized pulse sequences at higher field strengths.

2.5.1 Motor Cortex

Reduction in the levels of motor cortex tNAA or tNAA/tCr is the most consistent ^{1}H-MRS finding in ALS (reported in over 15 studies) [84-98]. Most of these studies were cross-sectional and applied single-voxel spectroscopy at 1.5 T. In all cases, the reductions were interpreted as indicating cortical neuronal loss or dysfunction. Those that reported tNAA/tCr generally attributed the reduction to a change in tNAA rather than a change in tCr. However, some evidence indicates that cortical tCr levels may be increased in ALS [88], which could reduce the specificity of this ratio measure as a marker of neuronal integrity.

A few studies have also reported lower ratios of tNAA to total choline (tNAA/tCho) [94, 99] or to mIns (tNAA/mIns) [85, 91]. Strong reductions in these measures in ALS may indicate a combination of neuronal loss and gliosis. Total choline (tCho) is the sum of compounds phosphocholine and glycerophosphocholine, which are important intermediates in cell membrane synthesis and catabolism [100]. Early studies reported elevations in tCho that could reflect increased glial cellularity or myelin breakdown [94]. However, recent studies have not substantiated this finding. The tNAA/mIns ratio may be a more robust indicator of neuronal injury associated with gliosis. Compared with tCho findings, increased mIns levels have been reported more frequently in ALS, albeit with some inconsistency as well. In one cross-sectional study, motor cortex tNAA/mIns showed superior sensitivity and specificity in distinguishing patients from healthy controls compared to other ratio measures [91].

Across multiple studies, motor cortex tNAA and its ratios have correlated significantly with ALSFRS-R, clinical UMN burden, and El Escorial diagnostic class [101]. These measures may also have the ability to predict survival and monitor treatment response [92, 99].

Only a few longitudinal ^{1}H-MRS studies have been performed, and these have reported either negative findings [93, 96] or decline in motor cortex tNAA or its ratios [94, 102, 103]. Longitudinal trends in other regions and in other metabolites have not been investigated.

In addition to tNAA, alterations in motor cortex Glu have been identified with ^{1}H-MRS. However, the direction in which Glu levels change in ALS is unclear. A few studies observed elevations in Glx, which may support an excitotoxic disease mechanism [88, 90]. However, other groups found reductions in Glu, which could reflect glutamatergic neuron loss [86, 104]. Studies conducted at ultra-high field will help clarify the direction of Glu abnormalities in ALS.

Motor cortex reductions in GSH and GABA have also been reported recently [88, 98]. Lower GABA in ALS may indicate loss of cortical inhibition, while lower GSH may be a marker of oxidative stress. In these studies, no significant correlations were observed between the metabolites and clinical severity scores. GSH and GABA are more difficult to quantify reliably than other metabolites. The findings of these studies may depend on the particular methodology used for detection and quantification and therefore need to be confirmed.

2.5.2 Corticospinal Tract

A few ^{1}H-MRSI studies have examined tNAA alterations in brain regions containing pyramidal white matter tracts. Reduced tNAA/tCho or tNAA/tCr were discovered in areas including the precentral gyrus white matter, corona radiata, and posterior limb of the internal capsule. Significant differences with controls were also observed when comparing the mean tNAA or tNAA/tCho levels calculated for the “whole” corticospinal tract within the brain. Notably, one study observed an expected somatotopic relationship between tNAA/tCho levels in the upper limb corticospinal tract and contralateral finger-tapping speed [105]. Significant correlations were also reported between mean corticospinal tract tNAA and ALSFRS-R [106].

Some of these studies have also tried to compare the disease information obtained from ^{1}H-MRSI with the corticospinal tract abnormalities observed using diffusion tensor imaging (DTI). One study demonstrated that corticospinal tract tNAA has greater ability to distinguish patients from controls compared to typical DTI measures such as fractional anisotropy and mean diffusivity [106].

2.5.3 Brainstem

Due to voxel size limitations and its caudal location in the head, ^{1}H-MRS assessment of the brainstem is typically more challenging than intracranial regions. Thus, only a few studies have examined metabolic alterations in the brainstem in ALS.

The findings from these studies, however, have been generally consistent. All studies reported reductions in tNAA or tNAA/tCr levels [88, 107-109]. In addition, two of the studies reported elevated Glx or Glx/tCr levels in the pons or medulla [88, 109]. These metabolic abnormalities were also related to region-specific function. For example, tNAA/tCr reductions were only observed in patients with prominent bulbar weakness [108], and Glx/tCr levels significantly correlated with ALSFRS bulbar subscores [109].

2.5.4 Spinal Cord

Spinal cord ^{1}H-MRS has been performed in ALS but is very challenging due to the region's deep location, severe local field inhomogeneities, and high susceptibility to subject and cord motion. These factors substantially reduce the SNR. A few studies in the cervical spine reported reductions in tNAA/tCr and tNAA/mIns [110, 111].

3

Test-Retest Reproducibility of ^{1}H-MRS: 3.0 versus 7.0 Tesla

3.1 Chapter Preface

Demonstrating adequate reliability of the measurement method is a critical step in biomarker validation and application in clinical trials. Multiple studies have reported high test-retest reproducibility of ^{1}H-MRS measurements [112-114]; however, the potential differences in reproducibility between different methodologies and field strengths have not been explored. The measurement reliability of specific metabolites depends on these factors. Here we studied the field dependence of ^{1}H-MRS test-retest reproducibility across the neurochemical profile of the brain obtained with a state-of-the-art semi-LASER sequence [115]. The same pulse sequence and parameters were used at 3 and 7 T to conduct serial measurements in healthy volunteers. Measurement precision was then compared between the field strengths for different brain regions. The results of this study help to inform the decision on the appropriate field strength to use for studying specific metabolites.

These results are published in the paper “Test-Retest Reproducibility of Neurochemical Profiles with Short-Echo, Single-Voxel MR Spectroscopy at 3T and 7T” [116].

3.2 Introduction

In vivo ^{1}H magnetic resonance spectroscopy (MRS) enables non-invasive detection of cellular and metabolic alterations in diseases of the central nervous system and therefore is ideally suited to play a role in the development of diagnostic protocols, preventative strategies, and therapeutic interventions [52]. With increasing availability of high and ultra-high magnetic field scanners comes a need to characterize the benefits of the increased sensitivity and resolution that they provide [83, 117, 118]. Systematic investigations of these benefits will facilitate informed choice of field strength for robust clinical applications of the technique.

Clinical applicability of MRS depends upon the test-retest reproducibility in the neurochemical concentrations measured since disease related changes can be detected in individuals only if they are higher than the day-to-day experimental and physiological variability. Test-retest coefficients of variance (CVs) have been reported for many experimental configurations for 3-7 major metabolites, quantified primarily with the standard STEAM and PRESS sequences [119-126].

However the field dependence of test-retest CVs is largely unexplored. In this respect, Cramér-Rao Lower Bound (CRLB) estimates of minimum variance can provide insights. The CRLBs have been shown by simulations [117] and in practice [83, 118, 119, 127] to be lower at higher field, predicting lower test-retest CVs at higher field. However, only a few studies have investigated whether the lower CRLBs indeed translate to lower test-retest CVs at higher field [119, 125].

Meanwhile, neurochemical profiles of 10-18 metabolites are increasingly being reported at both 3 T [113, 118, 128-130] and 7 T [118, 131-135] using highly optimized, short echo localization sequences such as STEAM, SPECIAL and semi-LASER, which minimize apparent T_2 relaxation and *J*-coupling evolution that counteract the sensitivity gains, particularly at 7 T. Of these, semi-LASER [49, 115] was recently shown to provide excellent between-site reproducibility at 3 T [113] and 7 T [135], documenting its suitability for multi-site trials. In addition, good between-session reproducibility of the sequence was demonstrated for selected VOI at 3 T [128] and 7 T [135]. However, its

limits for test-retest reproducibility of neurochemical profiles and how these compare at 3 T vs. 7 T remain to be established.

Therefore the goal of this study was to compare test-retest reproducibility of neurochemical profiles obtained with semi-LASER at 3 T versus 7 T, with state-of-the art hardware at each field. We investigated whether improvements in CRLB at ultra-high vs. high field lead to better test-retest reproducibility, and which metabolites critically need the sensitivity and spectral resolution at 7 T to manifest clinically applicable reproducibility. A secondary goal was to determine the number of repeat measurements needed for a robust estimation of test-retest CVs, as between-session test-retest reproducibility investigations typically use only one repeat measurement.

The same subjects were scanned at both 3 T and 7 T using the best hardware available to us and matched software on a clinical platform. We utilized coils that were capable of achieving sufficient B_1 for spectroscopy (with minimal chemical shift displacement) in deep brain regions at both fields. We focused on two brain regions that are of interest for neurological diseases and that present different levels of technical challenges for MRS: the posterior cingulate, a key node in the default mode network [136], which is affected in a number of neurological and psychiatric disorders [137, 138], and the cerebellum, which is affected in multiple movement disorders [139], and is technically more challenging for study by MRS (due to its caudal location in the brain and broader intrinsic linewidths than most other cortical areas).

3.3 Methods

Subjects and study design

Six healthy volunteers (males, 32 ± 8 years) participated in the study after giving written informed consent using procedures approved by the Institutional Review Board: Human Subjects Committee of the University of Minnesota. Volunteers were scanned 4 times at 3 T and 4 times at 7 T, once weekly for each field strength, except for one subject who was scanned 5 times at 3 T and twice at 7 T and another subject who was scanned 5 times at 7 T.

MR protocol

Studies were performed with a 3 T whole-body Siemens Tim Trio and a 7 T whole body Siemens MAGNETOM scanner (Siemens Medical Solutions, Erlangen, Germany). At 3 T, the standard body RF coil was used for radiofrequency transmission and the 32-channel phased-array Siemens head coil was used for signal reception. At 7 T, a 16-channel transceiver array coil [140] allowed B_1^+ shimming as described previously [133]. T_1-weighted MPRAGE images (3 T: repetition time (TR) = 2530 ms, echo time (TE) = 3.65 ms, flip angle = 7˚, slice thickness = 1 mm, 224 slices, field-of-view (FOV) = 256 x 176 mm^2, matrix size = 256 x 256; 7 T: TR = 2500 ms, TE = 2.4 ms, flip angle = 5˚, slice thickness = 1 mm, 176 slices, FOV = 232 x 256 mm^2, matrix size = 232 x 256) were acquired to position the volume-of-interest (VOI) for MRS. Proton spectra were acquired from the posterior cingulate cortex (PCC, 2.0 x 2.0 x 2.0 cm^3) and cerebellar vermis (CBM, 1.0 x 2.5 x 2.5 cm^3). Reproducible voxel placement was based on anatomical landmarks: For the PCC, the anterior inferior corner of the voxel was placed at the splenium of the corpus callosum and the anterior superior corner was below the cingulate sulcus. The surfaces, lobes, lobules and fissures of the cerebellum were used for CBM.

After selecting the VOI and B_1^+ shimming at 7 T [133], first- and second-order B_0 shims were adjusted in each VOI using FASTMAP (fast, automatic shimming technique by mapping along projections) with echo-planar imaging readout [141]. Next, B_1 levels for localization pulses and water suppression in semi-LASER were adjusted [113]. Metabolite and water reference spectra were acquired using a modified semi-LASER sequence [115] (TE = 28 ms at 3 T and 26 ms at 7 T, TR = 5 s, 64 transients, as described previously [113]. Finally, fully relaxed unsuppressed water signals were acquired at TE's ranging from 28-4000 ms (TR = 15 s) to estimate the cerebrospinal fluid (CSF) contribution to each VOI [142].

Spectral post-processing and quality control (QC)

Single-shot spectra were post-processed in Matlab, including Eddy current correction, removal of shots affected by subject motion, frequency correction using a cross-correlation algorithm and phase correction using a least-square fit algorithm [113], and

then averaged. Summed spectra were visually assessed for extraneous coherences and spectra excluded from further analysis if such coherences were noted.

To evaluate the between-session reproducibility of voxel placement, the MPRAGE image from the first session was used as a reference to which images from later sessions were aligned linearly (6 degrees of freedom) together with VOI masks in FSL-FLIRT registration tool (http://fsl.fmrib.ox.ac.uk/fsl/fslwiki/FLIRT). The proportion of the volume that is shared by at least three of the four VOI masks to the VOI volume was calculated and expressed in percent. This approach was chosen to treat the 4 sessions as 'exchangeable' rather than identifying one of them post-hoc as a 'gold standard' session to which the others should be compared, which may introduce a bias if the reference VOI has poor overlap with the other 3 even if the other 3 VOI overlap well.

Metabolite quantification

Metabolites were quantified using LCModel [55]. The model spectra for alanine (Ala), aspartate (Asp), ascorbate (Asc), glycerophosphocholine (GPC), phosphocholine (PC), creatine (Cr), phosphocreatine (PCr), γ-aminobutyric acid (GABA), glucose (Glc), glutamine (Gln), glutamate (Glu), glutathione (GSH), *myo*-inositol (Ins), lactate (Lac), *N*-acetylaspartate (NAA), *N*-acetylaspartylglutamate (NAAG), phosphoethanolamine (PE), *scyllo*-inositol (sIns) and taurine (Tau) were simulated using density matrix formalism [143] based on previously reported chemical shifts and coupling constants [67, 144]. Macromolecule spectra acquired from the occipital cortex of 4-5 volunteers at each field using an inversion recovery technique (TR = 2.5 s, inversion time TI = 0.75 s at 3 T and TR = 2 s, TI = 0.69 s at 7 T) [83] were also included in the basis set. The validity of using a general macromolecule spectrum for fitting spectra from multiple brain regions was recently demonstrated [56, 145].

Metabolite concentrations were determined after correcting for tissue water and CSF content, and the T_2 of water in LCModel (version 6.3-0G), as described previously [113]. A water content of 82% was assumed [146]. The % CSF contribution was obtained from a bi-exponential fit of the integrals of water spectra at different TE values [142]. A water T_2 of 120 ms was used at 3 T and 87 ms at 7 T, based on the assumption that the T_2 of

water under Carr-Purcell conditions is 1.5x longer than the measured free precession T_2 [113]. Metabolites quantified with CRLB > 50% were classified as not detected [147]. Only metabolites quantified with mean CRLB ≤ 20% were included in the neurochemical profile of each brain region at each field. If the correlation between two metabolites was consistently very high (correlation coefficient < -0.7), their sum was reported [147], e.g. total creatine (tCr, Cr + PCr) and total choline (tCho, GPC + PC).

Statistical analysis

Summaries were calculated per field strength for each region. Spectral quality was quantified by water linewidth and SNR in the frequency domain (SNR_{freq}). Voxel placement reproducibility was assessed by within-voxel CSF fraction and % voxel overlap between sessions. These quantities were each compared across regions within field strength, and across field strengths within region, using linear mixed models to account for the multiple scans per person.

Neurochemical concentrations (summed over 64 transients per scan per subject), and CRLBs of concentrations, were summarized per person using intra-subject means across all scans. Between-session CV of concentration was calculated for the i^{th} subject and m^{th} metabolite across repeat scans as intra-subject sample standard deviation (SD) divided by intra-subject sample mean:

$$\text{intra-subject } CV = CV_{im} = {}^{s_{im}}\!/_{\bar{x}_{im}}.$$

Since some concentrations were excluded according to CRLB criteria (see above), all included concentrations were used in computing these means and SDs. A confidence interval (CI) for each CV_{im} was calculated using the modified McKay approximation [148]. To examine the robustness of the intra-subject CVs to the number of repeat scans, the intra-subject CV and CI calculations were repeated using each person's first 2, then 3 and then 4 scans. For each number of scans used (2, 3, and 4), means across the 6 participants of the intra-subject CVs were calculated:

$$\hat{\mu}_m^{CV} = \frac{1}{6}\sum_{i=1}^{6} CV_{im};$$

means of the endpoints of the CV_{im} CIs were also calculated. Next, using all scans per person, intra-subject CVs were summarized across people using inter-subject means (as in the above equation) and using inter-subject SDs:

$$\hat{\sigma}_m^{CV} = \sqrt{\frac{1}{5}\sum_{i=1}^{6}\left(CV_{im} - \hat{\mu}_m^{CV}\right)^2};$$

similar inter-subject means and SDs were computed for the intra-subject mean CRLBs. Concentrations, CVs and mean CRLBs were compared between field strengths (for each region separately) using paired Wilcoxon tests because of mild non-normality. Lastly, intra-subject between-session CV was separately re-computed five times: including the first 2, 4, 8, 16, and 32 transients from each scan; these were then compared to the original summaries using 64 transients from each scan.

3.4 Results

Using an MRS protocol that involved B_0 shimming with FASTMAP, voxel-based B_1 adjustment, localization by semi-LASER [115] and single-shot phase/frequency correction, consistently high quality spectra were obtained in both brain regions at both fields. The high reproducibility of spectral quality and pattern within individuals is demonstrated in Figure 3.1. Based on QC criteria, 1 spectrum from the cerebellum (of a total of 23 spectra) and 2 spectra from the posterior cingulate (of 23 spectra) at 7 T were excluded from further analysis. None of the 25 spectra available for each region at 3 T were excluded.

As expected, the PCC spectra had narrower linewidths and better SNR than CBM spectra (Table 3.1). Frequency domain SNR (SNR_{freq}) was better at 7 T for CBM, but not for PCC (Table 3.1), underlining the importance of the many factors that determine the SNR in addition to field strength, such as coil configurations. Voxel placement consistency was demonstrated both by CSF contribution to each VOI and by between-session voxel overlap (Table 3.1, $p > 0.05$, 3 T vs. 7 T).

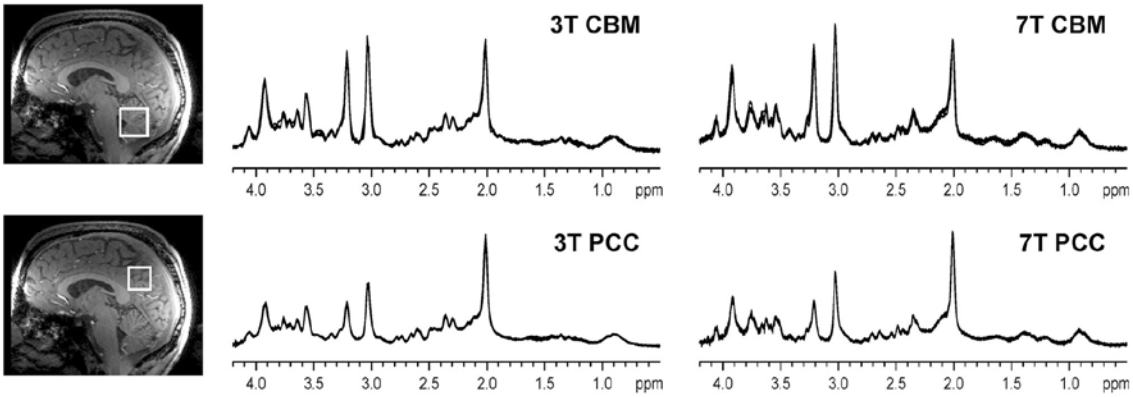

Figure 3.1 Reproducibility of spectral quality and pattern. All spectra obtained in one subject are shown (semi-LASER, TE = 28 ms at 3T and 26 ms at 7T, TR = 5 s, 64 transients), with the spectra obtained per brain region/field overlaid in each panel. The voxel locations are shown on the T_1-weighted images acquired at 3T. Spectra were apodized with linebroadening (1 Hz) and Gaussian multiplication ($\sigma = 0.12$ s) for display purposes. PCC: posterior cingulate cortex, CBM: cerebellar vermis.

Table 3.1 Spectroscopic parameters measured in two brain regions and two fields

	3T		7T	
	PCC	CBM	PCC	CBM
Number of spectra (N)	25	25	21	22
Water linewidth (Hz)	6.6 ± 0.4	7.5 ± 0.9**	12.1 ± 1.0	14.3 ± 1.2**
SNR_{freq}[a]	234 ± 57	127 ± 29**	181 ± 28*	141 ± 21*,**
CSF fraction (%)	6.1 ± 2.5	7.6 ± 3.3	5.5 ± 1.6	7.8 ± 2.6
Voxel overlap (%)[b]	91 ± 5	90 ± 2	88 ± 5	90 ± 4

Values given are inter-subject mean ± inter-subject standard deviation of the intra-subject means. PCC: posterior cingulate cortex; CBM: cerebellar vermis.

[a]SNR was measured in the frequency domain (defined as peak height divided by root mean square noise) based on tNAA in non-apodized spectra.

[b]Fraction of total voxel volume that is shared in at least three of the four scanning sessions

* $p < 0.01$, 3T vs. 7T (within region)

** $p < 0.001$, PCC vs. CBM (within field)

A larger number of metabolites had mean CRLB ≤ 20% at 7 T than at 3 T for both VOI (Figure 3.2), despite a lower SNR_{freq} for PCC at 7 T. Metabolites such as GABA, Lac, PE and NAAG passed the CRLB filter only at 7 T, while Glc passed the filter only at 3 T for

both regions and sIns passed the filter only at 3 T for PCC. The concentrations obtained at the two fields were comparable with few exceptions, such as NAA, Glu and Gln, which were estimated at higher levels at 7 T likely due differences in the fitted spline baselines.

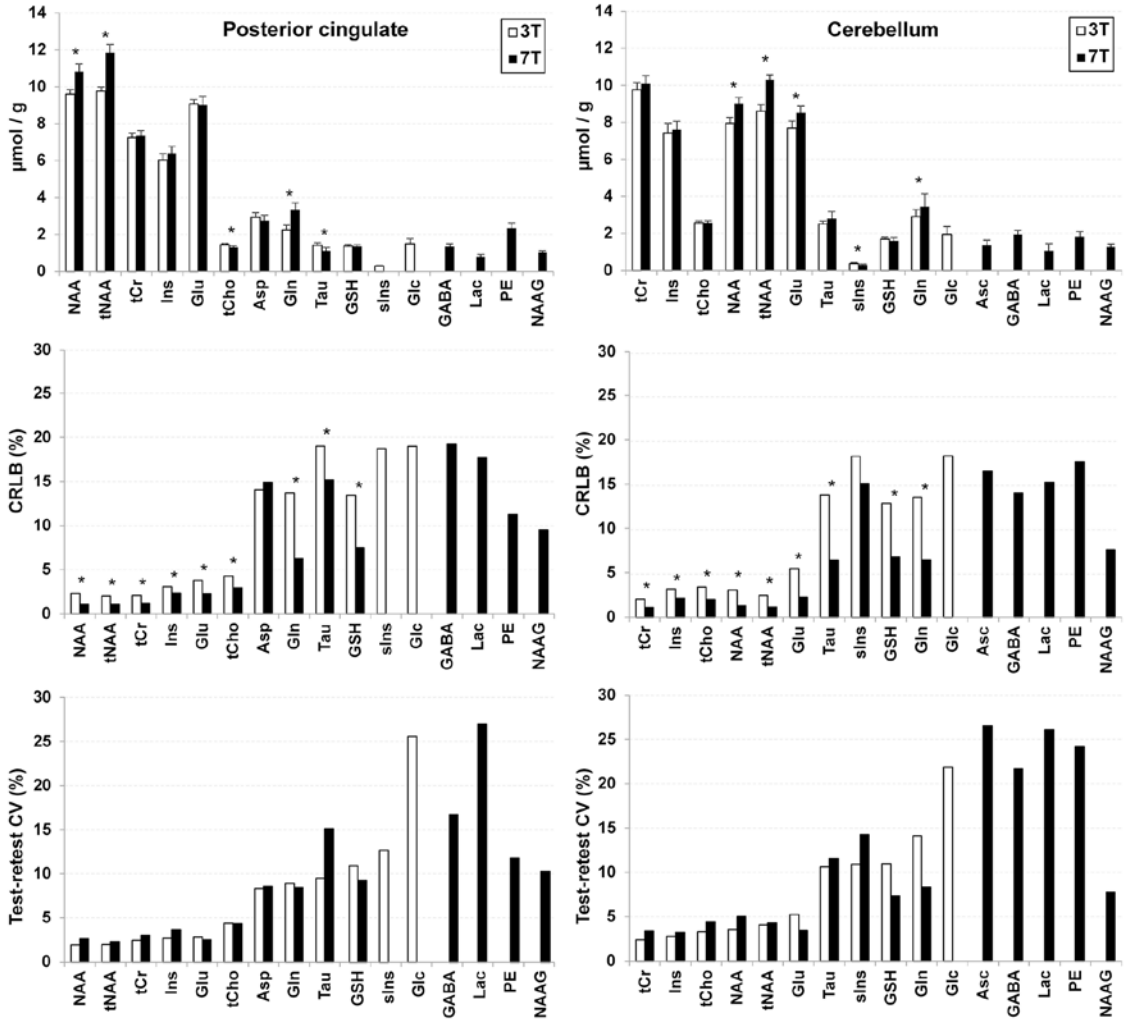

Figure 3.2 Mean metabolite concentrations, Cramér-Rao lower bounds (CRLB) and between-session CVs obtained with semi-LASER (TE = 28 ms at 3T and 26 ms at 7T, TR = 5 s, 64 transients) in the two brain regions at both field strengths. Only metabolites with mean CRLB ≤ 20% are shown. Error bars represent inter-subject SD of intra-subject means. Means include all scans of each subject, i.e. up to 5 scans at each field strength. **p* < 0.05, 3T vs. 7T.

To determine the number of repeat measurements needed for a robust evaluation of intra-subject test-retest reproducibility, between-session CVs were calculated for each of 2, 3 and 4 repeat measurements. Between-session CVs tended to be underestimated for most metabolites with only 2 scans, although the mean CVs were similar with 2, 3 and 4 measurements (Figure 3.3, top). On the other hand, the robustness of the intra-subject CV estimates increased substantially (inter-subject means of the intra-subject CI widths decreased substantially) from 2 to 3 repeat scans, while the improvement from 3 to 4 scans was smaller (Figure 3.3, bottom).

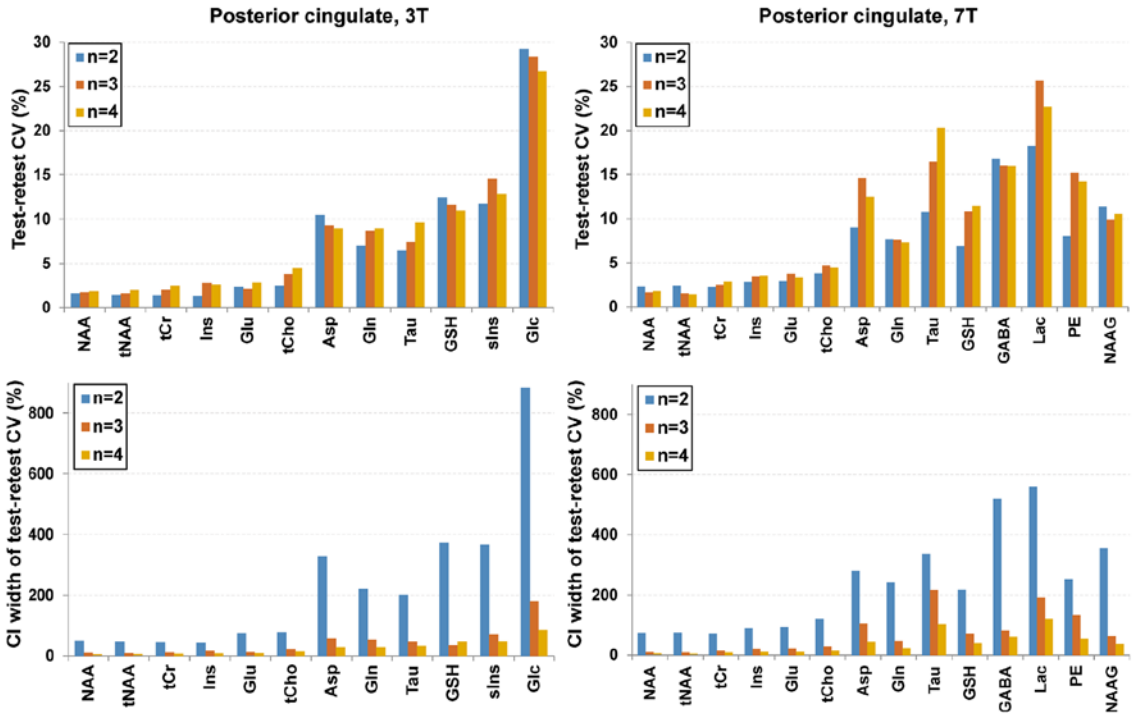

Figure 3.3 Mean between-session CVs (SD/mean, top row) and inter-subject means of the intra-subject confidence interval widths for between-session CVs (bottom row) for posterior cingulate neurochemical profiles, obtained with 2, 3 or 4 repeat scans. Similar results were obtained for the CBM (not shown).

Mean CRLBs were lower at 7 T than at 3 T for almost all metabolites while between-session CVs were comparable at the two fields (Figure 3.2). Trends for lower CVs at 7 T were detected for Glu, Gln and GSH in CBM. Therefore, while the CRLB provided a rough estimate of test-retest reproducibility, they did not fully reflect the true relative reproducibility at the 2 field strengths. Notably, NAA, tCr, tCho, Ins and Glu were

quantified with between-session CVs of ≤ 5% even at 3 T. To investigate whether with the very high spectral quality we have reached a physiological threshold upon which reproducibility cannot be further improved, we analyzed between-session CVs of subspectra. Namely, we summed the first 2, 4, 8, 16 and 32 shots of all spectra and thereby evaluated the between-session reproducibility of spectra with varying SNR at each field (Figure 3.4). This analysis showed that the between-session CVs were indeed lower with shorter acquisitions at 7 T than at 3 T for most metabolites in PCC. For example, the between-session CVs had already leveled off at 2-4 shots for NAA, at 8 shots for tCr and tCho and at 16 shots for Ins at 7 T, while they continuously improved with increasing acquisition duration, i.e. increasing SNR, at 3 T. In CBM, mean between-session CVs for Glu, Gln and GSH were lower at 7 T vs. 3 T across acquisition times.

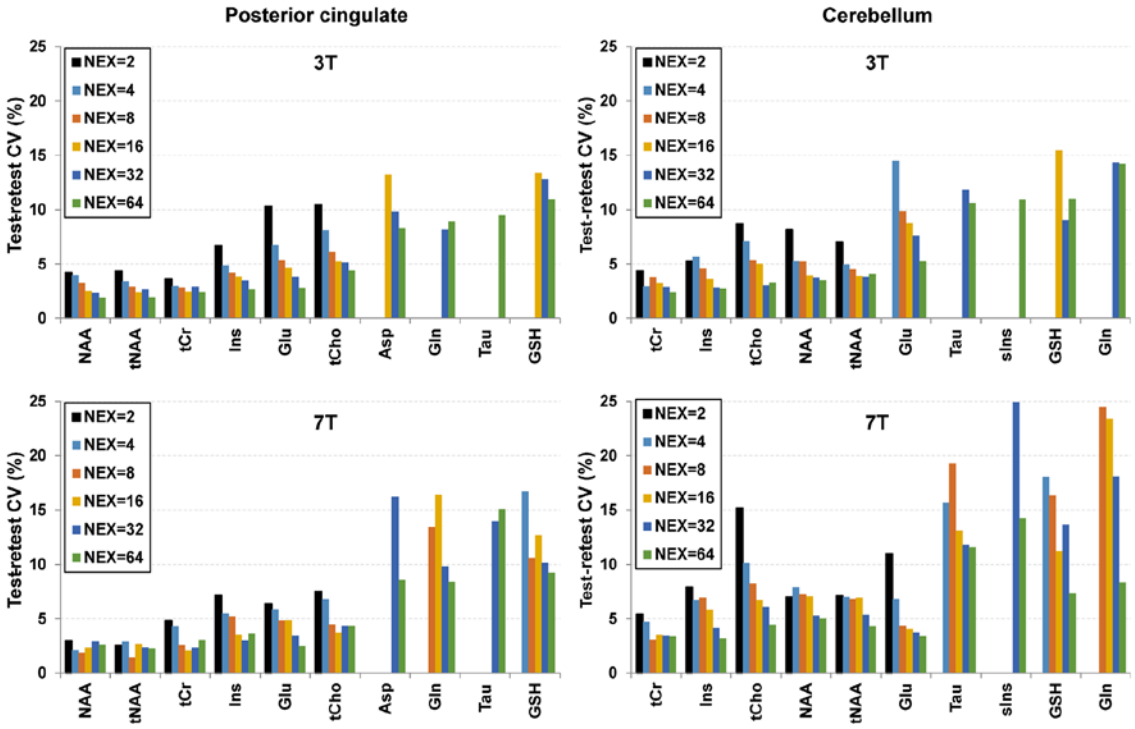

Figure 3.4 Mean between-session CVs obtained by averaging the first 2, 4, 8, 16, 32 and 64 transients (NEX) of spectra from the two brain regions and field strengths. Only metabolites that passed the CRLB reliability criteria are shown, e.g. weakly represented metabolites such as Asp, Gln, Tau and GSH are not reliably quantified in spectra with 2 transients.

3.5 Discussion

Here we examined the test-retest reproducibility of neurochemical profiles using state-of-the-art MRS methodology at high (3 T) and ultra-high (7 T) field with an unprecedented number of retests. We demonstrated excellent reproducibility with standard clinical 3 T hardware and a FASTMAP + semi-LASER based MRS protocol. We further showed that more neurochemicals are detected reliably at 7 T vs. 3 T even when SNR_{freq} was lower at 7 T. Importantly, the reproducibility advantages of 7 T were realized primarily for coupled metabolites such as Glu, Gln and GSH, and for experimental conditions with low SNR. We further showed that the CRLB and test-retest reproducibility do not necessarily improve together.

Sequences such as semi-LASER are increasingly utilized at high field primarily because they minimize chemical shift displacement, which is a major drawback of the standard full intensity sequence PRESS at high field. While these sequences are not standard, they are available as work-in-progress packages on major clinical scanner platforms. Hence the assessment of their within-person reproducibility is critical for their utility in longitudinal clinical applications. To accomplish this, we focused on two clinically relevant VOI. Better linewidths and SNR were obtained for PCC than CBM, because CBM has more microscopic heterogeneities and is located further away from the receive coils. Still, the MRS protocol used here provided spectra with excellent SNR and linewidths with ~5 minute data averaging from both brain regions at both fields (Figure 3.1, Table 3.1). Importantly we aimed at a practical field comparison here, using matched software and the best hardware available to us to consistently achieve sufficient B_1 at both fields because of the challenges to perfectly match hardware for a strict field comparison. Indeed these challenges have resulted in a wide range of reported SNR improvements at ultra-high vs. high field [117]. Note however that despite the differences in coil configurations at the two field strengths, the relationship between the SNR_{freq} at 3 T vs. 7 T corresponded well with theoretical predictions for the CBM. Namely, a ~22% increase in SNR_{freq} is expected at 7 T vs. 3 T for this voxel (SNR_{freq} is proportional to $SNR_{time}/\Delta\nu_{Hz}$, where $\Delta\nu_{Hz}$ is the spectral linewidth in Hz. Since theory predicts a linear dependence of SNR_{time} on B_0 [149], $SNR_{freq} \sim B_0/\Delta\nu_{Hz}$), i.e. the increase in SNR_{time} is

largely offset by the increase in linewidth. The observed 11% increase in SNR_{freq} (Table 3.1) is close to the theoretical prediction; hence observations for this VOI are generalizable for 3 T vs. 7 T comparisons. In addition, the conclusions on test-retest repeatability were the same for the two VOI, further supporting the generalizability of the findings.

The SNR_{freq} was lower at 7 T for PCC, likely because the 32 channel receive array at 3 T provided superior sensitivity relative to the 16 channel T/R array for peripheral VOI such as the PCC. Hence, SNR improvements at 7 T vs. 3 T can vary widely depending on the RF coil characteristics and the relative location of the VOI to the receive coils. Importantly, CRLB were lower at 7 T for both VOI, leading to more metabolites being quantified with mean CRLB ≤ 20% (Figure 3.2) despite the loss in SNR_{freq} in PCC, and therefore are likely due to the resolution enhancement at 7 T. Note that Kreis recently cautioned against quality filtering based on relative CRLBs (in %), and laid out cases where such filtering can lead to biased concentrations in cohort data and wrong conclusions in group comparisons [150]. Here we used the 20% CRLB threshold to identify the neurochemicals that were most reliably quantified [147] at each field rather than for group comparisons, consistent with the recommendation to utilize the relative CRLB to define which metabolites should be evaluated at all [150]. Also note that all metabolites that were quantified with mean CRLB ≤ 20% were also quantified with CRLB < 50% in the majority of the spectra, thereby avoiding biases in metabolite selection for reporting.

The extent of improvement in CRLB at 7 T vs. 3 T differed substantially among neurochemicals, as also shown previously [83, 121, 125, 127]. Namely, the greatest improvements were observed for *J*-coupled metabolites such as Glu, Gln, GSH and GABA (Figure 3.2) due to increased spectral dispersion at 7 T, fully consistent with recent simulations [117]. Glc is a known exception to this trend [83] and is more reliably quantified at 3 T because of a simpler spectral pattern. Despite these improvements we also noted that more spectra were excluded from analysis at 7 T due to unwanted coherences, which were encountered in a larger fraction of spectra likely because of less consistent performance of OVS pulses due to B_1 inhomogeneities at 7 T.

We also investigated the extent to which a single retest is sufficient to provide a robust estimate of between-session CVs. We found that mean CVs were similar with 2, 3 and 4 measurements, with only small trends upon increasing the number of retest measurements (Figure 3.3). This was because skewness and outliers were absent from the current dataset. Skewness or outliers could cause large changes in the CV or confidence interval estimates when including one or two more data points in the CV calculation. Our analysis showed that 3 repeat measurements instead of 2 can substantially improve the robustness of the estimate for datasets without skewness/outliers.

The between-session CVs observed here (Figure 3.2) were lower than almost all prior reports of MRS reproducibility [119-126, 151], except for a recent 3 T study [130]. Notably, that study utilized the same 32 channel RF coil on the same clinical 3 T platform with a non-standard sequence and also investigated reproducibility for a VOI in the PCC. The mean between-session CVs for PCC were lower for multiple metabolites (NAA, tCr, tCho, Ins, Glu) in our study vs. the Wijtenburg et al. study [130], while they were the same (Gln) or higher for others (Asp, GSH). While there were multiple methodological differences between the two studies, including the pulse sequences used and LCModel basis sets (e.g. we included experimentally acquired macromolecule spectra), together these studies demonstrate the advantages of utilizing optimized MRS methodology on standard clinical 3 T hardware for improved reproducibility of neurochemical profile quantification. Note however that when using semi-LASER for clinical cohort comparisons, age [152], disease [153], metabolite [154] and region [155] associated variance in T2 needs to be considered at the TEs achievable with the sequence. In addition to optimized MRS methodology, reproducible voxel placement (Table 3.1) was clearly also an important factor in the high reproducibility in metabolite concentrations. Note that the approach we chose to report voxel overlap (fraction shared by at least 3 VOI) was appropriate since the voxel was not placed based on a reference session (e.g. session #1). Also note that the reproducibility of metabolite concentrations may be further improved by automating VOI placement using atlas-based approaches [156].

Importantly, lower CRLBs did not necessarily translate to lower CVs at 7 T (Figure 3.2). However, the sample size was only 6 for the pairwise comparison of CVs at 3 T vs. 7 T, therefore notable differences in mean CVs of Glu, Gln and GSH at 3 T vs. 7 T remained as trends. Analysis of sub-spectra with a reduced number of scans demonstrated that we reached a minimum achievable CV threshold with a lower number of transients than 64 at 7 T for multiple metabolites and that test-retest CVs are indeed lower at 7 T than at 3 T with shorter acquisitions (Figure 3.4).

3.6 Relevance to the Study of ALS

This work demonstrated very high test-retest reproducibility for the measurements of major metabolites at both 3 and 7 T. However, except for one study at 3 T [96], all longitudinal ^{1}H-MRS studies in ALS thus far have been performed at 1.5 T. Furthermore, the study at 3 T did not report the number of transients per scan, making it unclear whether they achieved substantial gains in measurement precision. Thus, the majority of studies have not utilized the increased measurement precision associated with higher field strengths, which may be a reason for the mixed findings in longitudinal ^{1}H-MRS literature (either negative or reported tNAA decline).

Major metabolites such as tNAA and mIns may be sensitive biomarkers in ALS. However, there is also strong interest in weakly represented coupled metabolites such as GSH and GABA, each of which have been investigated only once in ALS. Without spectral editing, these metabolites showed better reproducibility at 7 T compared to 3 T. Thus, we employed this study's sequence and parameters at 7 T to examine the full neurochemical profile in patients with ALS. Our ^{1}H-MRS experiments in ALS will be described in the next two chapters.

4

A ^{1}H-MRS Study of ALS at 7 Tesla: Cross-sectional Findings

4.1 Chapter Preface

This chapter describes the cross-sectional analysis of ^{1}H-MRS data acquired at 7 T from an early-stage ALS cohort. Comparisons of metabolite levels between disease and control groups are described as well as correlation analyses with clinical status. We were particularly interested in the group comparison of motor cortex GSH levels, which are purportedly lower in ALS according to a recent study performed at 3 T [98]. Thus, in addition to the GSH quantification at 7 T, we also ran a GSH-editing protocol at 3 T to replicate this previous finding and to determine whether the choice of methodology impacts the results obtained for this metabolite. The results from this study are published in the paper "Ultra-High Field Proton MR Spectroscopy in Early-Stage Amyotrophic Lateral Sclerosis" [157]. The longitudinal follow-up of this cohort was performed only at 7 T and will be discussed in the next chapter.

In this chapter, unpublished data on the diagnostic sensitivity and specificity of ^{1}H-MRS measures and additional correlations with novel measures of clinical burden are also presented. The Methods section contains descriptions of the methods used in these additional analyses.

4.2 Introduction

Amyotrophic lateral sclerosis (ALS) is a fatal adult-onset motor neuron disease characterized by progressive and irreversible loss of voluntary muscle function. Affected persons generally die within two to four years after symptom onset, and riluzole — an FDA-approved drug for ALS — has provided only a modest benefit in prolonging survival [158, 159]. On *post-mortem* exam, ALS is distinguished from other motor neuron diseases by the selective degeneration of both the upper motor neurons (UMNs) that descend from the primary motor cortex to the brainstem and spinal cord and the lower motor neurons (LMNs) that project peripherally to the musculature. The diagnosis of ALS currently depends upon the clinician's ability to detect signs of UMN and LMN dysfunction through physical examination. While electrophysiological testing can provide additional supportive evidence of LMN dysfunction, the reliability of tools for quantitatively and objectively measuring UMN degeneration in ALS has not been established. Such tools could help identify biomarkers of disease activity in the brain that are critical for evaluating treatment efficacy in therapeutic trials for ALS [160].

Single-voxel proton magnetic resonance spectroscopy (^{1}H-MRS) is an advanced magnetic resonance imaging (MRI) technique for examining the neurochemistry of the brain. Whereas conventional brain MRI is unremarkable in ALS [161], ^{1}H-MRS has revealed various neurochemical abnormalities that may indicate underlying disease processes, including gliosis, glutamate excitotoxicity, and oxidative stress. ^{1}H-MRS studies over the years in humans with ALS have suggested abnormal levels of the following brain metabolites: *N*-acetylaspartate (NAA, marker of neuronal integrity) [88, 89, 103]; *myo*-inositol (mIns, putative marker of glial cells) [86, 91]; glutamate (Glu, excitatory neurotransmitter) [90]; γ-aminobutyric acid (GABA, inhibitory neurotransmitter) [88]; and glutathione (GSH, thiol antioxidant) [98]. Nearly all of these studies included the primary motor cortex and its underlying white matter as a region of investigation.

The most commonly reported finding across ^{1}H-MRS studies of ALS to date is lower levels of NAA in the motor cortex, indicating neuronal loss and/or dysfunction. However, apart from this finding, alterations in the levels of other metabolites have been reported

inconsistently in ALS literature. For example, only a few studies reported a significant elevation in motor cortex mIns levels [86, 91], while the majority did not. In addition, it remains unclear as to whether motor cortex Glu levels are higher or lower in ALS, as differences from controls have been reported in both directions [86, 88, 90, 104]. This discrepancy may stem from the difficulty in quantifying Glu at low field strengths due to its considerable overlap with glutamine (Gln), resulting in the reporting of Glu and Gln as a sum termed Glx. Furthermore, in two relatively recent studies, lower GABA and GSH levels were observed in the motor cortex of patients using edited ^{1}H-MRS techniques at 3 T [88, 98]. GABA and GSH may mark states of cortical hyperexcitability and chronic oxidative stress, respectively, in ALS [79, 162] and require further investigation with advanced ^{1}H-MRS methods.

Neurochemical profiles that consist of 10-15 metabolites can be reliably quantified with ^{1}H-MRS at 7 T [83, 116]. A major advantage of increasing the magnetic field to 7 T is improved resolution of the overlapping *J*-coupled resonances of Gln, Glu, GSH, and GABA, resulting in quantification of these metabolites with excellent test-retest reproducibility [114, 116] and without the need for metabolite-specific spectral editing. The purpose of the present study was to utilize our advanced 7 T ^{1}H-MRS protocol to establish the neurochemical profiles of an early-stage ALS cohort and compare them with a cohort of matched healthy controls. Specifically, the study was designed to (1) clarify discrepancies in the literature regarding metabolite concentrations in ALS by using state-of-the-art ^{1}H-MRS technology at 7 T and (2) investigate the dependence of neurochemical abnormalities on clinical measures of functional status, upper motor neuron disease burden, and diagnostic classification. We selected volumes-of-interest (VOI) in the motor cortex and pons, which are regions that show histopathologic evidence of neurodegeneration in ALS [4, 17]. On the same participants, we also performed edited ^{1}H-MRS at 3 T for measuring GSH levels in the motor cortex, which were recently reported to be lower in ALS versus controls [98]. Finally, we examined the relationships between brain metabolite levels and measures of clinical status, including ALS Functional Rating Scale-Revised (ALSFRS-R) scores, upper motor neuron (UMN) burden scores, and El Escorial diagnostic criteria.

4.3 Methods

Study Participants and Design

A total of 38 volunteers (20 individuals with ALS and 18 healthy controls, matched by age-range and sex-ratio) were enrolled in the study after giving written informed consent using procedures approved by the Institutional Review Board: Human Subjects Committee of the University of Minnesota. All volunteers with ALS were recruited from the ALS Association Certified Treatment Centers of Excellence at the University of Minnesota and Hennepin County Medical Center and fulfilled the revised El Escorial Criteria [163] for clinically possible (N = 8), probable (N = 8), or definite (N = 4) ALS. Two volunteers were withdrawn from the study after enrollment: 1 control volunteer with evidence of neurologic disease and 1 individual with ALS who was unable to undergo scanning due to claustrophobia.

Participants underwent both 3 and 7 T MR scanning no more than one week apart and a neuromuscular examination by a board-certified neurologist on the day of the 3 T scan (19 subjects with ALS, 17 healthy controls total). At 7 T, MR spectra were acquired from two VOIs: primary motor cortex and pons. At 3 T, spectra were acquired from the primary motor cortex only. In subjects with ALS, the motor cortex VOI was selected in the hemisphere contralateral to the more clinically affected side of the body. In controls, the hemispheres were chosen so that the cohorts would have similar proportions of left- and right-sided scans. The neuromuscular exam was used to determine the clinical characteristics of subjects with ALS, including the more affected side of the body, the El Escorial diagnosis, and a score on a novel upper motor neuron (UMN) burden scale. Active riluzole use at the time of the exam was also recorded in order to account for the drug's potential effect on metabolite concentrations [88]. Disease duration and site of onset were obtained from patient medical records. Disease duration was calculated as the time from the first symptom occurrence to the date of the MR exam. The UMN burden score was based on neurologic exam signs and was used to measure the extent of UMN involvement in subjects with ALS. This score was generated by assigning point values of "1" to the presence of upper motor neuron signs in the cranial, cervical, and lumbosacral cord segments. Specifically, six signs were used in the rating: 1) pathologic jaw jerk, 2)

slow tongue coordination, 3) abnormal upper limb reflexes (increased biceps reflex, triceps reflex, brachioradialis reflex, and/or finger flexors), 4) upper limb spasticity, 5) abnormal lower limb reflexes (increased patellar reflex, Achilles reflex, and/or extensor plantar response), 6) lower limb spasticity. Summing the points resulted in a total scale ranging from 0 to 6 (a higher score indicating greater UMN burden). All subjects with ALS were also evaluated with the ALS Functional Rating Scale-Revised (ALSFRS-R) as a measure of global disease severity [39]. The ALSFRS-R consists of 12 physical function queries that address bulbar, respiratory, gross motor, and fine motor domains. It yields a composite score ranging from 0 (most severe) to 48 (no disability). Participant characteristics are summarized in Table 4.1.

*Unpublished methods: Other clinical rating systems were also used to generate scores of UMN and LMN burden. First, UMN scores for the upper limbs were determined using a modified version of the established Penn scale [164]. Second, a novel system developed by the Clinical Research in ALS and Related Disorders for Therapeutic Development (CReATe) Consortium was used to quantify UMN and LMN burden in the right/left upper limb, lower limb, and cranial regions. Scoring components for each system are provided in the Appendix.

Data Acquisition

Proton MRS studies were performed on a 7 T whole body Siemens MAGNETOM scanner and a 3 T whole body Siemens Tim Trio scanner (Siemens Medical Solutions, Erlangen, Germany). At 7 T, a 16-channel transceiver array coil [140] allowed B_1^+ shimming as described previously [133]. T_1-weighted MPRAGE images were acquired to position the VOI for MRS using the following parameters: repetition time (TR) = 2500 ms, echo time (TE) = 2.4 ms, flip angle = 5°, slice thickness = 1 mm, number of slices = 176, field of view = 232 x 256 mm^2, and matrix size = 232 x 256. VOI placement was based on anatomical landmarks. For the primary motor cortex, a 2.2 x 2.2 x 2.2 cm^3 voxel was placed in the area representing the upper limb and aligned parallel to the dura mater in the coronal orientation in order to maximize inclusion of the cortical surface (Figure 4.2). The upper limb portion of the motor homunculus was specifically selected because a

large majority of subjects with ALS were predicted to have some degree of upper limb involvement during the time of scanning. For the pons, a 1.6 x 1.6 x 1.6 cm^3 voxel was aligned parallel to the pontomedullary junction in the sagittal orientation to maximize inclusion of pons tissue (Figure 4.1). This voxel included both LMN and UMN structures that undergo pathological changes in ALS.

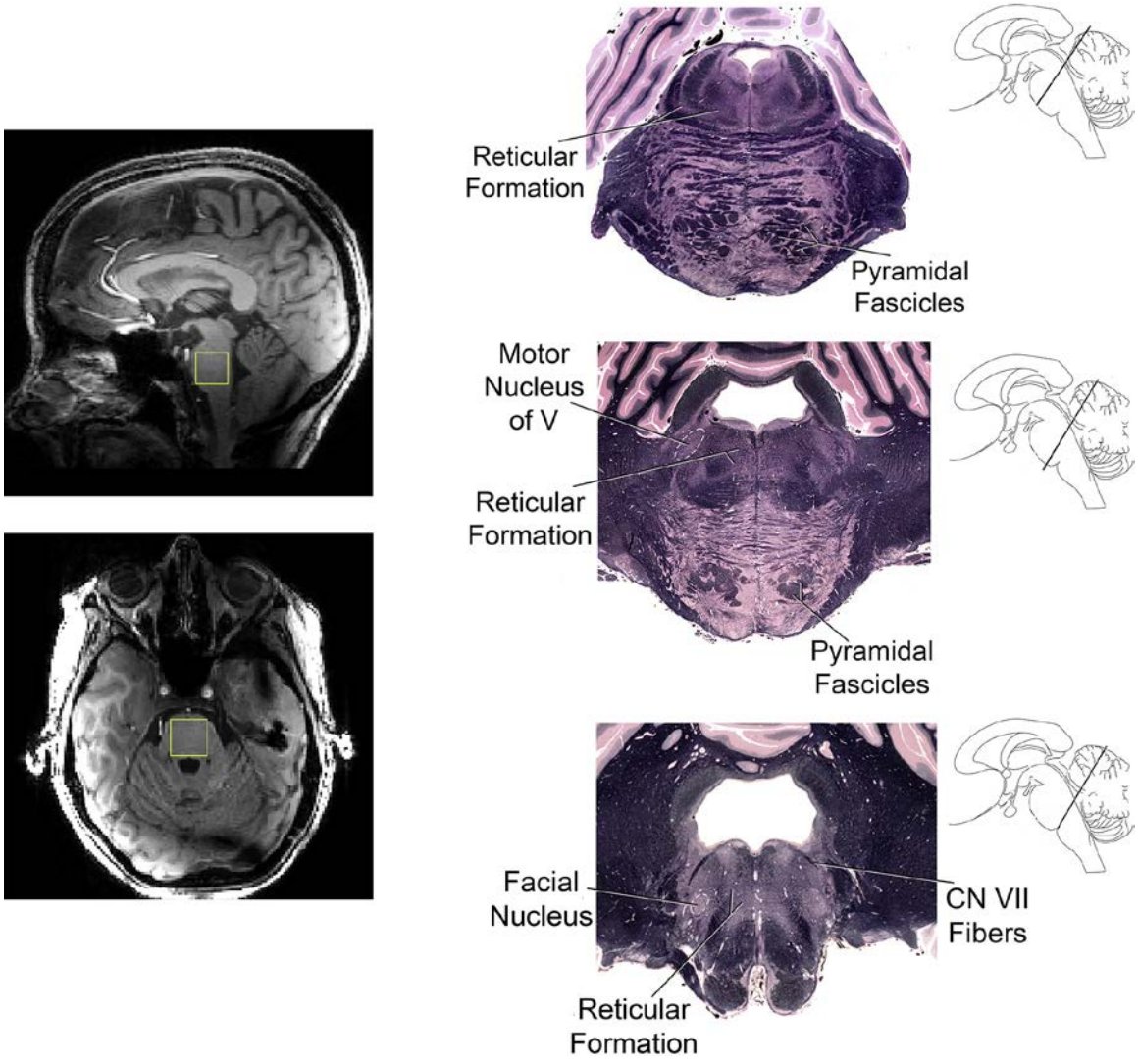

Figure 4.1 Diagram illustrating ALS-relevant neuroanatomic structures within the pons voxel. Left: Pons voxel placement in sagittal and axial views. Right: Contained structures that show degenerative changes in ALS are labeled and include the pontine pyramidal fascicles, cranial motor nuclei and efferent fibers, and the reticular formation (see Section 1.3.1 Neuropathology). Note that cranial nerve VII fibers also wrap medially around the abducens nucleus (not labelled). Photos of histological brainstem slices are reused with permission from the University of Minnesota Medical School Neuroanatomy Course.

After B_1^+ shimming and VOI selection, first- and second-order B_0 shims were adjusted in the VOI using FASTMAP (a fast, automatic shimming technique by mapping along projections) with an echo planar imaging readout [141]. Then, B_1 levels required for localization and water suppression were adjusted, as described previously [116]. Metabolite and water reference spectra were acquired using a modified semi-LASER sequence [115] (TR = 5 s, TE = 26 ms, 64 averages). In addition, fully relaxed unsuppressed water signals were acquired at TEs ranging from 28 to 4000 ms (TR = 15 s) to estimate the cerebrospinal fluid (CSF) contribution to the VOI [142].

At 3 T, radiofrequency transmission was performed with the built-in body coil, and signal was received with a 32-channel receive-only head coil. T_1-weighted MPRAGE images were obtained for VOI positioning (TR = 2.6 s, TE = 2.43 ms, flip angle = 7°, slice thickness = 1 mm, number of slices = 224, field of view = 256 x 256 mm^2, and matrix size = 256 x 256). Spectra were acquired from a 3.5 x 2.5 x 2.3 cm^3 VOI placed in the motor cortex using the MEGA-PRESS sequence [165, 166] (TR = 2 s, TE = 68 ms, 512 averages) with editing pulse (180° Shinnar-Le Roux; duration, 22.7 ms; bandwidth, 52 Hz) applied at 4.56 ppm and 7.5 ppm. The larger VOI relative to that selected at 7 T included areas of the motor cortex corresponding to the face and lips, in addition to upper limb (Figure 4.4).

Data Post-processing and Quality Control

For 7 T data, single-shot metabolite spectra were corrected for frequency and phase fluctuations as well as residual eddy currents before summing [167]. Summed spectra were then visually inspected for the presence of unwanted coherences. Signal-to-noise ratio (SNR) measurements were made on the raw spectra by taking the ratio of the NAA methyl resonance at 2.02 ppm and root mean square of the noise measured from -4 to -2 ppm. Linewidth was measured as the full-width at half-maximum of the unsuppressed water reference spectrum. Spectra were excluded from further analysis if SNR < 25. Based on this criterion, three spectra from the pons were excluded.

For 3 T data, edit-off and edit-on spectra were corrected for phase and frequency fluctuations before subtracting to generate difference spectra. Edit-off and edit-on spectra were visually inspected for unwanted coherences. Difference spectra were also inspected for small frequency shifts between edit-off and edit-on spectra.

Metabolite Quantification

Summed 7 T spectra were analyzed with LCModel (version 6.3-0G) [55]. The basis set for LCModel contained 19 metabolites that were simulated using a density matrix approach [143] based on previously reported chemical shifts and coupling constants [67, 168]: alanine (Ala), aspartate (Asp), ascorbate (Asc), glycerophosphocholine (GPC), phosphocholine (PCho), creatine (Cr), phosphocreatine (PCr), γ-aminobutyric acid (GABA), glucose (Glc), glutamine (Gln), glutamate (Glu), glutathione (GSH), *myo*-inositol (mIns), lactate (Lac), *N*-acetylaspartate (NAA), *N*-acetylaspartylglutamate (NAAG), phosphoethanolamine (PE), *scyllo*-inositol (sIns), and taurine (Tau). The basis set also included a macromolecule spectrum that was measured previously using an inversion recovery technique in 5 healthy subjects (TR = 2 s, inversion time = 685 ms, 640 averages total, occipital cortex) [56, 83]. Absolute metabolite concentrations were determined by utilizing the unsuppressed water spectrum as an internal reference and correcting for tissue water and CSF content [116]. A tissue water content of 82% was assumed for the motor cortex and pons [146]. The T_2 relaxation of tissue water was taken into account in the LCModel fitting by assuming values of 68 ms for the motor cortex and 74 ms for the pons. These assumptions were determined by acquiring a series of unsuppressed water signals at different echo times (TE = 28-4000 ms, TR = 15 s) in the respective VOI in ten healthy control subjects and fitting their integrals with a biexponential function. For the biexponential fit, the T_2 of CSF was fixed at 565 ms, which was measured using the same sequence in the lateral ventricles of four healthy subjects (TE = 28-4000 ms, TR = 15 s, VOI = 0.125-0.360 mL). The measured free precession T_2 values of tissue water in the motor cortex (45.4 ± 2.5 ms) and pons (48.9 ± 0.9 ms) were multiplied by a factor of 1.5 assuming Carr-Purcell conditions [167]. The % CSF contribution to each VOI was also obtained by fitting the integrals of the

unsuppressed water spectra acquired in each VOI at different TE values with a biexponential decay function [142].

The 3 T MEGA-PRESS edit-off and difference spectra were analyzed with LCModel (version 6.3-1J) using a protocol nearly identical to that described above. However, NAA was separated into singlet and multiplet, and tCr was separated into CH_3 and CH_2 groups. The difference spectra were analyzed with the basis set that contained simulated information for NAA and GSH using previously described fitting parameters [154]. For edit-off data, absolute metabolite concentrations were obtained by utilizing an unsuppressed water reference spectrum and correcting for tissue water and CSF content. The CSF content was determined by segmenting the MPRAGE images using the SPM8 software package and then applying iterative threshold selection to obtain within-VOI fractions of gray matter, white matter, and CSF, as described previously [112]. A tissue water content of 82% was assumed and the T_1 of tissue water of 1.08 s and T_2 of 95 ms were used [169, 170].

For each region, only metabolites quantified with mean Cramér-Rao Lower Bounds (CRLB) ≤ 20% were selected for analysis. In addition, metabolites were reported only as sums if they correlated strongly with each other ($r < -0.7$), as in the cases of total creatine (tCr; Cr+PCr) and total choline (tCho; GPC+PCho). Additionally, total NAA (tNAA; NAA+NAAG) and metabolite ratios (i.e., mIns/tCr, tNAA/tCr, NAA/mIns, tNAA/mIns) were reported in order to compare with prior work performed at lower field. The sums Glc+Tau and Glu+Gln (Glx) were also reported if any metabolite within each pair did not meet mean CRLB ≤ 20% criterion. Lac at 7 T was not quantified in the motor cortex of 6 subjects with ALS and 5 healthy controls due to the presence of unwanted coherences near 1.3 ppm.

Statistical Analysis

Except for left/right hemisphere and male/female scan counts, all measures were compared between the two cohorts using unpaired, two-tailed Student's t-tests. Group comparisons of the count data were made using Fisher's exact tests. Neurochemical levels were compared between the cohorts using t-tests and then two-way ANOVA to

adjust for hemisphere scanned (motor cortex data only). Age and sex were not included as covariates in the models because they were similar between the ALS and control groups. The neurochemical levels were also compared pairwise across El Escorial diagnostic subgroups and controls using one-tailed t-tests (with the direction pre-specified according to disease severity in the diagnostic subgroups); a step-down Bonferroni procedure was used to correct type I error for multiple comparisons [171]. Comparisons in tNAA levels assumed that Definite ALS < Probable ALS < Possible ALS < Controls because these levels were expected, based on literature, to become lower as more disease signs appear [93, 103]. Conversely, mIns levels were expected to be higher in disease and comparisons assumed that Definite ALS > Probable ALS > Possible ALS > Controls [86, 91]. For Glu level comparisons, two-tailed t-tests were performed between subgroups and controls because there was no obvious expectation that Glu levels are altered in one direction as opposed to the other. Neurochemical levels were also compared across riluzole-treatment subgroups using pairwise two-tailed *t*-tests between riluzole-users, riluzole-non-users, and control groups, while again applying the step-down Bonferroni correction. Pearson's correlation tests were used to examine possible linear relationships between neurochemical levels and clinical status measures.

*Unpublished methods: Diagnostic sensitivity and specificity were assessed for metabolites that demonstrated the most significant differences between patients and controls. The 'ROCR' package in R (version 3.4.2) was used to generate receiver-operator characteristic (ROC) curves and to estimate area-under-the-curve (AUC). Sensitivity and specificity at the optimal cut-off were calculated from logistic regression model predictions of success (disease) and failure (no disease).

As a supplement to the El Escorial diagnostic subgroup analysis, metabolite levels were compared across King's disease stages, which were estimated from ALSFRS-R scores using an algorithm described previously [43]. King's stages 1 and 2 were considered "early" stages, while stages 3 and 4 were considered "advanced". Corrections for multiple comparisons were applied (same as above).

4.4 Results

Cohort characteristics

Motor cortex ^{1}H-MRS data were obtained at both 3 T and 7 T for all 19 subjects with ALS and 17 controls. Five subjects were unable to complete the exam's second half, which was allotted for pons data acquisition. For two of these subjects, pons data were acquired successfully at 6-month follow-up visits and were used in the analysis. Three subjects also had larger heads that resulted in increased coil loading. For these subjects, pons spectra were acquired with subadiabatic RF transmit power and were excluded due to low SNR. Thus, data from a total of 15 subjects with ALS and 15 controls were used in the pons ^{1}H-MRS analysis.

The ALS and control cohorts were matched on average for age and sex for both regions examined (Table 4.1). For motor cortex data, the cohorts were also approximately matched for brain hemisphere scanned. In the ALS cohort, 4 out of 19 subjects had bulbar-onset ALS, and of these, only one did not exhibit signs of upper limb involvement during the time of scanning. Compared to most prior studies [88, 91, 172], our ALS cohort had a higher mean ALSFRS-R score, indicating that the subjects as a group had milder disease. Scores on the UMN burden scale also indicated that they had mild upper motor neuron involvement on average. Lastly, seven subjects within the scanning cohort were classified by El Escorial criteria as having possible ALS. Subjects within this particular subgroup had the fewest disease signs, and their ALSFRS-R scores were significantly higher than the subjects with probable or definite ALS (Table 4.3). Notably, the subjects with probable and definite ALS also had mean ALSFRS-R scores higher than those commonly reported in literature.

Spectral quality in subjects with ALS and controls

High-SNR metabolite spectra were obtained at 7 T from the motor cortex and pons of subjects with ALS and healthy controls (Figure 4.2). No differences in spectral quality were apparent between the groups, while differences were observed between the two regions as expected. Pons spectra had lower SNR and broader linewidths than motor

cortex spectra (Table 4.1). The spectral patterns were also distinct between the regions and noted to be characteristic of the motor cortex and pons. Similarly, comparable spectral quality was obtained in ALS and control groups at 3 T.

Table 4.1 Clinical and ^{1}H-MRS characteristics by group and brain region examined

	Motor Cortex			Pons		
Clinical parameters	ALS (N = 19)	Controls (N = 17)	*P*-values	ALS (N = 15)	Controls (N = 15)	*P*-values
Sex ratio, male:female	10:9	10:7	0.75*	8:7	8:7	1*
Age, years	57 ± 9 [31-74]	57 ± 9 [30-69]	1	56 ± 10 [31-70]	56 ± 9 [30-69]	0.92
Brain hemisphere scanned, left:right	8:11	8:9	1*	N/A	N/A	
Disease duration, months	40.2 ± 43.0 [3.5-147.8]	N/A		37.0 ± 40.2 [3.5-147.8]	N/A	
Site of onset, limb:bulbar	15:4	N/A		12:3	N/A	
El Escorial Diagnosis (no. of patients)	Possible (7) Probable (8) Definite (4)	N/A		Possible (6) Probable (7) Definite (2)	N/A	
King's Disease Stage (no.of patients)	Stage 1 (6) Stage 2 (6) Stage 3 (6) Stage 4 (1)	N/A		Stage 1 (6) Stage 2 (5) Stage 3 (3) Stage 4 (1)	N/A	
Current riluzole use, yes:no	8:11	N/A		6:9	N/A	
ALSFRS-R score	39.8 ± 5.6 [26-45]	48 ± 0	<0.001	40.6 ± 5.2 [26-45]	48 ± 0	<0.001
UMN score	2.5 ± 1.3 [1-6]	N/A		2.3 ± 1.1 [1-5]	N/A	
7 T MRS quality parameters						
Signal-to-noise ratio	205 ± 37	201 ± 35	0.72	45 ± 9	53 ± 17	0.11
Water linewidth, Hz	10 ± 2	11 ± 2	0.53	16 ± 2	15 ± 2	0.15
% CSF	11.3 ± 5.3	10.2 ± 3.9	0.55	0.9 ± 0.3	1.1 ± 0.3	0.26

Data are given as mean ± SD or counts. *denotes *p*-values that are from Fisher's exact tests. Other *p*-values are from unpaired, two-tailed *t*-tests.

The CSF content within the motor cortex and pons VOIs was not significantly different between subjects with ALS and controls; therefore there was no indication of atrophy in these regions due to disease. In the motor cortex at 7 T, eleven metabolites had mean CRLB ≤ 20%: Gln, Glu, GSH, Lac, mIns, NAA, NAAG, tCho, tCr, tNAA, and Glc+Tau. Notably, the major metabolites (tNAA, tCho, tCr, mIns) as well as Glu, Gln, and GSH were each quantified with mean CRLB less than 10%, consistent with prior findings at 7 T using semi-LASER [116]. In the pons, the CRLB criteria were fulfilled by the same metabolites as above, with the exception of GSH and Gln; the sum Glx (Glu+Gln) was therefore reported. Asc measurements in the pons also passed the mean CRLB ≤ 20% criterion.

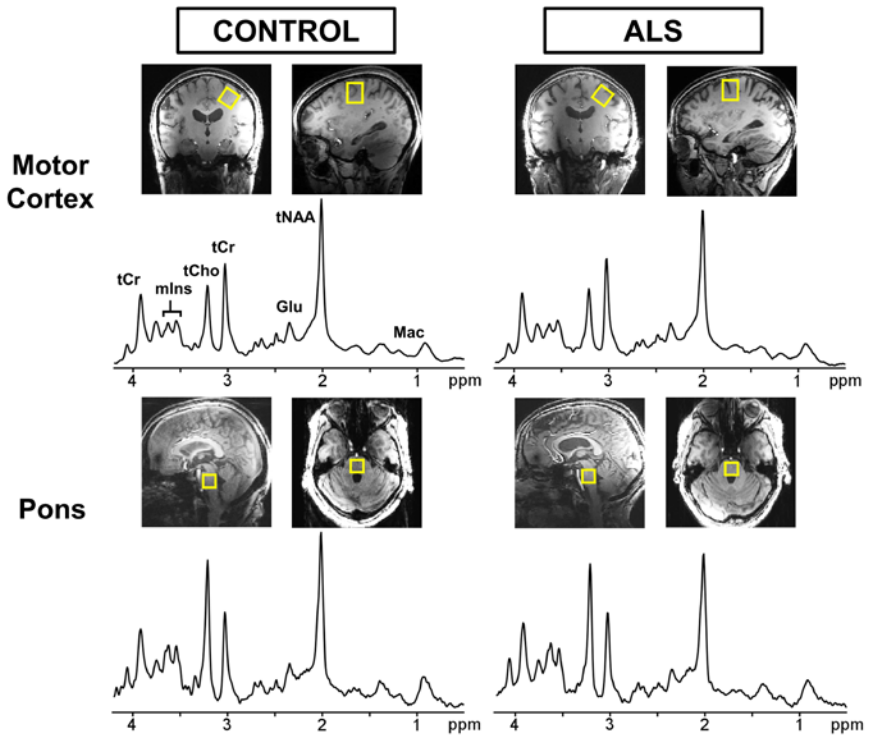

Figure 4.2 Localized proton spectra obtained from the motor cortex (top) and pons (bottom) at 7 T using semi-LASER (TE = 26 ms, TR = 5 s, 64 averages). A 2.2 x 2.2 x 2.2 cm^3 voxel (shown on T_1-weighted images) was selected in the motor cortex and angulated parallel to the slope of the dural surface in the coronal orientation. A 1.6 x 1.6 x 1.6 cm^3 voxel was selected to cover nearly the entire pons region. The spectra are shown with 1-Hz exponential and 5-Hz Gaussian weighting. Left: healthy control (68 year-old female); right: subject with ALS (64 year-old female)

Neurochemical alterations in ALS

Metabolite concentrations from the motor cortex and pons of subjects with ALS and controls were quantified at 7 T (Figure 4.3, Table 4.2). In the motor cortex, the greatest group differences were seen in the levels of mIns. Subjects with ALS had significantly higher mIns levels and mIns/tCr ratio than controls (both $p < 0.01$). In addition, participants with ALS had significantly lower NAA/mIns and tNAA/mIns ratios than controls (both $p < 0.01$). In the pons, subjects with ALS had significantly lower NAAG and tNAA/mIns ratio compared to controls ($p < 0.01$ and $p = 0.04$, respectively). Analysis of the edit-off data acquired at 3 T from the larger motor cortex VOI (Figure 4.4) produced similar findings; significantly lower NAA/mIns and tNAA/mIns ratios (both $p < 0.01$) were observed in subjects with ALS versus controls. No differences in

GSH levels were observed between the ALS and healthy control cohorts using either non-edited ^{1}H-MRS at 7 T or edited ^{1}H-MRS at 3 T.

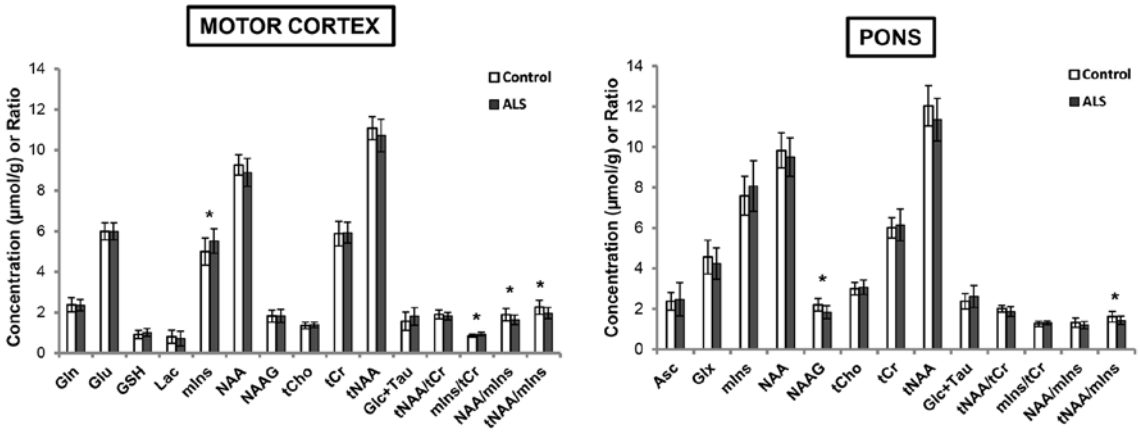

Figure 4.3 Neurochemical profiles of healthy controls and subjects with ALS obtained at 7 T (shown as mean concentration and standard deviation bars). Only neurochemicals that were quantified with mean CRLB ≤ 20% are plotted. Motor cortex: ALS (N = 19), controls (N = 17). Pons: ALS (N = 15), controls (N = 15). Asc, ascorbate; Glc+Tau, glucose+taurine; Gln, glutamine; Glu, glutamate; Glx, glutamate+glutamine; GSH, glutathione; Lac, lactate; mIns, *myo*-inositol; NAA, *N*-acetylaspartate; NAAG, *N*-acetylaspartylglutamate; tCho, phosphocholine+glycerophosphocholine; tCr, creatine+phosphocreatine; tNAA, *N*-acetylaspartate+*N*-acetylaspartylglutamate.
*p < 0.05 from ANOVAs adjusting for brain hemisphere scanned

Table 4.2 Metabolite concentrations (µmol/g) and ratios in subjects with ALS and controls

	Motor Cortex			Pons		
Metabolites	ALS (N = 19)	Controls (N = 17)	*P*-values	ALS (N = 15)	Controls (N = 15)	*P*-values
Gln	2.36 ± 0.29	2.38 ± 0.35	0.86	-	-	-
Glu	5.99 ± 0.42	5.99 ± 0.41	0.99	-	-	-
GSH	1.01 ± 0.19	0.91 ± 0.20	0.14	-	-	-
Lac	0.71 ± 0.36	0.79 ± 0.33	0.57	-	-	-
mIns	5.51 ± 0.60	5.00 ± 0.67	0.01	8.07 ± 1.25	7.59 ± 0.96	0.25
NAA	8.90 ± 0.69	9.27 ± 0.50	0.08	9.51 ± 0.95	9.83 ± 0.87	0.35
NAAG	1.82 ± 0.32	1.81 ± 0.29	0.94	1.84 ± 0.32	2.20 ± 0.31	<0.01
tCho	1.39 ± 0.13	1.35 ± 0.16	0.50	3.07 ± 0.36	2.99 ± 0.31	0.51
tCr	5.93 ± 0.51	5.88 ± 0.60	0.76	6.15 ± 0.78	6.01 ± 0.50	0.58
tNAA	10.72 ± 0.79	11.08 ± 0.57	0.13	11.35 ± 1.05	12.03 ± 1.00	0.07
Glx	-	-	-	4.24 ± 0.76	4.56 ± 0.84	0.28
Glc+Tau	1.80 ± 0.44	1.57 ± 0.46	0.13	2.61 ± 0.54	2.37 ± 0.39	0.18
Metabolite Ratio						
tNAA/tCr	1.82 ± 0.18	1.90 ± 0.21	0.13	1.87 ± 0.26	2.01 ± 0.17	0.06
mIns/tCr	0.93 ± 0.09	0.85 ± 0.08	0.01	1.29 ± 0.06	1.26 ± 0.12	0.22
NAA/mIns	1.63 ± 0.23	1.89 ± 0.29	<0.01	1.20 ± 0.18	1.32 ± 0.23	0.12
tNAA/mIns	1.97 ± 0.27	2.26 ± 0.35	<0.01	1.45 ± 0.20	1.61 ± 0.26	0.04
GSH/tCr	0.17 ± 0.03	0.15 ± 0.02	0.10	-	-	-

Data are given as mean ± SD. *P*-values are from ANOVAs adjusting for hemisphere scanned. Note: Glx was not reported in the motor cortex since Gln and Glu were each quantified with mean CRLB ≤ 20%. Gln, Glu, and GSH in the pons did not meet this criterion.

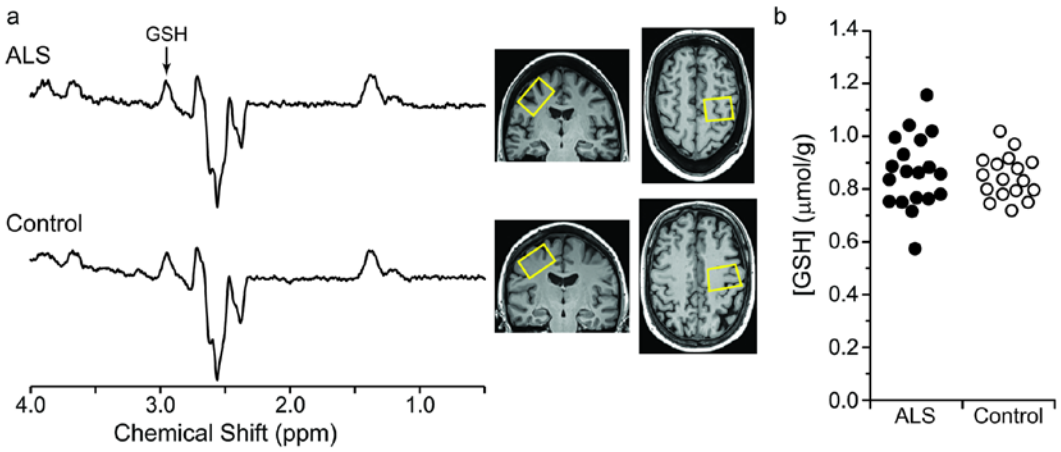

Figure 4.4 GSH-edited spectra and GSH concentrations from the motor cortex of subjects with ALS and healthy controls using MEGA-PRESS at 3 T (TE = 68 ms, TR = 2 s, 512 averages). (a) Representative difference spectra acquired in a subject with ALS (top) and healthy control (bottom). Motor cortex voxel placement (3.5 x 2.5 x 2.3 cm^3) is shown on T_1-weighted images. Spectra are shown with 1-Hz exponential line broadening and with vertical scale adjusted using NAA resonance. (b) GSH concentrations quantified using LCModel in subjects with ALS and controls; $p = 0.6$ from ANOVA adjusting for brain hemisphere scanned

In order to investigate whether neurochemical levels were different for different diagnostic categories, the ALS cohort was separated into El Escorial diagnostic classifications (Figure 4.5A, Table 4.3). Total NAA levels in the motor cortex were the lowest in subjects with definite ALS and were significantly different in these subjects compared to those with possible ALS ($p = 0.04$) and healthy controls ($p = 0.04$). *Myo*-inositol levels in the motor cortex were significantly higher in subjects with probable ALS than in controls ($p = 0.02$). Finally, Glu levels in subjects with either probable or definite ALS were significantly lower compared to those with possible ALS (both $p = 0.01$). In addition, since most prior ^{1}H-MRS studies only enrolled subjects with definite and probable ALS and reported their results from whole cohort comparisons versus controls, we also pooled these two subgroups ($N = 12$; ALSFRS-R mean ± SD = 37.3 ± 5.7) and compared their neurochemical levels to those of subjects with possible ALS (ALSFRS-R mean ± SD = 44.1 ± 0.7) and healthy controls. In the motor cortex, combined probable/definite ALS had lower tNAA than possible ALS and controls (both $p = 0.03$), higher mIns than controls ($p < 0.01$), and lower Glu than possible ALS ($p < 0.01$).

The analysis of King's disease stage subgroups revealed neurochemical differences similar to those observed between El Escorial diagnostic categories. Compared to the other groups, the advanced-stage patients (Stages 3 or 4) had significantly higher mIns levels and lower tNAA and Glu levels (Figure 4.5B).

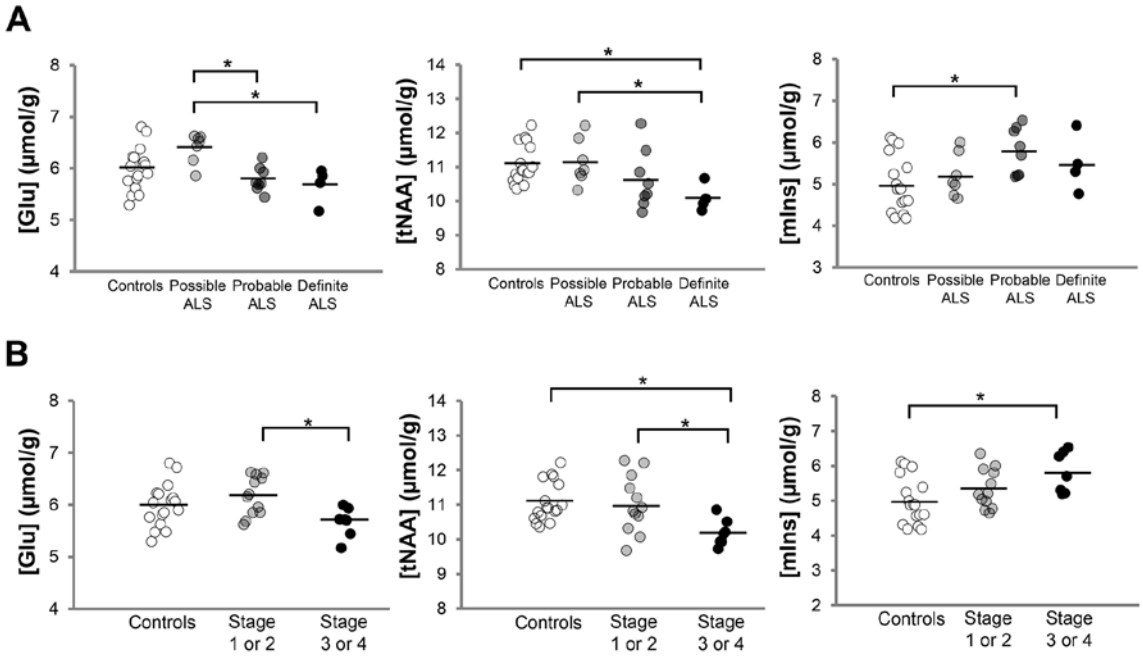

Figure 4.5 Motor cortex NAA, mIns, and Glu levels differ between healthy controls and ALS subgroups classified by El Escorial diagnostic criteria (A) and King's disease staging (B). Controls (N = 17); ALS diagnostic subgroups: definite (N = 4), probable (N = 8), possible (N = 7). King's staging subgroups: Stages 3 or 4 = "Advanced" (N = 7), Stages 1 or 2 = "Early" (N = 12). For tNAA and mIns comparisons, one-tailed Student's t-tests were performed because the expected group differences are unidirectional. For the Glu comparison, two-tailed t-tests were performed as no such assumption was made. *indicates $p < 0.05$ corrected for multiple comparisons.

Table 4.3 Motor cortex metabolite concentrations (µmol/g) in El Escorial subgroups

	ALS			
	Definite (N = 4)	Probable (N = 8)	Possible (N = 7)	Controls (N = 17)
Glu	5.68 ± 0.35[5]	5.79 ± 0.24[4]	6.40 ± 0.29	5.99 ± 0.41
mIns	5.49 ± 0.68	5.80 ± 0.56[2]	5.20 ± 0.52	5.00 ± 0.67
tNAA	10.10 ± 0.41[3,5]	10.64 ± 0.87	11.16 ± 0.66	11.08 ± 0.57
tNAA/mIns	1.86 ± 0.24	1.85 ± 0.26[2]	2.16 ± 0.22	2.26 ± 0.35
ALSFRS-R	39.8 ± 2.2[5]	36.1 ± 6.6[4]	44.1 ± 0.7	N/A

Data are given as mean ± SD. Numeric superscripts denote $p < 0.05$ (Type 1 error corrected) from unpaired Student's t-tests: [1]Possible vs. Controls; [2]Probable vs. Controls; [3]Definite vs. Controls; [4]Probable vs. Possible; [5]Definite vs. Possible; [6]Definite vs. Probable

Unlike their dependence on El Escorial classification, neurochemical levels did not vary in relation to the severity of UMN dysfunction. Subjects with ALS were separated into subgroups consisting of those with higher burden (UMN score ≥ 3) and those with lower burden (UMN score < 3); no differences in the levels of metabolites were observed between these subgroups.

We also investigated the potential effects of riluzole treatment on neurochemical levels (Table 4.4). In the motor cortex, no significant metabolite differences were observed between 8 subjects with ALS who were using riluzole at the time of MR scanning and 11 subjects who were not. When compared with healthy controls, riluzole-non-users had lower tNAA/mIns ($p = 0.04$). In the pons, no significant differences were observed among riluzole-users, riluzole-non-users, and healthy controls.

Table 4.4 Metabolite concentrations (μmol/g) in riluzole-users and -non-users with ALS

	Motor Cortex			**Pons**		
	ALS			ALS		
Metabolites	Riluzole-users (N = 8)	Riluzole-non-users (N = 11)	Controls (N = 17)	Riluzole-users (N = 6)	Riluzole-non-users (N = 9)	Controls (N = 15)
Gln	2.22 ± 0.30	2.37 ± 0.22	2.38 ± 0.35	-	-	-
Glu	6.02 ± 0.44	5.86 ± 0.36	5.99 ± 0.41	-	-	-
GSH	1.05 ± 0.24	0.98 ± 0.17	0.91 ± 0.20	-	-	-
mIns	5.52 ± 0.79	5.43 ± 0.51	5.00 ± 0.67	8.13 ± 1.55	8.04 ± 1.10	7.59 ± 0.96
tCho	1.39 ± 0.14	1.37 ± 0.14	1.35 ± 0.16	3.13 ± 0.47	3.03 ± 0.29	2.99 ± 0.31
tCr	5.70 ± 0.53	6.03 ± 0.51	5.88 ± 0.60	6.02 ± 0.84	6.23 ± 0.77	6.01 ± 0.50
tNAA	10.88 ± 0.97	10.44 ± 0.52	11.08 ± 0.57	10.81 ± 0.76	11.71 ± 1.10	12.03 ± 1.00
Glx	-	-	-	4.00 ± 0.69	4.40 ± 0.81	4.56 ± 0.84
Glc+Tau	1.69 ± 0.50	1.87 ± 0.43	1.57 ± 0.46	2.38 ± 0.55	2.77 ± 0.51	2.37 ± 0.39
Metabolite Ratio						
tNAA/tCr	1.92 ± 0.22	1.74 ± 0.11	1.90 ± 0.21	1.81 ± 0.15	1.90 ± 0.29	2.01 ± 0.17
mIns/tCr	0.97 ± 0.12	0.90 ± 0.07	0.85 ± 0.08	1.34 ± 0.11	1.29 ± 0.08	1.26 ± 0.12
tNAA/mIns	2.02 ± 0.42	1.93 ± 0.16*****	2.26 ± 0.35	1.36 ± 0.17	1.48 ± 0.22	1.61 ± 0.26
ALSFRS-R	41.9 ± 3.2	38.4 ± 6.6	-	42.7 ± 2.9	39.2 ± 6.0	-

Data are given as mean ± SD. *****$p < 0.05$ (Type 1 error corrected) from unpaired Student's t-test between riluzole-non-users and healthy controls.

Correlations with functional status

Metabolite levels and ratios in the motor cortex significantly correlated with ALSFRS-R scores, but not with disease duration or any of the UMN burden scales. Specifically,

moderate positive correlations were observed between ALSFRS-R and ratios of tNAA/tCr (r = 0.61; $p < 0.01$) and tNAA/mIns (r = 0.56; $p = 0.01$). Weaker correlations were seen between ALSFRS-R and absolute concentrations of tNAA (r = 0.46; $p = 0.05$), Glu (r = 0.48; $p = 0.04$), and mIns (r = -0.42; $p = 0.07$). Metabolite levels in the pons did not correlate with any of the clinical measures.

Significant correlations were also observed between motor cortex tNAA/mIns and CReATe LMN scores of the contralateral upper limb (Figure 4.6). Whole-limb LMN scores were moderately correlated with tNAA/mIns (r = -0.54, $p = 0.02$). However, the strength of the correlation increased when using only the strength scores of distal limb muscle groups (r = -0.63, $p < 0.01$). Unexpectedly, trends were also seen between ipsilateral upper limb LMN scores and motor cortex tNAA/mIns. Metabolite levels did not correlate with CReATe LMN scores of the bulbar or lower limb regions.

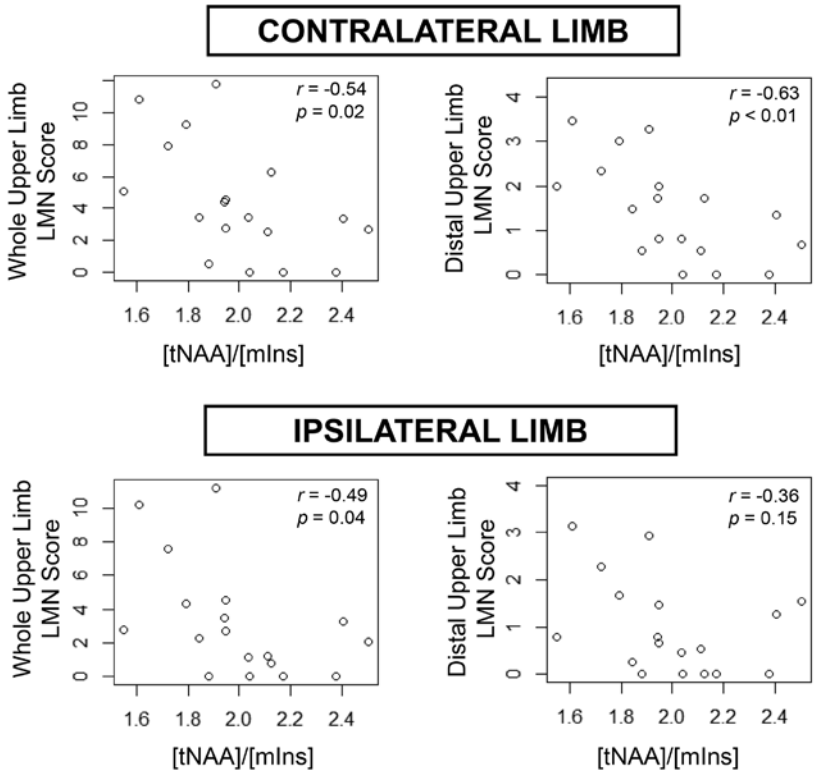

Figure 4.6 Upper limb motor cortex tNAA/mIns correlates with CReATe upper limb LMN scores in patients with ALS. The strongest correlation was observed using scores from the distal portion of the contralateral limb. *P*-values and *r* coefficients were obtained from Pearson's test of correlation.

4.5 Discussion

To date, only a limited number of studies have utilized *in vivo* ^{1}H-MRS at ultra-high field (7 T) for investigating neurochemical alterations associated with neurological diseases. These few studies have reported abnormalities in Parkinson's disease, Huntington's disease, adrenoleukodystrophy, and schizophrenia [173-177], while many other conditions have not been explored with ^{1}H-MRS at 7 T. Aside from research abstracts [172, 178], this is the first report of neurochemical alterations in ALS determined via ^{1}H-MRS at 7 T. In addition, only two other studies have reported ^{1}H-MRS data from subjects with early-stage ALS [96, 102]. Consistent with previous reports, our data at 7 T indicate that people with ALS have metabolite alterations in the motor cortex and pons (Figure 4.3). In particular, the tNAA/mIns ratio was significantly lower in these areas in affected subjects compared to healthy controls and suggests neurodegenerative changes [91, 138]. Importantly, we also observed that the levels of NAA, mIns, and Glu depend on El Escorial diagnostic categories and King's stages (Figure 4.5).

Using an optimized semi-LASER protocol at 7 T, we acquired proton spectra with high SNR and resolution from subjects with ALS and healthy controls. Relative to the motor cortex, the lower spectral quality obtained from the pons was expected and due to multiple factors, including smaller voxel size, deeper brain location, and increased intrinsic field inhomogeneities [115]. The increased sensitivity and spectral dispersion at 7 T allowed us to quantify a greater number of metabolites compared to previous ^{1}H-MRS studies of ALS at lower fields. However, a few metabolites with low abundance (i.e., GABA, Asp, PE) did not pass the mean CRLB $\leq$ 20% criterion, which was unlike recent data on the test-retest reproducibility of 7 T ^{1}H-MRS in the cerebellum and cingulate cortex [116]. Thus, the detectability of metabolites by ^{1}H-MRS depends on brain region in addition to data acquisition methodology and magnetic field strength.

This study was partly motivated by a recent report that described lower levels of GSH in the motor cortex of subjects with ALS using spectral editing at 3 T [98]. In addition to our advanced ^{1}H-MRS protocol at 7 T, we performed the previously-described protocol on the same subjects at 3 T in order to compare GSH quantitation in ALS across these two methods. The results were the same using both methods, with no differences

observed in GSH levels and significant differences observed in tNAA/mIns ratio in the motor cortex between groups. The discrepancy between our GSH findings and those of the previous study is likely not explained by differences in methodology. Both studies used similar edited ^{1}H-MRS protocols at 3 T, but in our study the size of the motor cortex VOI was larger (20.1 versus 12.5 ml) [98]. Furthermore, our smaller motor cortex VOI at 7 T (10.6 ml) also did not reveal a GSH difference between ALS and controls. Instead, differences in the characteristics of the studies' cohorts may be important. Our study had a larger sample size and a potentially earlier-stage ALS cohort. The mean ALSFRS-R score of our cohort was among the highest of all ALS cohorts studied to date using ^{1}H-MRS (ALSFRS-R mean ± SD = 39.8 ± 5.6). Notably, while the previous study reported a mean ALSFRS-R score similar to ours, it was calculated using data from only half of their cohort (N = 6). Thus, a difference between the cohorts' disease severities may explain the difference in results. Our data show that GSH levels are not different from controls in people with ALS who possess relatively high functional status. Whether these levels change as ALS progresses needs to be examined further through longitudinal investigations.

Previous studies also reported alterations in the levels of NAA and Glx in the motor cortex and pons of humans with ALS [88, 90]. The present study suggests that the levels of these metabolites are not significantly altered in these regions early in ALS. In particular, no differences in these metabolite levels were observed when comparing the entire early-stage ALS cohort with healthy controls (Figure 4.3). Rather, group differences in motor cortex NAA and Glu levels became apparent only when performing comparisons with a subgroup of individuals with greater disease burden (i.e., subjects with probable/definite ALS [ALSFRS-R mean ± SD: 37.3 ± 5.7]). This finding is remarkable in the context of previous literature, in which many studies restricted their enrollment to probable or definite ALS. These studies commonly reported lower motor cortex NAA in subjects with ALS than in controls, suggesting neuronal loss and/or dysfunction [88, 91, 103]. Notably, the few studies that did not observe alterations in NAA included (1) a study of an early-stage cohort [96] and (2) a study of

possible/suspected ALS [102]. Thus, motor cortex NAA levels appear dependent on disease stage, which likely explains differences in findings.

This is one of the first ^{1}H-MRS studies of ALS to report absolute Glu levels in the motor cortex. Due to lower sensitivity and spectral resolution, previous studies at lower field strengths only reported Glx, a sum of Glu and Gln. Multiple contradictory reports have indicated either higher or lower levels of Glx in subjects with ALS [86, 88, 90, 104], and therefore the absolute quantification of Glu is essential for determining the true direction of Glu alteration in ALS. Recently, Ratai *et al.* described lower motor cortex Glu levels in 13 subjects with ALS compared to 12 healthy controls [85]. In the present study, we analyzed a larger sample of subjects and did not observe differences in Glu levels between the cohorts. However, the El Escorial subgroup comparison suggests that motor cortex Glu levels also depend on disease stage in ALS. Lower Glu levels in subjects with probable/definite ALS than in those with possible ALS suggest glutamatergic neuron loss/dysfunction with progressing disease. This is further supported by earlier work in *post-mortem* human tissue that demonstrated neuronal loss as well as markedly lower Glu levels in the motor cortex in end-stage ALS [4, 75].

Due to its potential as a glial cell marker [68, 69], mIns has been quantified in the brain extensively using *in vivo* ^{1}H-MRS. Elevated mIns levels have been reported for several neurodegenerative diseases, including Alzheimer's disease [179], Huntington's disease [180], hereditary ataxias [181, 182], and ALS [88, 91]. In these cases, investigators interpreted the elevated levels as an indication of gliosis, a proliferative response by glial cell types to neuronal injury. In ALS, gliosis is commonly seen on post-mortem exam and includes increased numbers of reactive astrocytes and activated microglia in the motor cortex [4, 7]. Prior work in ALS using a positron emission tomography (PET) tracer that binds specifically to these cells has shown evidence of gliosis in the motor cortex *in vivo* [183-185]. This PET biomarker also positively correlates with mIns levels, according to a recent pilot investigation [186]. Consistent with these previous studies, we observed higher mIns levels in the motor cortex in subjects with ALS than in healthy controls. Importantly, this group difference was primarily driven by higher mIns levels in those with probable ALS. Similar to tNAA and Glu, mIns levels in subjects with possible ALS

were not significantly different from controls (Fig. 4). Thus, mIns levels appear to increase with progressing disease in ALS. Notably, a prior study that enrolled subjects at a similarly early disease stage (ALSFRS-R mean ± SD = 40.1 ± 4.3) reported no differences in mIns levels [96].

One of the limitations of this study is the relatively small sample sizes of each El Escorial subgroup. In particular, the pons data were acquired from fewer subjects, which may have impacted our ability to detect subgroup differences in neurochemical levels in this region. Secondly, while the El Escorial classifications provide information on disease extent according to the number of regions affected by ALS, they were designed as a tool for providing diagnostic certainty rather than an indicator of disease stage. Furthermore, the El Escorial criteria require counting both UMN and LMN clinical signs in order to determine the classification. Therefore, novel classification schemes based only on clinical signs of UMN dysfunction may be better for assessing the extent of disease within the brain. In this study, there were no associations between our novel UMN burden score and neurochemical levels in subjects with ALS. There were also no differences in neurochemical levels between those with greater burden (UMN score ≥ 3) and those with lesser burden (score < 3). Incorporating additional components into our rating scale that are recognized as highly sensitive to UMN dysfunction, such as finger- and foot-tapping speed, may provide a better means of separating disease cohorts according to the severity of UMN burden.

Notably, motor cortex tNAA ratios also showed highly significant correlations with contralateral upper limb LMN scores measured using the novel CReATe system. This new finding confirms the expected relationship between brain and body that is governed by the motor cortex's somatotopic organization. The strongest correlation was observed with distal upper limb LMN scores, which makes sense given that the motor cortex voxel was positioned specifically over the hand knob area. The finding also suggests that changes at the UMN level are not independent of changes at the LMN level, which supports the current model of disease focality and spread [35]. Interestingly, we also found that the tNAA ratios were associated to a lesser extent with ipsilateral upper limb LMN dysfunction. This is consistent with the idea that the disease spreads from the most

affected neuroanatomical areas to contiguous tissue (in this case from the contralateral anterior horn to the ipsilateral anterior horn of a cervical cord segment). Longitudinal studies that investigate how the relationship between these region-specific UMN and LMN measures evolves over time may better inform us on regional spread.

In conclusion, the data from this study suggest that differences between disease cohorts, particularly in subjects' functional status and El Escorial classification, may be responsible for the discrepancies in the literature regarding the concentrations of MRS-measured metabolites in ALS. In addition, alterations in MRS-measured metabolites, namely NAA, mIns, and Glu, are restricted to individuals with ALSFRS-R scores lower than 44. Notably, these three metabolites show weak-to-moderate correlations with ALSFRS-R scores, suggesting that their levels change with disease severity. Longitudinal studies to monitor this ALS cohort, particularly those individuals with possible ALS, will be critical for evaluating the sensitivity of these and additional metabolites to disease progression in ALS.

4.6 Chapter Summary

Consistent with prior literature [88, 91], the cross-sectional analysis of baseline data revealed that patients with ALS have metabolic alterations in the brain compared to healthy controls. Comparisons between whole cohorts showed that the differences are statistically significant for certain metabolites, but the effect size is small. The results at 3 and 7 T are also very comparable, with both methods showing (1) no differences in motor cortex GSH and (2) lower levels of motor cortex tNAA/mIns in ALS. Overall, the most interesting findings from the analysis are related to the various correlations between ^{1}H-MRS measures and clinical status.

Our results extend previous work that reported a significant correlation between motor cortex tNAA/tCr and El Escorial diagnostic category [101]. Here we observed that three motor cortex metabolites (tNAA, mIns, and Glu) correlate with diagnostic category and with King's disease stage. Like several previous studies [88, 90, 96], we also observed significant or near-significant correlations between these metabolites and total ALSFRS-

R (with motor cortex tNAA ratios showing the strongest associations). Lastly, our data revealed an expected anatomic relationship between upper limb motor cortex tNAA/mIns and contralateral upper limb LMN scores. No relationships were observed with clinical UMN burden scores, which are generally poor measures of UMN dysfunction. Importantly, the clinical correlations with disease severity and staging suggest that ^{1}H-MRS can provide sensitive biomarkers of ALS progression.

4.6.1 Potential as a Diagnostic Biomarker

The results of these cross-sectional analyses suggest that ^{1}H-MRS currently has limited diagnostic value. The El Escorial diagnostic subgroup comparison shows that metabolite levels lack sensitivity in patients with milder severity. Stratification by King's stages also confirms this, as patients at Stages 1 and 2 did not have values that were significantly different from healthy controls.

The most significant difference between patients and healthy controls was observed in motor cortex tNAA/mIns levels. However, the ROC curve analysis showed low diagnostic accuracy for this measure in distinguishing patients with possible ALS from controls (71% sensitivity, 65% specificity, and 60% AUC). The measure had greater accuracy in identifying patients with probable or definite ALS (89% sensitivity, 76% specificity, and 81% AUC), which was expected as these diagnostic classes were primarily responsible for the significant differences between the cohorts. These latter values are generally comparable to those reported by another group who studied only probable and definite ALS [91].

The low diagnostic accuracy of motor cortex tNAA/mIns is perhaps not surprising since it is not a UMN-specific measure. Reduced tNAA/mIns has been reported in different brain regions in ALS [187] and other neurodegenerative diseases [188, 189] and thus can broadly reflect dysfunction in multiple neuronal populations. The motor cortex voxel contains not only UMNs but other neuronal cell types and glia. In early-symptomatic ALS, the motor cortex may undergo selective UMN degeneration that is difficult to detect with ^{1}H-MRS. Later-stage disease may involve both UMNs and other surrounding cell types, which may boost the sensitivity of tNAA/mIns.

The search for a diagnostic marker is an important area of ALS biomarker research. Patients often go through multiple referrals before an official diagnosis is made. The diagnostic delay prevents early treatment but also makes it very difficult to study early-symptomatic ALS, which can build our understanding of how the disease propagates. In particular, to investigate the hypothesis that the disease begins focally and then spreads neuroanatomically, patients must be studied at the earliest disease stages.

Combination with other sensitive neuroimaging techniques may be able to enhance the diagnostic accuracy of ^{1}H-MRS. In one study, a multi-modal analysis of corticospinal tract DTI fractional anisotropy and motor cortex ^{1}H-MRS biomarkers resulted in improvement of DTI's ability to distinguish patients with ALS from healthy controls [190]. Studies examining whether a multi-modal approach can improve ^{1}H-MRS's diagnostic accuracy have not been performed.

5

A ^{1}H-MRS Study of ALS at 7 Tesla: Longitudinal Findings

5.1 Chapter Preface

In the previous chapter, we described the cross-sectional analysis of an early-stage cohort, which identified potential markers of disease progression. Here we focus on a longitudinal study design that evaluated neurochemical changes in this cohort over one year. The objective of this study was to assess the sensitivity of ^{1}H-MRS biomarkers to disease progression by comparing their time trends to those of established clinical measures, particularly the ALSFRS-R. In addition, we examined the heterogeneity among patients in their regional progression and its relationship to neurochemical changes in specific brain areas. Finally, the study included analyses to determine the prognostic value of ^{1}H-MRS biomarkers. Data on the prediction of survival, participant withdrawal, and clinical progression are presented.

In this chapter, the results of the longitudinal neurochemical trend analyses and the patient withdrawal prediction analysis have been submitted for publication. Other predictive analyses are included here as supplementary information to this thesis.

5.2 Introduction

Functional decline in amyotrophic lateral sclerosis (ALS) is driven by progressive upper and lower motor neuron (UMN and LMN) degeneration. However, longitudinal changes in UMN integrity are not directly assessed by clinical and electrophysiological methods. Neuroimaging may provide sensitive and objective measures of progressive motor neuron dysfunction in the brain [191].

Proton magnetic resonance spectroscopy (^{1}H-MRS) detects abnormal brain neurochemistry in ALS [84, 85, 88, 91, 157]. Reproducible findings include altered levels of motor cortex *N*-acetylaspartate (NAA; neuronal marker) [84, 88] and *myo*-inositol (mIns; putative glial marker) [88, 157] — in particular, a lower total NAA to mIns ratio (tNAA/mIns) in patients than in controls [91, 157] — as well as elevated levels of brainstem Glx (glutamate + glutamine) [88, 109].

In cross-sectional studies, tNAA/mIns and Glx levels correlate with disease severity measures, suggesting that they change longitudinally with ALS progression [85, 88, 109, 157]. However, longitudinal studies in ALS are few and have demonstrated conflicting results regarding changes in ^{1}H-MRS measures over time [93, 94, 96, 102, 103].

In this study, people with early-stage ALS and matched healthy controls were evaluated across 12 months at approximately 6-month intervals. We measured motor cortex tNAA/mIns and pons Glx levels using an optimized, ultra-high field ^{1}H-MRS technique shown to have high test-retest reproducibility [116]. Cross-sectional findings in this cohort were described in the last chapter and published [157]. Here we examined longitudinal trends and the prognostic value of ^{1}H-MRS measures alongside scores of functional impairment and UMN burden. To identify the neurochemical changes associated with regional loss of function, we stratified patients according to their rates of upper limb and bulbar functional decline.

5.3 Methods

Study Participants and Design

Patients who met revised El Escorial Criteria [163] for clinically possible, probable, or definite ALS were recruited from the ALS Association Certified Treatment Centers of Excellence at the University of Minnesota and Hennepin County Medical Center. Healthy control volunteers were recruited from the general public and selected to match the patient group on mean age and sex ratio. Twenty-two patients and 28 controls were screened using the following exclusion criteria: (1) presence of neurologic illnesses other than ALS, (2) inability to tolerate MRI scanning, and (3) failure to meet MRI safety requirements. After screening, 20 patients and 19 controls were enrolled as study participants (Figure 5.1).

Participants underwent MRI and clinical assessments at baseline (Visit 1) and returned for repeat assessments after approximately 6 and 12 months (Visits 2 and 3). Sample size was estimated from a preliminary analysis of 5 patients who completed baseline and 6-month follow-up exams and showed decline in motor cortex tNAA/mIns levels (SD = 0.2). Twenty patients scanned longitudinally gave 85% power to detect a motor cortex tNAA/mIns decline of 0.13 using paired *t*-test (α-level = 0.05).

Clinical Assessments

At Visit 1, each participant underwent a neurologic examination by a neuromuscular neurologist. A UMN burden score for each upper limb was generated using a modification of a rating system described previously [164]. The following signs were tallied for a score out of 5: pathologically brisk reflexes (biceps, triceps, and finger flexors), Hoffman's sign, and upper limb spasticity.

Functional impairment was measured at all 3 visits using the ALS Functional Rating Scale-Revised (ALSFRS-R) and its region-specific subscales [39]. The total ALSFRS-R score was used as a measure of global disability (0 most severe – 48 normal). The bulbar subscore equaled the sum of ALSFRS-R questions 1 to 3, and the upper limb subscore equaled the sum of questions 4 to 6 (0 most severe – 12 normal, for each region). Clinical

staging was abstracted from the ALSFRS-R using an algorithm developed by King's College London (Stage 1 mild – Stage 4 advanced) [43]. Cognitive and behavioral status was assessed at all visits using the Edinburgh Cognitive Behavioral ALS Screen (ECAS) [44]. Scores on the total ECAS and its ALS-specific component were recorded. Current riluzole use was documented to evaluate its potential effects on longitudinal neurochemical trends. Disease duration was calculated as the interval from the date of symptom onset to the date of the MRI exam. All clinical assessments were performed within one week of the MRI exam.

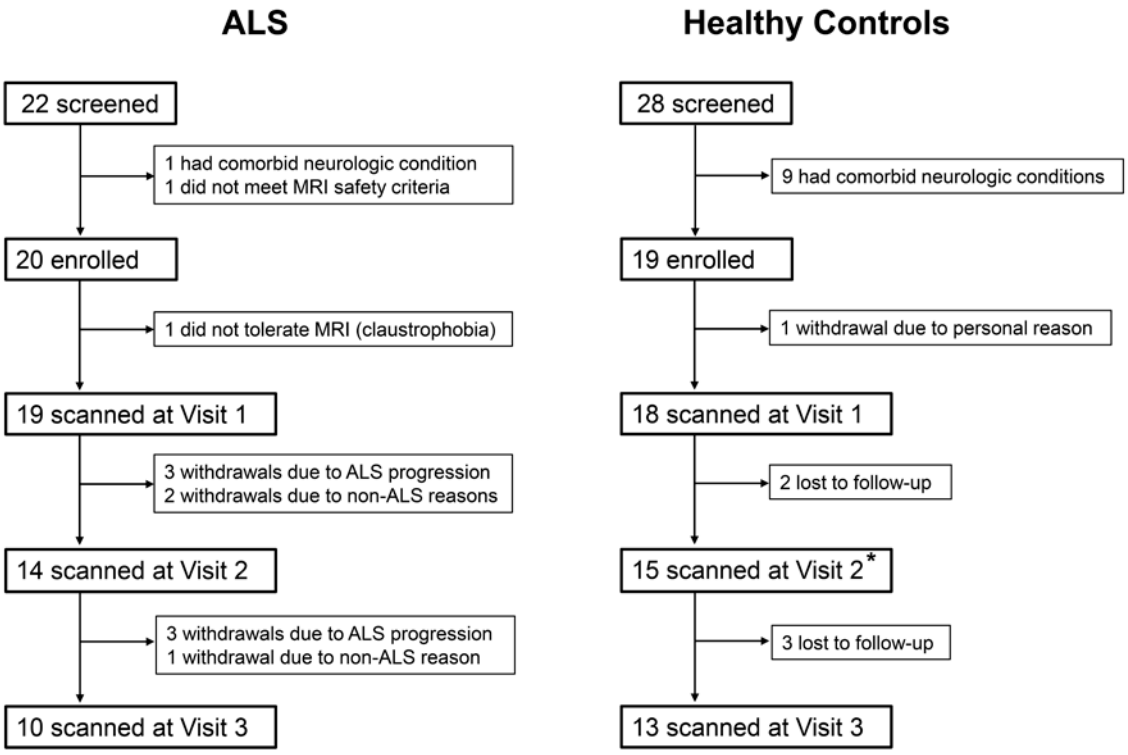

Figure 5.1 Flow diagram of study participation
Participant withdrawals were recorded as being either due to ALS progression or due to reasons unrelated to ALS. Lost to follow-up refers to participants who discontinued follow-up but did not communicate any reason for withdrawal.
*One control participant missed Visit 2 but returned for Visit 3.

^{1}H-MRS Protocol

All ^{1}H-MRS data were acquired as described in our previous report on Visit 1 results [157]. Briefly, studies were performed on a 7 tesla (T) whole body Siemens

MAGNETOM scanner using a 16-channel head transceiver array coil with B_1^+ shimming [133]. T_1-weighted MPRAGE images were acquired for ^{1}H-MRS voxel placement. Voxels were manually placed in the upper limb region of the primary motor cortex (22 x 22 x 22 mm^3) and the pons (16 x 16 x 16 mm^3). In patients, the motor cortex voxel was positioned in the hemisphere contralateral to the more clinically affected upper limb. For patients who did not have upper limb involvement at the time of Visit 1, the hemisphere was selected contralateral to the side of the body with greater overall disease involvement. In controls, hemispheres were chosen such that the ratio of left- to right-sided scans was comparable in both cohorts. The 'AutoAlign' option on the Siemens console was applied to achieve reproducible voxel placement across each participant's series of scans. Metabolite spectra were acquired from each voxel using semi-LASER localization [115] (repetition time TR = 5 s, echo time TE = 26 ms, 64 averages). Unsuppressed water reference spectra were collected for metabolite quantification. Total scan duration was approximately one hour, with the pons acquisition conducted during the second half of the session.

Spectral post-processing and quantification were performed using automated methods to eliminate observer bias. During post-processing, spectra were corrected for frequency and phase fluctuations and lineshape distortions [113]. Signal-to-noise ratio (SNR) was measured on summed metabolite spectra by dividing the height of the NAA peak at 2.01 ppm by the root mean square of the noise measured from -4 to -2 ppm. Linewidth was measured as the full-width at half-maximum of the water reference signal. To minimize bias during spectral quality assessment, an exclusion criterion of SNR < 25 was used to reject low quality spectra.

Metabolite spectra were quantified with LCModel (version 6.3-0G) [55] as described previously [157]. A basis set contained model spectra for macromolecules and 19 metabolites: alanine, aspartate, ascorbate, glycerophosphocholine, phosphocholine, creatine, phosphocreatine, γ-aminobutyric acid, glucose, glutamine (Gln), glutamate (Glu), glutathione, mIns, lactate, NAA, *N*-acetylaspartylglutamate (NAAG), phosphoethanolamine, *scyllo*-inositol, and taurine. Metabolite concentrations in tissue were determined by water scaling and adjusted for cerebrospinal fluid (CSF) within the

voxel [116]. In the motor cortex, we analyzed the total NAA (tNAA: NAA + NAAG) to mIns ratio, a potential marker and predictor of progressive neurodegeneration [91]. This measure correlated significantly with ALSFRS-R [157] and UMN burden [85] in earlier cross-sectional studies, including our published analysis of Visit 1 data. In the pons, we analyzed Glx (Glu + Gln), which also correlated with disease severity measures in cross-sectional studies [88, 109].

Measurement reliability was assessed using Cramér-Rao Lower Bounds (CRLB) estimates from LCModel. Only those metabolites quantified with mean CRLB ≤ 20% were examined longitudinally. In the pons, individual concentrations for Gln and Glu were not reported since Gln did not pass the CRLB criterion [157]. Additionally, correlated metabolites ($r < -0.5$) were analyzed only as sums (e.g., tCho [phosphocholine+glycerophosphocholine], tCr [creatine+phosphocreatine], and tNAA).

Statistical Analysis

All analyses were performed using R version 3.4.2. Comparisons of binary data (sex, hemisphere scanned, and riluzole use) were performed using Fisher's exact tests. Other measures (e.g., age, clinical scores, and spectral quality parameters) were compared between groups at each visit using Student's *t*-tests. Using all participants who completed 2 or 3 visits, linear mixed-effects models estimated time trends (linear slopes) in motor cortex tNAA/mIns, pons Glx, and clinical measures in whole cohorts and in patient subgroups. Age and sex were not included as covariates due to their similarity by design between cohorts. Mean slope estimates in patients were tested against no change over time and against mean slope estimates in controls. Patients were classified into those with stable function and those with declining function (defined as a negative slope in ALSFRS-R subscore over the observation period). Patients were also divided into riluzole users and non-users, and their mean slope estimates were compared to examine the effect of riluzole on neurochemical trends. Linear models were used to estimate each patient's individual trajectory in motor cortex tNAA/mIns, pons Glx, UMN burden scores, and ALSFRS-R scores over time. Spearman's rank test examined correlations

between the estimated slopes of the metabolites and the estimated slopes of the clinical scores.

We conducted predictive analyses on motor cortex tNAA/mIns and pons Glx levels measured at Visit 1. Student's *t*-tests were used to compare these levels between patients who withdrew due to ALS progression and patients who completed the study, while excluding withdrawals due to non-ALS reasons. To determine ability to predict change in ALSFRS-R, we examined correlations between metabolite levels at Visit 1 and patient-specific ALSFRS-R slope estimates.

Linear mixed models were also used to examine longitudinal change in the absolute concentrations of metabolites quantified with mean CRLB $\leq$ 20%. This exploratory analysis did not include Type 1 error corrections for multiple testing.

Additional Methods: In addition to the on-site ALSFRS-R scores obtained at each scan visit, ALSFRS-R scores were retrieved from medical records of patient clinic visits. These clinic ALSFRS-R scores were first gathered at the clinic date closest in time to the first scan visit and recorded for each subsequent clinic visit for 18 months ($\pm$ 2 months) or until the last visit if death occurred within 18 months. For each assessment, the answers to all 12 questions were also obtained, allowing for calculation of the ALSFRS-R subscores. Eighteen-month follow-up was chosen as this is the upper limit for typical phase III trial duration. Using the same methods described above, Visit 1 metabolite levels were examined for their ability to predict clinic ALSFRS-R slopes.

Survival analyses were carried out in two ways using the 'survival' package in R. First, Visit 1 metabolite levels were assigned as covariates in a Cox proportional hazards model. A measure of progression rate at Visit 1, called ΔFS, was also included as a covariate for comparison of predictor performance. ΔFS is a widely recognized predictor of survival in ALS and is calculated with the following formula [192]:

$$\Delta FS = (48 - \text{ALSFRS-R at Visit 1})/(\text{disease duration at Visit 1})$$

Hazard ratios were obtained for each covariate as an estimate of its association with survival time. Second, all Visit 2 and 3 metabolite data were added in a time-updated extended Cox model. This analysis was performed because the hazard risk may change

over time with the follow-up values. Follow-up of survival status ended on October 26, 2017, approximately 46.2 months after the first scan date of the study's first participant with ALS.

Study withdrawers and completers were also compared in their ΔFS at Visit 1 using *t*-tests as above.

For each participant, the percent voxel overlap between visits was determined. Voxel masks from later visits were registered to the same space as the T_1-weighted image from Visit 1 using the method described in the test-retest reproducibility study [116]. However, instead of calculating the overlap shared among multiple voxels, percent overlap was calculated using Visit 1's voxel mask as a reference. This approach was performed because later visit scans used the AutoAlign feature to copy the first visit's voxel placement. Means and standard deviations of percent voxel overlap relative to Visit 1 are presented in Table 5.1.

5.4 Results

Cohort Characteristics

The demographics and clinical features of participants at each visit are displayed in Table 5.1. Participant exclusions and withdrawals are shown in Figure 5.1.

Patients and controls at Visit 1 were well-matched on age-range, sex ratio, and hemisphere scanned. Matching on age-range and sex ratio was retained across Visits 2 and 3. At Visit 1, most patients (12 out of 19, 63%) were in King's disease stages 1 or 2. This proportion was similar at Visit 2 (10/14 = 72%) and lower at Visit 3 (3/10 = 30%). Mean ALSFRS-R scores also indicated that the patient cohort was mildly disabled at Visits 1 and 2 and more severely disabled at Visit 3. UMN burden scores were determined for the upper limb contralateral to the scanned hemisphere. Mean scores indicated mild UMN dysfunction in 19 patients at Visit 1 and in 7 patients who returned at Visit 3. Total ECAS scores were lower in patients compared to controls at all visits, but the differences did not reach statistical significance.

Table 5.1 Cohort Characteristics: Clinical Information and Spectroscopic Parameters*

	Visit 1		Visit 2		Visit 3	
	ALS	**Control**	**ALS**	**Control**	**ALS**	**Control**
Sample size n	19	18	14	15	10	13
Time of exam after Visit 1, months	–	–	6.6 ± 1.1	6.3 ± 0.8	12.8 ± 1.4	12.3 ± 1.0
Sex ratio, male:female	10:9	10:8	8:6	7:8	6:4	6:7
Age, years	57 ± 9 (31-74)	57 ± 9 (30-69)	58 ± 10 (32-71)	59 ± 7 (48-69)	58 ± 11 (32-70)	58 ± 10 (31-69)
Brain hemisphere scanned, left:right	8:11	8:10	5:9	7:8	3:7	6:7
Riluzole use, yes:no	8:11	–	7:7	–	4:6	–
Disease duration, months	40.3 ± 43.1 (3.5-148.1)	–	47.1 ± 49.4 (9.9-154.2)	–	43.2 ± 41.8 (15.9-156.5)	–
King's Disease Stage (no. of patients)	Stage 1 (6) Stage 2 (6) Stage 3 (6) Stage 4 (1)	–	Stage 1 (4) Stage 2 (6) Stage 3 (2) Stage 4 (2)	–	Stage 1 (1) Stage 2 (2) Stage 3 (2) Stage 4 (5)	–
ALSFRS-R Total Score (0 most severe – 48 normal)	39.8 ± 5.6 (26-45)	–	39.7 ± 4.1 (33-47)	–	36.4 ± 5.9 (26-45)	–
ALSFRS-R Upper Limb Subscore (0 most severe – 12 normal)	8.7 ± 3.2 (0-12)	–	9.3 ± 1.6 (7-12)	–	8.4 ± 1.8 (5-12)	–
ALSFRS-R Bulbar Subscore (0 most severe – 12 normal)	10.3 ± 1.9 (6-12)	–	9.7 ± 2.8 (4-12)	–	8.8 ± 3.8 (0-12)	–
Contralateral Upper Limb UMN Score** (0 normal – 5 most severe)	1.9 ± 1.7 (0-5)	–	–	–	1.9 ± 2.0 (0-5)	–
ECAS Total Score (0 most severe – 136 normal)	115.3 ± 6.5 (99-127)	119.3 ± 8.8 (103-129)	116.7 ± 8.2 (106-135)	123.0 ± 7.1 (107-132)	117.5 ± 6.6 (106-129)	122.4 ± 7.2 (108-134)
ECAS ALS-Specific Subscore (0 most severe – 100 normal)	86.3 ± 4.9 (74-95)	–	87.2 ± 6.3 (77-100)	–	86.6 ± 5.1 (80-97)	–
Motor Cortex Spectra SNR	205 ± 37	201 ± 34	215 ± 48	198 ± 45	208 ± 26	202 ± 44
Motor Cortex Spectra Linewidth, Hz	11 ± 2	11 ± 2	10 ± 2	11 ± 2	10 ± 2	11 ± 2
Motor Cortex % Voxel Overlap	–	–	86 ± 5	86 ± 6	86 ± 6	89 ± 4
Pons Spectra SNR	45 ± 10	53 ± 17	51 ± 10	56 ± 16	52 ± 10	62 ± 12
Pons Spectra Linewidth, Hz	16 ± 2	15 ± 2	14 ± 2	15 ± 2	15 ± 2	15 ± 2
Pons % Voxel Overlap	–	–	87 ± 9	89 ± 10	84 ± 6	88 ± 8

Data are given as counts or mean ± SD and range. Comparisons were made between patients and controls using Fisher's exact tests (sex ratio and brain hemisphere scanned) and unpaired, two-tailed Student's *t*-tests. Total ECAS scores trended lower in patients compared with controls at each visit. All other parameters were not different between groups. Abbreviations: ALSFRS-R = ALS Functional Rating Scale-Revised; UMN = upper motor neuron; ECAS = Edinburgh Cognitive-Behavioral ALS Screen.
*Pons spectra were acquired from fewer participants (see Results: ^{1}H-MRS Data Completeness and Quality).
**Neuromuscular examinations were conducted at Visits 1 and 3. Contralateral Upper Limb UMN burden was assessed in all patients at Visit 1 and in 7 patients at Visit 3.

^{1}H-MRS Data Completeness and Quality

Motor cortex metabolite spectra were acquired at each visit, and all datasets subsequently passed quality criteria. In contrast, fewer pons datasets were obtained. Thirteen pons acquisitions were incomplete due to participant discomfort during the latter half of the exam. Seven pons datasets were excluded due to SNR < 25. In total, usable pons spectra were acquired from 13 patients and 15 controls at Visit 1, 9 patients and 13 controls at Visit 2, and 9 patients and 10 controls at Visit 3.

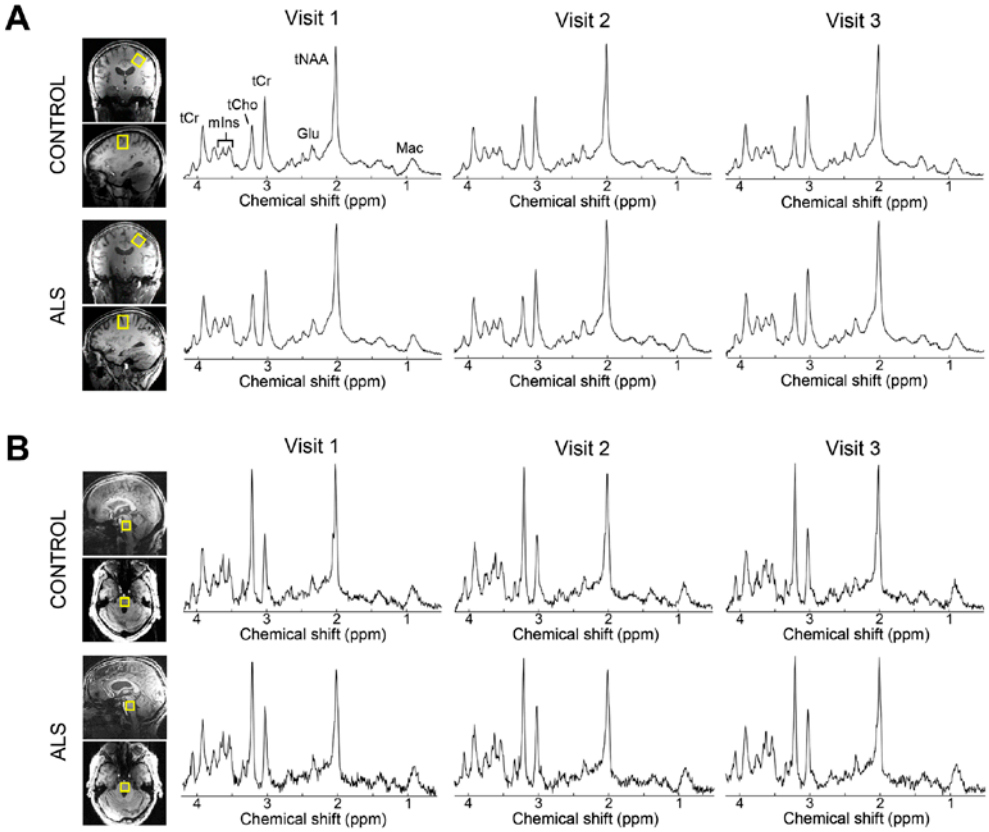

Figure 5.2 Proton spectra obtained from the motor cortex and pons of a patient and healthy control. Upper limb motor cortex spectra (A) and pons spectra (B) had high SNR that was reproducible across visits (semi-LASER: TR/TE = 5000/26 ms, 64 averages). Spectral SNR was not different between patients and controls using unpaired Student's t-test. Spectra are weighted with a 5-Hz Gaussian function for display purposes. Abbreviations: Glu, glutamate; Mac; macromolecules; mIns, *myo*-inositol; tCho, phosphocholine + glycerophosphocholine; tCr, creatine+phosphocreatine; tNAA, *N*-acetylaspartate + *N*-acetylaspartylglutamate.

Motor cortex and pons metabolite spectra that satisfied quality criteria had high SNR that was reproducible across visits (Table 5.1; Figure 5.2). The mean coefficient of variation in SNR across visits was 9.0% for motor cortex spectra and 12.4% for pons spectra. Motor cortex spectra had significantly higher SNR and narrower linewidths than pons spectra (both $p < 0.0001$). Patient and control spectra did not differ in SNR or linewidth. High percent voxel overlap was also observed across visits for both regions.

Analyses of Longitudinal Changes

As reported previously [157], the cross-sectional analyses of neurochemical levels at Visit 1 demonstrated significantly reduced motor cortex tNAA/mIns in patients, as well as positive correlations between this measure and ALSFRS-R.

In patients, ALSFRS-R total scores declined over the follow-up period at an average rate of -0.46 points per month ($p < 0.0001$; Table 5.2). ALSFRS-R subscores also declined, with the upper limb scores showing a stronger change over time than bulbar scores. Cognitive-behavioral and UMN burden scores for the contralateral upper limb did not change.

Table 5.2 Linear Trends in Clinical and Spectroscopy Measures*

	ALS			Controls		
Clinical Measures	**Mean change per mo.**	**SE**	***p*-value**	**Mean change per mo.**	**SE**	***p*-value**
ALSFRS-R Total	-0.46	0.07	< 0.0001	–	–	–
ALSFRS-R Upper Limb	-0.13	0.03	< 0.0001	–	–	–
ALSFRS-R Bulbar	-0.13	0.06	0.04	–	–	–
Contralateral Upper Limb UMN	-0.07	0.04	0.16	–	–	–
ECAS ALS-Specific	0.08	0.11	0.48	–	–	–
^{1}H-MRS Measures	**Mean change per yr.**	**SE**	***p*-value**	**Mean change per yr.**	**SE**	***p*-value**
Motor cortex tNAA/mIns	-0.126	0.049	0.01	-0.030	0.047	0.53
Pons Glx, µmol/g	0.570	0.178	< 0.01	0.414	0.308	0.19

P-values are from tests against null change over time.
Abbreviations: SE = standard error; ALSFRS-R = ALS Functional Rating Scale-Revised; UMN = upper motor neuron burden; ECAS = Edinburgh Cognitive-Behavioral Screen.
*Slope analyses were performed on longitudinal data from participants who completed two or three visits. The sample size was 14 patients and 16 controls for all analyses, except for the following: ALSFRS-R bulbar and pons Glx analyses (12 patients, 14 controls) and contralateral upper limb UMN burden analysis (7 patients).

Motor cortex tNAA/mIns levels significantly declined in patients over the follow-up period ($p = 0.01$). Additionally, pons Glx levels significantly increased in patients ($p = 0.003$). The rates of change in these measures were not significantly different between riluzole users and non-users (half of patients were riluzole users in each longitudinal analysis). Neither metabolite measure changed over time in controls. An exploratory analysis of absolute concentrations for 8 neurochemicals revealed no significant changes over time in patients or controls for either region, except for an increase in pons Glx levels in patients with ALS (Figure 5.3).

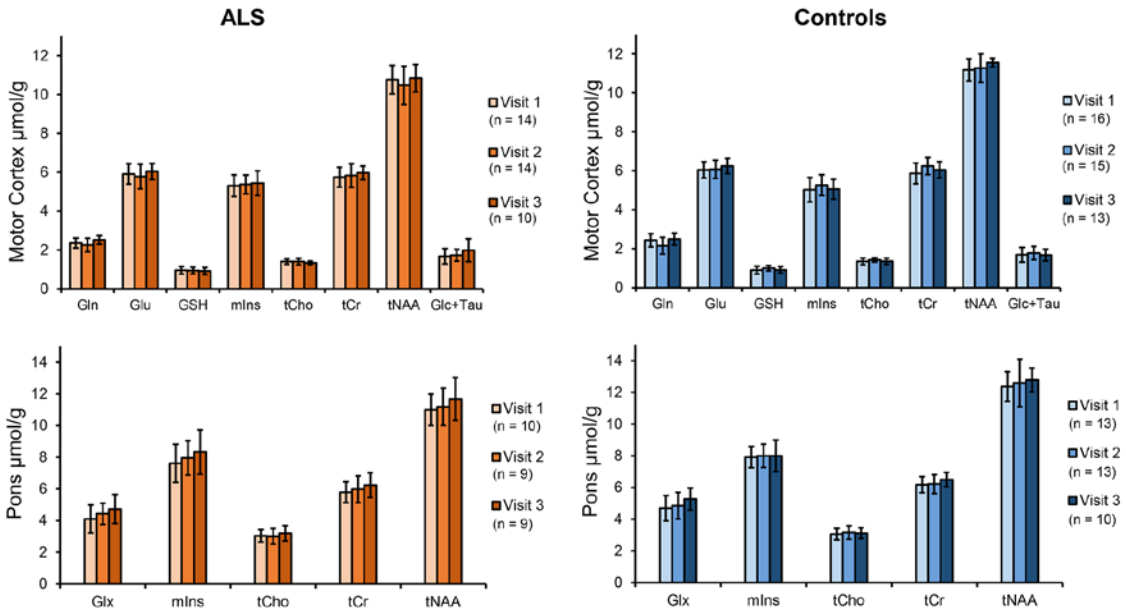

Figure 5.3 Absolute concentrations for metabolites quantified with mean CRLB ≤ 20%. Linear slope analysis showed that pons Glx levels in patients with ALS significantly increased across visits. Other metabolite levels were not different across visits for either region in patients or controls. Mean ± standard deviation bars were generated using the datasets from only those participants who completed at least two visits. Correlated metabolites ($r < -0.5$) were analyzed as sums (tCho, tCr, tNAA, and Glc+Tau).
Abbreviations: Glc, glucose; Gln, glutamine; Glu, glutamate; GSH, glutathione; mIns, *myo*-inositol; tCho, phosphocholine + glycerophosphocholine; tCr, creatine + phosphocreatine; tNAA, *N*-acetylaspartate + *N*-acetylaspartylglutamate; Tau, taurine.

To determine whether clinical subgroups drove the longitudinal changes in neurochemical levels, we stratified patients by progression of regional functional

impairment. Of the 14 patients with usable longitudinal motor cortex ^{1}H-MRS data, 9 experienced decline in ALSFRS-R upper limb subscores during the follow-up period (p < 0.0001; average rate = -0.21 points/month), while 5 remained stable (p = 1; average rate = 0 points/month). Motor cortex tNAA/mIns levels dropped significantly over time in the patients with declining upper limb function (p = 0.002) but did not change in those who were stable (p = 0.76; Figure 5.4). The functionally declining patients showed a significantly greater rate of decline in tNAA/mIns compared to controls (p = 0.04), while functionally stable patients did not (p = 0.94). The proportion of riluzole users was not significantly different between the functionally declining and functionally stable subgroups (5 out of 9 patients versus 2 out of 5 patients; Fisher's test).

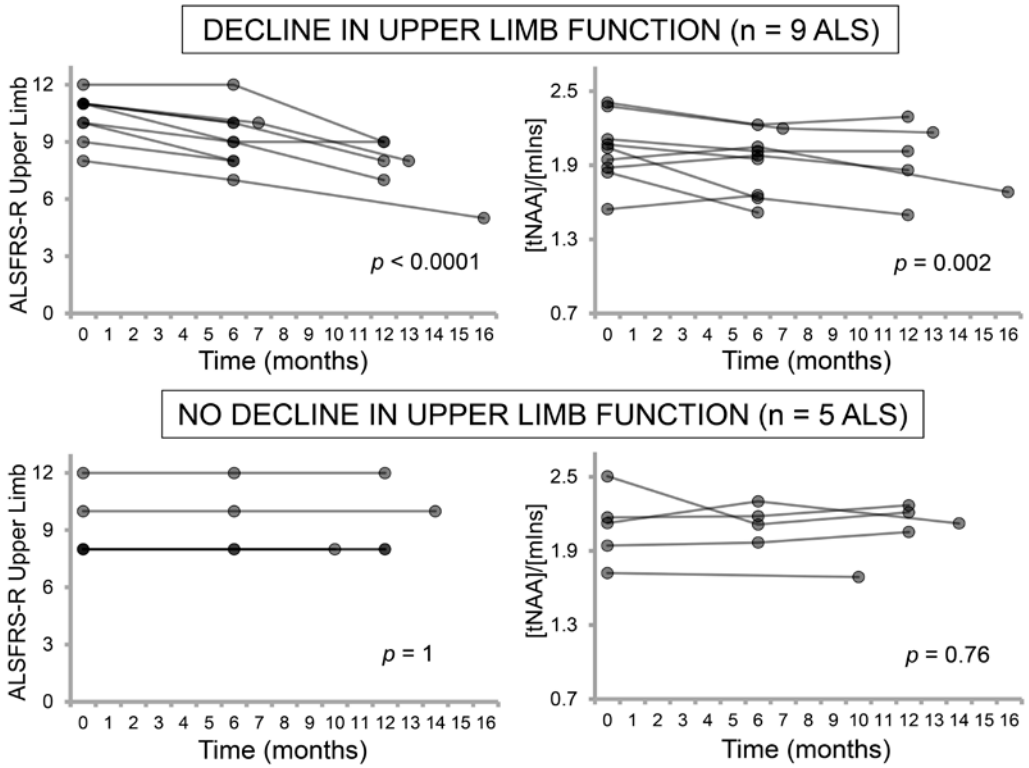

Figure 5.4 Longitudinal changes in motor cortex tNAA/mIns are related to progression of upper limb function. Patients who had declining ALSFRS-R upper limb scores over the follow-up period experienced decreasing tNAA/mIns over the same time window (both p < 0.01). In contrast, patients who had stable ALSFRS-R upper limb scores showed no change in tNAA/mIns over time. Analyses were performed on data from participants who completed two or three visits. *P*-values are from a test of the mean slope against no change over time.

Of the 12 patients with usable longitudinal pons ^{1}H-MRS data, 6 experienced decline in ALSFRS-R bulbar subscores during the follow-up period (p = 0.03; average rate = -0.26 points/month), while 6 remained stable (p = 0.52; average rate = 0.01 points/month). Pons Glx levels increased significantly over time in the patients with declining bulbar function ($p < 0.0001$) and did not change in those who were stable (p = 0.43; Figure 5.5). The proportion of riluzole users was equal in the functionally declining and functionally stable subgroups (3 out of 6 patients in each).

We also analyzed patients' individual trajectories in motor cortex tNAA/mIns, pons Glx, UMN burden scores, and ALSFRS-R scores (total, upper limb, and bulbar). The slopes of neurochemical levels over time did not correlate with the slopes of clinical measures.

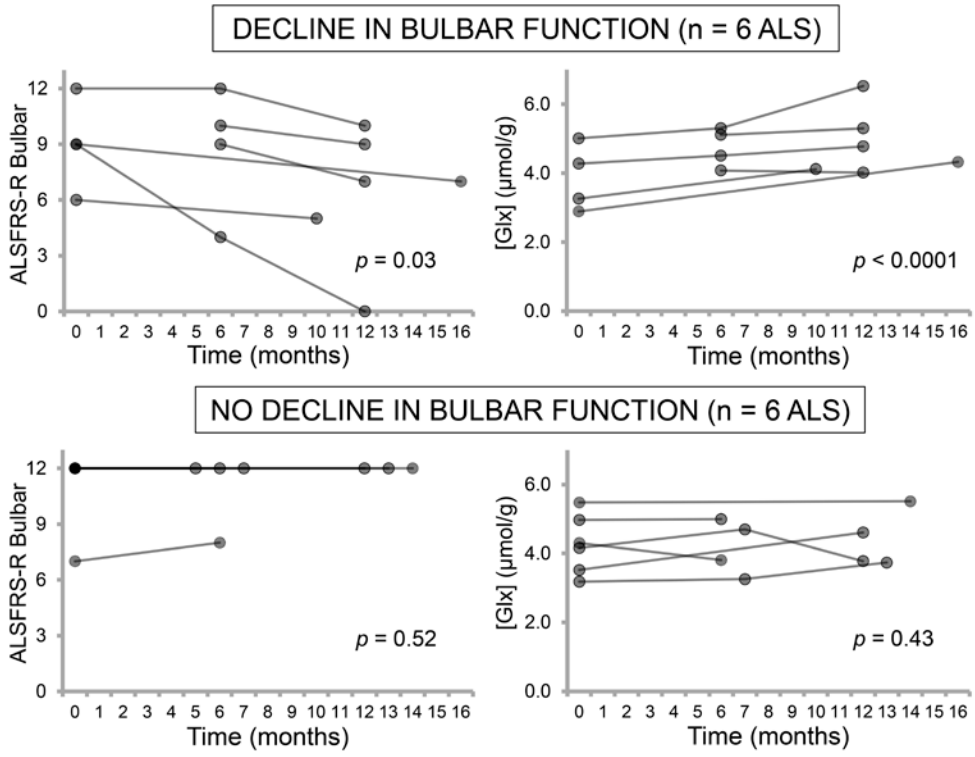

Figure 5.5 Longitudinal changes in pons Glx levels are related to progression of bulbar function. Patients who had declining ALSFRS-R bulbar scores over the follow-up period experienced increasing Glx levels in the pons over the same time window ($p <$ 0.0001). In contrast, patients who had stable ALSFRS-R bulbar scores showed no change in pons Glx levels over time. Analyses were performed on data from participants who completed two or three visits. *P*-values are from a test of the mean slope against no change over time.

Prediction of Patient Withdrawal

Neurochemical levels at Visit 1 were assessed for their ability to predict disease progression in patients. Specifically, we compared motor cortex tNAA/mIns levels at Visit 1 between 6 patients who withdrew from the study due to ALS progression and 10 patients who returned for all follow-up visits. Levels of tNAA/mIns were significantly lower in people who withdrew than in those who completed all visits ($p < 0.001$; Figure 5.6).

Compared with those who completed all visits, patients who withdrew due to ALS progression also had lower ALSFRS-R total and upper limb scores at Visit 1 ($p = 0.007$ and 0.02, respectively). However, overlap in the clinical scores between withdrawers and completers was substantially larger than the overlap in their tNAA/mIns levels (Figure 5.6). ΔFS and pons Glx at Visit 1 displayed no predictive ability.

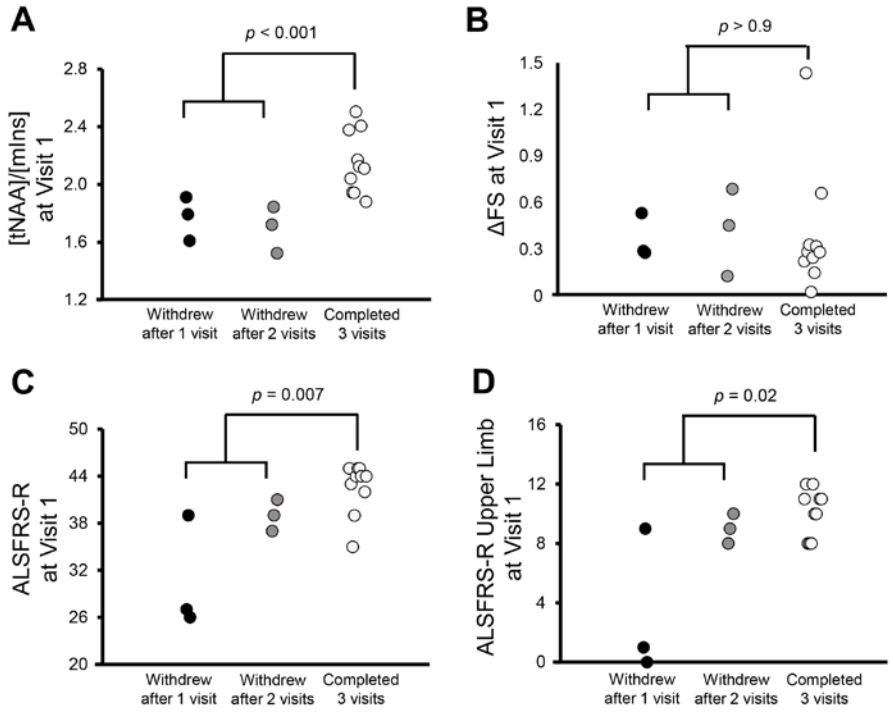

Figure 5.6 Comparison of motor cortex tNAA/mIns, ALSFRS-R, and ΔFS at Visit 1 between study withdrawers and completers. Patient subgroups were divided according to study withdrawal and completion. The most significant difference between groups was observed in the tNAA/mIns comparison ($p < 0.001$; unpaired, two-tailed *t*-tests).

Prediction of Clinical Progression

The estimation of ALSFRS-R slopes required at least 2 data points for each participant. Clinic ALSFRS-R slopes were not determined for 6 patients who either did not have more than 1 available clinic visit or were not followed for approximately 18 months. The average number of data points used for slope calculation was 2.7 ± 1.5 points for on-site ALSFRS-R and 4.5 ± 1.3 points for clinic ALSFRS-R.

In patients, motor cortex tNAA/mIns at Visit 1 did not correlate with change in ALSFRS-R total or upper limb scores over time. This was the case regardless of whether on-site or clinic ALSFRS-R slope estimates were used (Figure 5.7).

For 2 patients, pons datasets were not acquired successfully at Visit 1 but were acquired at Visit 2. Thus, these patients' Visit 2 pons Glx levels were included as baseline values in this analysis and the survival analysis (next section). Pons Glx levels at baseline did not correlate with change in on-site ALSFRS-R total or bulbar scores. However, they did significantly correlate with clinic ALSFRS-R total slopes ($r = -0.63$, $p = 0.04$). No significant correlations were observed between pons Glx at baseline and clinic ALSFRS-R bulbar slopes.

Prediction of Survival

We recorded 7 patient deaths over the course of the study (total study duration = 45.3 months). Cox regression analyses demonstrated no significant ability for motor cortex tNAA/mIns to predict reduced survival (Figure 5.8). Higher pons Glx at Visit 1 showed a trend for an association with increased risk of death ($p = 0.05$; hazard ratio = 7.4). However, the time-updated analysis showed no such relationship ($p = 0.48$). A trend between higher ΔFS at Visit 1 and reduced survival was also observed ($p = 0.11$; hazard ratio = 3.9).

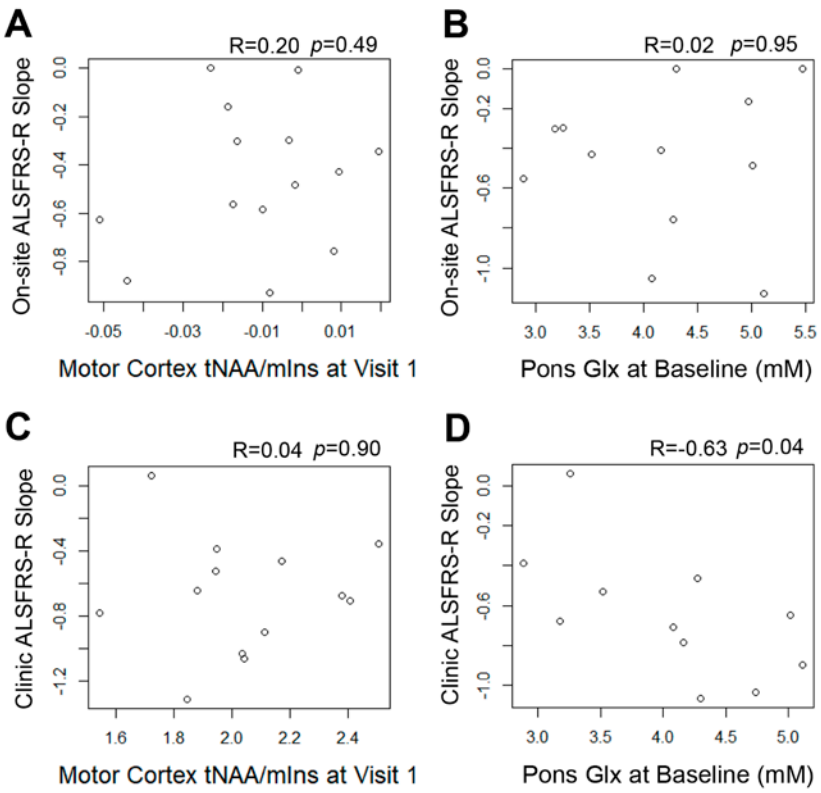

Figure 5.7 Correlation analyses between metabolite levels at baseline and patient-specific ALSFRS-R slope estimates. Panels A and B: On-site ALSFRS-R slopes vs metabolite levels. Panels C and D: Clinic ALSFRS-R slopes vs metabolite levels. A moderate correlation was observed between pons Glx levels at baseline and clinic ALSFRS-R slope estimates.

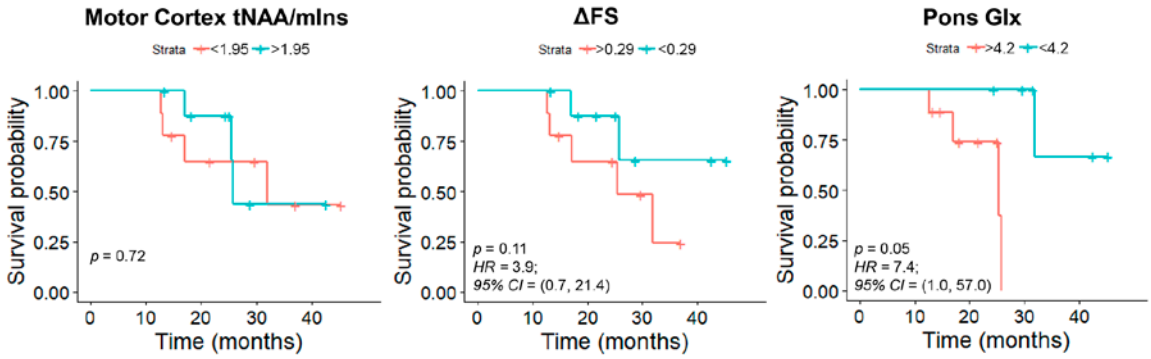

Figure 5.8 Kaplan-Meier survival curves for patient groups divided by median predictor values at baseline. Trends were observed in the abilities for pons Glx and ΔFS at baseline to predict survival. Note that the *p*-values displayed were obtained from Cox proportional hazards regression.

5.5 Discussion

This longitudinal study revealed changes in brain neurochemical levels over one year in people with ALS. These neurochemical changes were regionally related to functional decline (i.e., upper limb motor cortex tNAA/mIns and upper limb function, pons Glx and bulbar function). Additionally, motor cortex tNAA/mIns was a significant predictor of study withdrawal due to ALS progression.

Most ^{1}H-MRS studies in ALS to date have been cross-sectional and typically found lower tNAA and higher mIns levels in the motor cortex in patients compared to healthy controls [193]. Reduction in tNAA indicates neuronal loss and dysfunction, while elevation in mIns suggests gliosis [52]. Hence, the tNAA/mIns ratio may be a robust, pathologically relevant biomarker for ALS, especially since UMN degeneration in the disease is often accompanied by glial activation and proliferation [194]. Earlier work showed that tNAA/mIns was markedly lower in ALS motor cortex and had the best sensitivity and specificity among ^{1}H-MRS measures in distinguishing patients from controls [91]. Subsequent studies also observed moderate-to-strong correlations between this measure and clinical scores of disability (ALSFRS-R) and UMN burden [85, 157]. Here we report that motor cortex tNAA/mIns decreases longitudinally in patients, which extends previous cross-sectional findings and supports tNAA/mIns as a measure of progressive neurodegeneration in ALS.

The longitudinal ^{1}H-MRS literature in ALS has been inconsistent. Although a few studies reported declines in motor cortex tNAA or its ratios (i.e., tNAA/tCho, tNAA/tCr) [84, 94], other studies obtained negative results [93, 96, 102, 103]. Notably, these studies did not examine whether neurochemical changes in the scanned area of motor cortex are related to functional decline in the represented body region. Investigating this question is meaningful because the heterogeneity of disease spread in ALS may be driven by differences among patients in their pattern of motor cortex degeneration. In our stratification analysis, tNAA/mIns in the upper limb motor cortex declined in patients with worsening upper limb function but did not change in patients who were functionally stable. This suggests that tNAA/mIns in the upper limb motor cortex reflects the integrity of UMNs that control upper limb function. More broadly, however, our finding also

indicates that the degeneration of distinct regions of the motor cortex is variable in ALS. This may explain the mixed longitudinal results in literature, which were all obtained from analyses of small areas within the motor cortex. Furthermore, focal motor cortex changes appear to have functional consequences according to the cortical somatotopic map. Thus, stratification by functional decline may be necessary to detect neurochemical changes consistently in parts of the motor cortex. This regional dependence has also been suggested in a previous cross-sectional study, which reported that upper limb corticospinal tract tNAA/tCho correlated significantly with finger-tapping rate but not with foot-tapping or bulbar muscle syllable repeat rates [105].

In our analysis of absolute concentrations, motor cortex tNAA and mIns did not significantly change over time in patients with ALS. Therefore, the decline in tNAA/mIns is probably driven by associated disease processes that cause small but opposite changes in the two concentrations. The measurement of the tNAA/mIns ratio likely confers additional robustness in detecting neurodegenerative changes, particularly during early disease stages when neuronal and glial pathology may be modest. Notably, changes in tNAA/mIns were detected while observing no changes in clinical UMN burden over time. This reinforces the understanding that clinical scores based upon reflexes and tone are an imperfect surrogate for UMN degeneration. In particular, the physiology that underlies clinical UMN signs is complex, and the presentation of these signs may also be obscured by advanced lower motor neuron signs [195]. By contrast, ^{1}H-MRS can directly evaluate motor areas of the brain and may have greater sensitivity to progressive UMN degeneration.

We also observed that motor cortex tNAA/mIns may be prognostic, with the potential to identify patients who are likely to withdraw from a study due to progressive decline. This finding is especially relevant to clinical trial design, which would benefit greatly from accurate prognostic information during participant selection [196]. Relatedly, low cingulate cortex tNAA/mIns in normal individuals predicts the conversion to mild cognitive impairment and Alzheimer's disease [197, 198]. Together these studies suggest that tNAA/mIns has prognostic value for conditions that show both neuronal degeneration and gliosis.

The sum Glx is frequently reported in ^{1}H-MRS literature due to the difficulty in reliably separating the overlapping resonances of Glu and Gln. Alterations in Glx levels have been interpreted primarily as alterations in Glu, which accounts for approximately 80% of the sum in healthy brain regions [83]. In cross-sectional studies, authors reported elevated Glx in the brainstem in patients with ALS and suggested that this supports the role of excess Glu neurotransmission in motor neuron death [88, 109]. Our previously published analysis of Visit 1 data showed no differences in pons Glx levels between patients with relatively early-stage ALS and healthy controls [157]. However, longitudinal follow-up of these patients revealed increases in pons Glx levels over the subsequent year. These increases are likely unrelated to riluzole's purported antiglutamatergic activity [20], since trends in Glx were not different between riluzole users and non-users. Our findings suggest that pons Glx levels are normal in early-stage ALS and rise as the disease transitions to later stages. Consistently, the mean disability scores of the cohorts that were previously reported to have elevated Glx levels [88, 109] were more severe than our cohort at Visit 1. Longitudinal increases in Glx may reflect progressive abnormalities in Glu metabolism, which likely occur in ALS [199]. It may also indirectly support Glu excitotoxicity as a pathogenic mechanism, although this interpretation is tenuous as the Glu signal in ^{1}H-MRS principally arises from the intracellular compartment [200]. Lastly, the rise in Glx may also indicate increases in astroglial Gln [201].

The stratification analysis in patients showed that elevation in pons Glx is related to decline in bulbar function. This finding was somewhat surprising, given that the ALSFRS-R bulbar subscore is a rating of functions governed largely by medullary motor neurons (i.e., speech, swallowing, and salivation) [43]. The pons voxel in this study contains cranial motor nuclei and corticospinal fibers that are less directly involved in controlling these functions. However, it also includes corticobulbar projections to the medullary motor nuclei as well as extrapyramidal tracts that greatly influence axial muscle tone [18]. Thus, elevated Glx in the pons may represent abnormalities in these different areas, which affect a variety of bulbar and non-bulbar motor functions. Moreover, degenerative changes are likely to occur in the pons and medulla

simultaneously due to their anatomic proximity. Pons Glx may therefore indirectly reflect disease burden in the medulla.

Although longitudinal neurochemical trends were different between subgroups of patients with different rates of functional decline, correlations were not statistically significant between the individual slopes of neurochemical levels and slopes of ALSFRS-R scores. This is most likely due to the correlation tests being insufficiently powered. Several patients had ALSFRS-R slopes that were zero, and thus the range of slope values may be too restricted to observe a large correlation coefficient. Furthermore, slope estimates are associated with additional measurement error that will lead to a biased underestimation of the true correlation [202]. This attenuation effect may be prominent due to the considerable error associated with slopes calculated from only two or three data points.

The regional association between neurochemical changes and functional decline suggests that ^{1}H-MRS can inform us about disease spread in ALS. The pattern of disease spread is a subject of intense interest and, to date, has relied largely upon longitudinal clinical examinations and post-mortem histopathology [12, 35]. Unlike these methods, ^{1}H-MRS may provide direct *in vivo* information on disease progression within and between brain regions, e.g., by tracking neurochemical changes in different areas of motor cortex that control bulbar, upper limb, or lower limb function. Specifically, ^{1}H-MRS may be able to determine how motor areas of the brain are sequentially involved in ALS, which would help explain patterns of functional decline.

Our longitudinal cohort was small, with 10 patients undergoing scanning at all three visits. Additionally, the rate of ALSFRS-R decline in our cohort was approximately half the rate typically observed in natural history studies [203]. We detected statistically significant longitudinal changes in motor cortex tNAA/mIns and pons Glx levels despite these factors, which suggests that these measures are highly sensitive to disease progression in the brain. We expect that future investigations of larger cohorts with typical progression rates will help establish these as disease progression biomarkers in ALS.

Our study has some limitations in addition to small sample size. First, in order to achieve high measurement precision [116], we utilized an optimized ^{1}H-MRS technique at 7 T, which is currently unavailable in the clinical setting. Our findings would have greater clinical application if demonstrated on a widely available 3 T system. In our earlier work, comparisons of glutathione levels between patients with ALS and controls yielded similar results whether 3 T edited or 7 T unedited ^{1}H-MRS was performed [157]. Here we expect that unedited ^{1}H-MRS experiments at 3 T will confirm our present findings because tNAA/mIns and Glx each have comparable measurement precision at both field strengths. Specifically, the mean coefficients of variation for these measures at 3 and 7 T are each under 5% as calculated from prior test-retest data from the cortex [116]. Second, we used an established UMN burden scoring system that is based heavily on pathologic reflexes. In particular, reflexes in the upper limb reflect overlapping motor neuron pools and may be overrepresented in this system. A more comprehensive scoring system that grades the severity of spasticity and hyperreflexia, assigns weighting to individual components, and incorporates speed of repetitive movements may allow a better comparison with ^{1}H-MRS measures.

Overall, this study indicates that neurochemical changes in motor areas of the brain reflect disease progression in corresponding areas of the body. Subsequent studies may confirm the relationship between neurochemical changes and functional decline for other motor cortex regions, such as the lower limb and cranial representations. Ultimately, ^{1}H-MRS may provide outcome measures for monitoring and predicting disease progression in future therapeutic trials. In natural history studies, ^{1}H-MRS may also be useful for mapping the course of cerebral degeneration.

5.6 Chapter Summary

The main implication of this longitudinal study is that functional heterogeneity in ALS may be underpinned by variable degeneration within the brain that is detectable using ^{1}H-MRS. The work confirms the spatial specificity of the technique, as neurochemical derangements in motor areas of the brain are linked to functional decline in

corresponding body regions. This is especially the case for our analysis of tNAA/mIns, in which changes in the upper limb motor cortex were observed only in patients with upper limb functional decline. Similar to the previous chapter's correlation analysis of motor cortex tNAA/mIns and CReATe LMN scores, this finding reflects an expected somatotopic relationship.

We did not observe a decline in motor cortex Glu over time, even though the metabolite showed cross-sectional negative correlations with disability and disease stage. Although mostly intraneuronal, Glu is not cell type-specific and is involved in many cellular pathways. Thus, neuronal loss would probably have to be dramatic in order to observe significant decline in tissue Glu levels. In contrast, our cohort displayed mild-to-moderate disease progression based on our analysis of the longitudinal trends in clinical scores and other neurochemical levels.

The patient cohort in this study was assessed for three clinical outcomes: ALSFRS-R decline, mortality, and withdrawal due to progression. The high event rate (6 withdrawals due to progression and 7 deaths out of 19 patients) enabled analysis of the predictors of these outcomes. Compared to other predictors, such as ALSFRS-R and ΔFS, motor cortex tNAA/mIns showed the most significant ability to predict patient withdrawal.

5.6.1 Potential as a Prognostic Biomarker

Robust prognostic biomarkers can help address the problem of phenotypic heterogeneity in ALS. In particular, large clinical trials are needed mainly because of high variability in disease progression rate. Predictors of progression rate can be used to study more homogeneous groups.

This study identified motor cortex tNAA/mIns as having potential prognostic value. If accurate, the measure's ability to predict study withdrawal due to disease progression would have enormous application in the smaller phase II trials. However, since our sample size is small, with only 6 withdrawals due to ALS progression and 10 completers, this finding should be treated as preliminary.

In this study, motor cortex tNAA/mIns was not a significant predictor of clinical outcomes such as survival and ALSFRS-R decline. Higher pons Glx levels at baseline showed a trend in the prediction of reduced survival, but this disappeared after including the time-updated values in the extended Cox model. This extended model is likely more appropriate as we know that the metabolite levels vary with time. Notably, higher ΔFS at baseline also showed a trend in predicting reduced survival, which is consistent with previous literature [192]. Pons Glx at baseline also correlated significantly with clinic ALSFRS-R progression but not with on-site ALSFRS-R progression. This suggests that the slope estimations were different between the two sites, which is most likely due to the discrepancy among the sites in the number of data points used for slope calculation.

A previous study in a cohort of 63 patients reported decent accuracy for tNAA ratios in predicting reduced survival in ALS [99]. The larger sample size is an important consideration especially when predicting a highly variable measure such as survival. In ALS, survival time can depend on multiple factors, including the quality and availability of nutritional and respiratory support and decisions regarding when to withdraw life-sustaining treatment.

Previous studies have not examined the ability of ^{1}H-MRS to predict ALSFRS-R decline. This is surprising given that ALSFRS-R scores are relatively easy to track longitudinally, as the questionnaire is simple to administer and accurate scores can also be obtained over the phone. However, estimating ALSFRS-R decline may not be straightforward if the assumption of linearity is not true. Some observers have noted different rates of ALSFRS-R progression at different stages of the disease. In particular, a current hypothesis proposes that the earliest and latest stages are characterized by plateaus in ALSFRS-R, while the middle stages are marked by rapid decline. Thus, ALSFRS-R progression may be better modeled using curved functions [41, 204]. In this study, the linearity of individual ALSFRS-R progression could not be confidently ascertained, as each participant had only two or three data points for on-site ALSFRS-R and usually four or five data points for clinic ALSFRS-R followed across 18 months. Ultimately, the ability to predict ALSFRS-R progression is likely best assessed in a larger cohort of

patients at early disease stage with more frequent evaluations over time (e.g., once per month, as in recent clinical trials).

5.6.2 Potential as a Progression Biomarker

Of all the biomarker types, progression and pharmacodynamic biomarkers would have the most direct impact on drug development for ALS. Our study of longitudinal neurochemical change shows that ^{1}H-MRS biomarkers are sensitive to disease progression, but the heterogeneity in regional progression needs to be taken into account. Compared to total ALSFRS-R decline, changes in region-specific neurochemical levels are much weaker. The time trends are generally comparable between region-specific ALSFRS-R scores and neurochemical levels, but nonetheless the upper limb ALSFRS-R decline is still more significant than upper limb motor cortex tNAA/mIns decline. This may reflect that upper limb motor cortex tNAA/mIns is simply not as sensitive to disease progression as upper limb ALSFRS-R. Alternatively, this could indicate that our cohort suffered greater progression at the LMN level than at the UMN level, since ALSFRS-R is recognized as being more driven by LMN dysfunction [205]. This latter possibility may also explain why pons Glx levels showed more significant time trends, as the pons voxel contained LMN as well as UMN areas. Thus, motor cortex tNAA/mIns may be a very useful measure of UMN or, more broadly, cortical degeneration in ALS. Notably, progressive UMN dysfunction was not detected using a rating system based on traditional clinical UMN signs. Subsequent studies that compare longitudinal neurochemical trends in UMN-predominant and LMN-predominant ALS will help determine the value of ^{1}H-MRS as a biomarker of progression.

Conclusion

This work demonstrates that ^{1}H-MRS is capable of quantifying region-specific neurodegeneration in ALS. As a non-invasive *in vivo* technique, ^{1}H-MRS may have powerful application as a biomarker of progression and prognosis. Larger studies are obviously needed to confirm and establish its utility in clinical trials, but studies that examine more regions of the brain, particularly other areas within the motor cortex, are also necessary. In ALS, the regional degeneration of the brain is variable across patients, which makes it difficult to predict and select the areas that undergo progressive change. When applied simultaneously to multiple regions, the high spatial specificity of ^{1}H-MRS may help us define distinct patterns of motor cortex degeneration, which would be beneficial information during efficacy analysis and drug development. In particular, therapies designed for local application in the brain may be able to contain disease spread. In this regard, ^{1}H-MRSI may be the most appropriate tool for understanding cortical disease spread in ALS. Recent improvements in this technique have enabled the reliable quantification of measures such as tNAA/mIns and Glx in multiple regions simultaneously [206].

The information obtained from ^{1}H-MRS(I) regarding disease spread in ALS would be further strengthened by agreement with current models of neuropathological spread. In a recently proposed model of TDP-43 propagation [207], disease involvement begins in the motor cortex and subsequently spreads to (1) the reticular formation and other brainstem nuclei, (2) prefrontal, parietal, and striatal areas, and (3) the hippocampus and temporal lobe. Most, if not all, of these regions can be assessed by ^{1}H-MRS, and thus, future longitudinal studies may support and establish this model of disease spread.

Both the cross-sectional and longitudinal components of this study reflect that UMN and LMN degeneration in ALS are not independent of each other. Larger studies may examine the interdependence of motor area-specific neurochemical levels and region-specific measures of LMN dysfunction (e.g., electrophysiologic indices or sensitive clinical scores such as CReATe LMN). These studies could appropriately test whether the idea of disease focality and contiguous anatomic spread is an accurate model of regional disease propagation.

^{1}H-MRS is sensitive to metabolic changes in ALS, which by itself may robustly indicate neurodegeneration. However, other neuroimaging measures, such as structural and functional connectivity metrics and cortical thickness, are also abnormal in ALS and indicate different aspects of the disease. Thus, combining modalities may confer increased robustness in disease detection. Improvements in diagnostic sensitivity and specificity in ALS have been observed after integrating ^{1}H-MRS and DTI data [190]. Additionally, ^{1}H-MRS and DTI biomarkers have occasionally demonstrated prognostic value in separate studies. Combining them in a multimodal approach may provide gains in predictive power, with important consequences for clinical trial design.

Longitudinal studies using neuroimaging techniques such as ^{1}H-MRS have struggled so far to identify a biomarker of progression that can match the sensitivity and relatively low variability of the ALSFRS-R. For example, one study estimated the required sample size to detect a treatment effect as 94 participants per experimental arm for ALSFRS-R compared to over 500 per arm for DTI fractional anisotropy [208]. However, a clear limitation of the ALSFRS-R is that it does not provide specific information on the status of the cortical descending motor pathway and other brain areas of major disease

involvement. Therefore, neuroimaging techniques are still among the most likely options for discovering sensitive markers that are more related to the fundamental disease biology in ALS. Such markers would have a better ability to screen for disease-modifying treatments.

One of the main hurdles towards the clinical application of neuroimaging biomarkers is demonstrating measurement reproducibility. ^{1}H-MRS strongly meets this requirement, as shown by the work in this thesis and by other groups. To maximize precision, future ^{1}H-MRS biomarker evaluation work in ALS should utilize optimized pulse sequences and other state-of-the-art methodology.

The relevance of the biomarkers to clinical outcome is another major test. In this regard, ^{1}H-MRS has also stepped forward by showing significant correlations with established clinical measures in ALS, particularly the ALSFRS-R. This step is critical if biomarkers are expected to serve as substitutes for gold-standard clinical endpoints.

Considering all factors, the heterogeneity in ALS is perhaps the largest hindrance to the development of effective therapies. Discovering markers that can separate distinct phenotypes will make the population easier to study, in addition to powering clinical trials. The work of this thesis showed that ^{1}H-MRS biomarkers may reflect variability in regional functional decline, but other aspects of disease heterogeneity also need to be investigated such as LMN- versus UMN-predominant ALS and genotypic differences. Ultimately, ^{1}H-MRS biomarkers may aid in our search for treatments for this unrelenting disease. Future studies are necessary to define their potential contributions to both drug development and our biological understanding of the disease's progression and spread.

BIBLIOGRAPHY

1. Turner MR, Barnwell J, Al-Chalabi A, Eisen A. Young-onset amyotrophic lateral sclerosis: historical and other observations. Brain 2012;135(Pt 9):2883-2891.

2. Chio A, Logroscino G, Traynor BJ, et al. Global epidemiology of amyotrophic lateral sclerosis: a systematic review of the published literature. Neuroepidemiology 2013;41(2):118-130.

3. Hammer RP, Jr., Tomiyasu U, Scheibel AB. Degeneration of the human Betz cell due to amyotrophic lateral sclerosis. Exp Neurol 1979;63(2):336-346.

4. Udaka F, Kameyama M, Tomonaga M. Degeneration of Betz cells in motor neuron disease. A Golgi study. Acta Neuropathol 1986;70(3-4):289-295.

5. Rivara CB, Sherwood CC, Bouras C, Hof PR. Stereologic characterization and spatial distribution patterns of Betz cells in the human primary motor cortex. Anat Rec A Discov Mol Cell Evol Biol 2003;270(2):137-151.

6. Kamo H, Haebara H, Akiguchi I, Kameyama M, Kimura H, McGeer PL. A distinctive distribution of reactive astroglia in the precentral cortex in amyotrophic lateral sclerosis. Acta Neuropathol 1987;74(1):33-38.

7. Brettschneider J, Toledo JB, Van Deerlin VM, et al. Microglial activation correlates with disease progression and upper motor neuron clinical symptoms in amyotrophic lateral sclerosis. PLoS One 2012;7(6):e39216.

8. Jara JH, Genc B, Stanford MJ, et al. Evidence for an early innate immune response in the motor cortex of ALS. J Neuroinflammation 2017;14(1):129.

9. Kiernan JA, Hudson AJ. Changes in sizes of cortical and lower motor neurons in amyotrophic lateral sclerosis. Brain 1991;114 (Pt 2):843-853.

10. Nihei K, McKee AC, Kowall NW. Patterns of neuronal degeneration in the motor cortex of amyotrophic lateral sclerosis patients. Acta Neuropathol 1993;86(1):55-64.

11. Kang SH, Li Y, Fukaya M, et al. Degeneration and impaired regeneration of gray matter oligodendrocytes in amyotrophic lateral sclerosis. Nat Neurosci 2013;16(5):571-579.

12. Brettschneider J, Del Tredici K, Toledo JB, et al. Stages of pTDP-43 pathology in amyotrophic lateral sclerosis. Ann Neurol 2013;74(1):20-38.

13. Kato S, Takikawa M, Nakashima K, et al. New consensus research on neuropathological aspects of familial amyotrophic lateral sclerosis with superoxide

dismutase 1 (SOD1) gene mutations: inclusions containing SOD1 in neurons and astrocytes. Amyotroph Lateral Scler Other Motor Neuron Disord 2000;1(3):163-184.

14. Mori K, Weng SM, Arzberger T, et al. The C9orf72 GGGGCC repeat is translated into aggregating dipeptide-repeat proteins in FTLD/ALS. Science 2013;339(6125):1335-1338.

15. DeJesus-Hernandez M, Mackenzie IR, Boeve BF, et al. Expanded GGGGCC hexanucleotide repeat in noncoding region of C9ORF72 causes chromosome 9p-linked FTD and ALS. Neuron 2011;72(2):245-256.

16. Okamoto K, Hirai S, Shoji M, Senoh Y, Yamazaki T. Axonal swellings in the corticospinal tracts in amyotrophic lateral sclerosis. Acta Neuropathol 1990;80(2):222-226.

17. Smith MC. Nerve Fibre Degeneration in the Brain in Amyotrophic Lateral Sclerosis. J Neurol Neurosurg Psychiatry 1960;23(4):269-282.

18. Mukherjee A, Chakravarty A. Spasticity mechanisms - for the clinician. Front Neurol 2010;1:149.

19. Rothstein JD, Van Kammen M, Levey AI, Martin LJ, Kuncl RW. Selective loss of glial glutamate transporter GLT-1 in amyotrophic lateral sclerosis. Ann Neurol 1995;38(1):73-84.

20. Doble A. The pharmacology and mechanism of action of riluzole. Neurology 1996;47(6 Suppl 4):S233-241.

21. Vucic S, Ziemann U, Eisen A, Hallett M, Kiernan MC. Transcranial magnetic stimulation and amyotrophic lateral sclerosis: pathophysiological insights. J Neurol Neurosurg Psychiatry 2013;84(10):1161-1170.

22. Gurney ME, Pu H, Chiu AY, et al. Motor neuron degeneration in mice that express a human Cu,Zn superoxide dismutase mutation. Science 1994;264(5166):1772-1775.

23. Beal MF, Ferrante RJ, Browne SE, Matthews RT, Kowall NW, Brown RH, Jr. Increased 3-nitrotyrosine in both sporadic and familial amyotrophic lateral sclerosis. Ann Neurol 1997;42(4):644-654.

24. Ferrante RJ, Browne SE, Shinobu LA, et al. Evidence of increased oxidative damage in both sporadic and familial amyotrophic lateral sclerosis. J Neurochem 1997;69(5):2064-2074.

25. Yoshino H, Kimura A. Investigation of the therapeutic effects of edaravone, a free radical scavenger, on amyotrophic lateral sclerosis (Phase II study). Amyotroph Lateral Scler 2006;7(4):241-245.

26. Carri MT, Valle C, Bozzo F, Cozzolino M. Oxidative stress and mitochondrial damage: importance in non-SOD1 ALS. Front Cell Neurosci 2015;9:41.

27. Sasaki S, Iwata M. Ultrastructural study of synapses in the anterior horn neurons of patients with amyotrophic lateral sclerosis. Neurosci Lett 1996;204(1-2):53-56.

28. Smith EF, Shaw PJ, De Vos KJ. The role of mitochondria in amyotrophic lateral sclerosis. Neurosci Lett 2017.

29. Philips T, Rothstein JD. Glial cells in amyotrophic lateral sclerosis. Exp Neurol 2014;262 Pt B:111-120.

30. Xiao S, McLean J, Robertson J. Neuronal intermediate filaments and ALS: a new look at an old question. Biochim Biophys Acta 2006;1762(11-12):1001-1012.

31. Kim HJ, Taylor JP. Lost in Transportation: Nucleocytoplasmic Transport Defects in ALS and Other Neurodegenerative Diseases. Neuron 2017;96(2):285-297.

32. Nonaka T, Masuda-Suzukake M, Arai T, et al. Prion-like properties of pathological TDP-43 aggregates from diseased brains. Cell Rep 2013;4(1):124-134.

33. Lee S, Kim HJ. Prion-like Mechanism in Amyotrophic Lateral Sclerosis: are Protein Aggregates the Key? Exp Neurobiol 2015;24(1):1-7.

34. Parvizi J, Coburn KL, Shillcutt SD, Coffey CE, Lauterbach EC, Mendez MF. Neuroanatomy of pathological laughing and crying: a report of the American Neuropsychiatric Association Committee on Research. J Neuropsychiatry Clin Neurosci 2009;21(1):75-87.

35. Ravits JM, La Spada AR. ALS motor phenotype heterogeneity, focality, and spread: deconstructing motor neuron degeneration. Neurology 2009;73(10):805-811.

36. Phukan J, Elamin M, Bede P, et al. The syndrome of cognitive impairment in amyotrophic lateral sclerosis: a population-based study. J Neurol Neurosurg Psychiatry 2012;83(1):102-108.

37. Renton AE, Majounie E, Waite A, et al. A hexanucleotide repeat expansion in C9ORF72 is the cause of chromosome 9p21-linked ALS-FTD. Neuron 2011;72(2):257-268.

38. Neumann M, Sampathu DM, Kwong LK, et al. Ubiquitinated TDP-43 in frontotemporal lobar degeneration and amyotrophic lateral sclerosis. Science 2006;314(5796):130-133.

39. Cedarbaum JM, Stambler N, Malta E, et al. The ALSFRS-R: a revised ALS functional rating scale that incorporates assessments of respiratory function. BDNF ALS Study Group (Phase III). J Neurol Sci 1999;169(1-2):13-21.

40. Bedlack RS, Vaughan T, Wicks P, et al. How common are ALS plateaus and reversals? Neurology 2016;86(9):808-812.

41. Gordon PH, Cheng B, Salachas F, et al. Progression in ALS is not linear but is curvilinear. J Neurol 2010;257(10):1713-1717.

42. Roche JC, Rojas-Garcia R, Scott KM, et al. A proposed staging system for amyotrophic lateral sclerosis. Brain 2012;135(Pt 3):847-852.

43. Balendra R, Jones A, Jivraj N, et al. Estimating clinical stage of amyotrophic lateral sclerosis from the ALS Functional Rating Scale. Amyotroph Lateral Scler Frontotemporal Degener 2014;15(3-4):279-284.

44. Abrahams S, Newton J, Niven E, Foley J, Bak TH. Screening for cognition and behaviour changes in ALS. Amyotroph Lateral Scler Frontotemporal Degener 2014;15(1-2):9-14.

45. Hahn EL. Spin Echoes. Physical Review 1950;80(4):580-594.

46. Carr HY, Purcell EM. Effects of Diffusion on Free Precession in Nuclear Magnetic Resonance Experiments. Physical Review 1954;94(3):630-638.

47. Frahm J, Merboldt KD, Hänicke W, Haase A. Stimulated echo imaging. Journal of Magnetic Resonance (1969) 1985;64(1):81-93.

48. Garwood M, DelaBarre L. The return of the frequency sweep: designing adiabatic pulses for contemporary NMR. J Magn Reson 2001;153(2):155-177.

49. Scheenen TW, Klomp DW, Wijnen JP, Heerschap A. Short echo time 1H-MRSI of the human brain at 3T with minimal chemical shift displacement errors using adiabatic refocusing pulses. Magn Reson Med 2008;59(1):1-6.

50. Tkáč I, Gruetter R. Methodology of H NMR Spectroscopy of the Human Brain at Very High Magnetic Fields. Appl Magn Reson 2005;29(1):139-157.

51. Gruetter R. Automatic, localized in vivo adjustment of all first- and second-order shim coils. Magn Reson Med 1993;29(6):804-811.

52. Öz G, Alger JR, Barker PB, et al. Clinical proton MR spectroscopy in central nervous system disorders. Radiology 2014;270(3):658-679.

53. Michaeli S, Garwood M, Zhu XH, et al. Proton T2 relaxation study of water, N-acetylaspartate, and creatine in human brain using Hahn and Carr-Purcell spin echoes at 4T and 7T. Magn Reson Med 2002;47(4):629-633.

54. Deelchand DK, Henry PG, Marjańska M. Effect of Carr-Purcell refocusing pulse trains on transverse relaxation times of metabolites in rat brain at 9.4 Tesla. Magn Reson Med 2015;73(1):13-20.

55. Provencher SW. Estimation of metabolite concentrations from localized in vivo proton NMR spectra. Magn Reson Med 1993;30(6):672-679.

56. Schaller B, Xin L, Gruetter R. Is the macromolecule signal tissue-specific in healthy human brain? A (1)H MRS study at 7 Tesla in the occipital lobe. Magn Reson Med 2014;72(4):934-940.

57. Rigotti DJ, Inglese M, Babb JS, et al. Serial whole-brain N-acetylaspartate concentration in healthy young adults. AJNR Am J Neuroradiol 2007;28(9):1650-1651.

58. Miyake M, Kakimoto Y, Sorimachi M. A gas chromatographic method for the determination of N-acetyl-L-aspartic acid, N-acetyl-alpha-aspartylglutamic acid and beta-citryl-L-glutamic acid and their distributions in the brain and other organs of various species of animals. J Neurochem 1981;36(3):804-810.

59. Moffett JR, Namboodiri MA, Cangro CB, Neale JH. Immunohistochemical localization of N-acetylaspartate in rat brain. Neuroreport 1991;2(3):131-134.

60. Simmons ML, Frondoza CG, Coyle JT. Immunocytochemical localization of N-acetyl-aspartate with monoclonal antibodies. Neuroscience 1991;45(1):37-45.

61. Urenjak J, Williams SR, Gadian DG, Noble M. Specific expression of N-acetylaspartate in neurons, oligodendrocyte-type-2 astrocyte progenitors, and immature oligodendrocytes in vitro. J Neurochem 1992;59(1):55-61.

62. Moffett JR. N-acetylaspartate : a unique neuronal molecule in the central nervous system. Adv Exp Med Biol. 2006, New York; Springer. p.

63. Ariyannur PS, Moffett JR, Manickam P, et al. Methamphetamine-induced neuronal protein NAT8L is the NAA biosynthetic enzyme: implications for specialized acetyl coenzyme A metabolism in the CNS. Brain Res 2010;1335:1-13.

64. Wiame E, Tyteca D, Pierrot N, et al. Molecular identification of aspartate N-acetyltransferase and its mutation in hypoacetylaspartia. Biochem J 2009;425(1):127-136.

65. Rothstein JD, Tsai G, Kuncl RW, et al. Abnormal excitatory amino acid metabolism in amyotrophic lateral sclerosis. Ann Neurol 1990;28(1):18-25.

66. Pouwels PJ, Frahm J. Differential distribution of NAA and NAAG in human brain as determined by quantitative localized proton MRS. NMR Biomed 1997;10(2):73-78.

67. Govindaraju V, Young K, Maudsley AA. Proton NMR chemical shifts and coupling constants for brain metabolites. NMR Biomed 2000;13(3):129-153.

68. Glanville NT, Byers DM, Cook HW, Spence MW, Palmer FB. Differences in the metabolism of inositol and phosphoinositides by cultured cells of neuronal and glial origin. Biochim Biophys Acta 1989;1004(2):169-179.

69. Brand A, Richter-Landsberg C, Leibfritz D. Multinuclear NMR studies on the energy metabolism of glial and neuronal cells. Dev Neurosci 1993;15(3-5):289-298.

70. Fisher SK, Novak JE, Agranoff BW. Inositol and higher inositol phosphates in neural tissues: homeostasis, metabolism and functional significance. J Neurochem 2002;82(4):736-754.

71. Jackson PS, Strange K. Volume-sensitive anion channels mediate swelling-activated inositol and taurine efflux. Am J Physiol 1993;265(6 Pt 1):C1489-1500.

72. Epand RM. Features of the Phosphatidylinositol Cycle and its Role in Signal Transduction. J Membr Biol 2017;250(4):353-366.

73. Karaca M, Frigerio F, Migrenne S, et al. GDH-Dependent Glutamate Oxidation in the Brain Dictates Peripheral Energy Substrate Distribution. Cell Rep 2015;13(2):365-375.

74. Cheung NS, Pascoe CJ, Giardina SF, John CA, Beart PM. Micromolar L-glutamate induces extensive apoptosis in an apoptotic-necrotic continuum of insult-dependent, excitotoxic injury in cultured cortical neurones. Neuropharmacology 1998;37(10-11):1419-1429.

75. Tsai GC, Stauch-Slusher B, Sim L, et al. Reductions in acidic amino acids and N-acetylaspartylglutamate in amyotrophic lateral sclerosis CNS. Brain Res 1991;556(1):151-156.

76. Perry TL, Krieger C, Hansen S, Eisen A. Amyotrophic lateral sclerosis: amino acid levels in plasma and cerebrospinal fluid. Ann Neurol 1990;28(1):12-17.

77. Marsman A, van den Heuvel MP, Klomp DW, Kahn RS, Luijten PR, Hulshoff Pol HE. Glutamate in schizophrenia: a focused review and meta-analysis of (1)H-MRS studies. Schizophr Bull 2013;39(1):120-129.

78. Lei H, Dirren E, Poitry-Yamate C, Schneider BL, Gruetter R, Aebischer P. Evolution of the neurochemical profiles in the G93A-SOD1 mouse model of amyotrophic lateral sclerosis. J Cereb Blood Flow Metab 2018:271678X18756499.

79. Bae JS, Simon NG, Menon P, Vucic S, Kiernan MC. The puzzling case of hyperexcitability in amyotrophic lateral sclerosis. J Clin Neurol 2013;9(2):65-74.

80. Rothman DL, Petroff OA, Behar KL, Mattson RH. Localized 1H NMR measurements of gamma-aminobutyric acid in human brain in vivo. Proc Natl Acad Sci U S A 1993;90(12):5662-5666.

81. Dringen R. Metabolism and functions of glutathione in brain. Prog Neurobiol 2000;62(6):649-671.

82. Terpstra M, Henry PG, Gruetter R. Measurement of reduced glutathione (GSH) in human brain using LCModel analysis of difference-edited spectra. Magn Reson Med 2003;50(1):19-23.

83. Tkáč I, Öz G, Adriany G, Uğurbil K, Gruetter R. In vivo 1H NMR spectroscopy of the human brain at high magnetic fields: metabolite quantification at 4T vs. 7T. Magn Reson Med 2009;62(4):868-879.

84. Pioro EP, Antel JP, Cashman NR, Arnold DL. Detection of cortical neuron loss in motor neuron disease by proton magnetic resonance spectroscopic imaging in vivo. Neurology 1994;44(10):1933-1938.

85. Atassi N, Xu M, Triantafyllou C, et al. Ultra high-field (7tesla) magnetic resonance spectroscopy in Amyotrophic Lateral Sclerosis. PLoS One 2017;12(5):e0177680.

86. Bowen BC, Pattany PM, Bradley WG, et al. MR imaging and localized proton spectroscopy of the precentral gyrus in amyotrophic lateral sclerosis. AJNR Am J Neuroradiol 2000;21(4):647-658.

87. Chan S, Shungu DC, Douglas-Akinwande A, Lange DJ, Rowland LP. Motor neuron diseases: comparison of single-voxel proton MR spectroscopy of the motor cortex with MR imaging of the brain. Radiology 1999;212(3):763-769.

88. Foerster BR, Pomper MG, Callaghan BC, et al. An imbalance between excitatory and inhibitory neurotransmitters in amyotrophic lateral sclerosis revealed by use of 3-T proton magnetic resonance spectroscopy. JAMA Neurol 2013;70(8):1009-1016.

89. Gredal O, Rosenbaum S, Topp S, Karlsborg M, Strange P, Werdelin L. Quantification of brain metabolites in amyotrophic lateral sclerosis by localized proton magnetic resonance spectroscopy. Neurology 1997;48(4):878-881.

90. Han J, Ma L. Study of the features of proton MR spectroscopy ((1)H-MRS) on amyotrophic lateral sclerosis. J Magn Reson Imaging 2010;31(2):305-308.

91. Kalra S, Hanstock CC, Martin WR, Allen PS, Johnston WS. Detection of cerebral degeneration in amyotrophic lateral sclerosis using high-field magnetic resonance spectroscopy. Arch Neurol 2006;63(8):1144-1148.

92. Kalra S, Tai P, Genge A, Arnold DL. Rapid improvement in cortical neuronal integrity in amyotrophic lateral sclerosis detected by proton magnetic resonance spectroscopic imaging. J Neurol 2006;253(8):1060-1063.

93. Mitsumoto H, Ulug AM, Pullman SL, et al. Quantitative objective markers for upper and lower motor neuron dysfunction in ALS. Neurology 2007;68(17):1402-1410.

94. Pohl C, Block W, Karitzky J, et al. Proton magnetic resonance spectroscopy of the motor cortex in 70 patients with amyotrophic lateral sclerosis. Arch Neurol 2001;58(5):729-735.

95. Rooney WD, Miller RG, Gelinas D, Schuff N, Maudsley AA, Weiner MW. Decreased N-acetylaspartate in motor cortex and corticospinal tract in ALS. Neurology 1998;50(6):1800-1805.

96. van der Graaff MM, Lavini C, Akkerman EM, et al. MR spectroscopy findings in early stages of motor neuron disease. AJNR Am J Neuroradiol 2010;31(10):1799-1806.

97. Wang S, Poptani H, Woo JH, et al. Amyotrophic lateral sclerosis: diffusion-tensor and chemical shift MR imaging at 3.0 T. Radiology 2006;239(3):831-838.

98. Weiduschat N, Mao X, Hupf J, et al. Motor cortex glutathione deficit in ALS measured in vivo with the J-editing technique. Neurosci Lett 2014;570:102-107.

99. Kalra S, Vitale A, Cashman NR, Genge A, Arnold DL. Cerebral degeneration predicts survival in amyotrophic lateral sclerosis. J Neurol Neurosurg Psychiatry 2006;77(11):1253-1255.

100. Miller BL. A review of chemical issues in 1H NMR spectroscopy: N-acetyl-L-aspartate, creatine and choline. NMR Biomed 1991;4(2):47-52.

101. Ellis CM, Simmons A, Andrews C, Dawson JM, Williams SC, Leigh PN. A proton magnetic resonance spectroscopic study in ALS: correlation with clinical findings. Neurology 1998;51(4):1104-1109.

102. Rule RR, Suhy J, Schuff N, Gelinas DF, Miller RG, Weiner MW. Reduced NAA in motor and non-motor brain regions in amyotrophic lateral sclerosis: a cross-sectional and longitudinal study. Amyotroph Lateral Scler Other Motor Neuron Disord 2004;5(3):141-149.

103. Unrath A, Ludolph AC, Kassubek J. Brain metabolites in definite amyotrophic lateral sclerosis. A longitudinal proton magnetic resonance spectroscopy study. J Neurol 2007;254(8):1099-1106.

104. Kalra S, Seres P, Choi C. In vivo quantification of excitatory and inhibitory neurotransmitters in amyotrophic lateral sclerosis. Proceedings of the International Society of Magnetic Resonance in Medicine 2013.

105. Govind V, Sharma KR, Maudsley AA, Arheart KL, Saigal G, Sheriff S. Comprehensive evaluation of corticospinal tract metabolites in amyotrophic lateral sclerosis using whole-brain 1H MR spectroscopy. PLoS One 2012;7(4):e35607.

106. Stagg CJ, Knight S, Talbot K, Jenkinson M, Maudsley AA, Turner MR. Whole-brain magnetic resonance spectroscopic imaging measures are related to disability in ALS. Neurology 2013;80(7):610-615.

107. Bradley WG, Bowen BC, Pattany PM, Rotta F. 1H-magnetic resonance spectroscopy in amyotrophic lateral sclerosis. J Neurol Sci 1999;169(1-2):84-86.

108. Cwik VA, Hanstock CC, Allen PS, Martin WR. Estimation of brainstem neuronal loss in amyotrophic lateral sclerosis with in vivo proton magnetic resonance spectroscopy. Neurology 1998;50(1):72-77.

109. Pioro EP, Majors AW, Mitsumoto H, Nelson DR, Ng TC. 1H-MRS evidence of neurodegeneration and excess glutamate + glutamine in ALS medulla. Neurology 1999;53(1):71-79.

110. Carew JD, Nair G, Andersen PM, et al. Presymptomatic spinal cord neurometabolic findings in SOD1-positive people at risk for familial ALS. Neurology 2011;77(14):1370-1375.

111. Ikeda K, Murata K, Kawase Y, et al. Relationship between cervical cord 1H-magnetic resonance spectroscopy and clinoco-electromyographic profile in amyotrophic lateral sclerosis. Muscle Nerve 2013;47(1):61-67.

112. Bednarik P, Moheet A, Deelchand DK, et al. Feasibility and reproducibility of neurochemical profile quantification in the human hippocampus at 3 T. NMR Biomed 2015;28(6):685-693.

113. Deelchand DK, Adanyeguh IM, Emir UE, et al. Two-site reproducibility of cerebellar and brainstem neurochemical profiles with short-echo, single-voxel MRS at 3T. Magn Reson Med 2015;73(5):1718-1725.

114. van de Bank BL, Emir UE, Boer VO, et al. Multi-center reproducibility of neurochemical profiles in the human brain at 7 T. NMR Biomed 2015;28(3):306-316.

115. Öz G, Tkáč I. Short-echo, single-shot, full-intensity proton magnetic resonance spectroscopy for neurochemical profiling at 4 T: validation in the cerebellum and brainstem. Magn Reson Med 2011;65(4):901-910.

116. Terpstra M, Cheong I, Lyu T, et al. Test-retest reproducibility of neurochemical profiles with short-echo, single-voxel MR spectroscopy at 3T and 7T. Magn Reson Med 2016;76(4):1083-1091.

117. Deelchand DK, Iltis I, Henry PG. Improved quantification precision of human brain short echo-time (1) H magnetic resonance spectroscopy at high magnetic field: a simulation study. Magn Reson Med 2014;72(1):20-25.

118. Mekle R, Mlynarik V, Gambarota G, Hergt M, Krueger G, Gruetter R. MR spectroscopy of the human brain with enhanced signal intensity at ultrashort echo times on a clinical platform at 3T and 7T. Magn Reson Med 2009;61(6):1279-1285.

119. Bartha R, Drost DJ, Menon RS, Williamson PC. Comparison of the quantification precision of human short echo time (1)H spectroscopy at 1.5 and 4.0 Tesla. Magn Reson Med 2000;44(2):185-192.

120. Brooks WM, Friedman SD, Stidley CA. Reproducibility of 1H-MRS in vivo. Magn Reson Med 1999;41(1):193-197.

121. Geurts JJ, Barkhof F, Castelijns JA, Uitdehaag BM, Polman CH, Pouwels PJ. Quantitative 1H-MRS of healthy human cortex, hippocampus, and thalamus: metabolite concentrations, quantification precision, and reproducibility. J Magn Reson Imaging 2004;20(3):366-371.

122. Hammen T, Stadlbauer A, Tomandl B, et al. Short TE single-voxel 1H-MR spectroscopy of hippocampal structures in healthy adults at 1.5 Tesla--how reproducible are the results? NMR Biomed 2005;18(3):195-201.

123. Kirov, II, George IC, Jayawickrama N, Babb JS, Perry NN, Gonen O. Longitudinal inter- and intra-individual human brain metabolic quantification over 3 years with proton MR spectroscopy at 3 T. Magn Reson Med 2012;67(1):27-33.

124. Schirmer T, Auer DP. On the reliability of quantitative clinical magnetic resonance spectroscopy of the human brain. NMR Biomed 2000;13(1):28-36.

125. Stephenson MC, Gunner F, Napolitano A, et al. Applications of multi-nuclear magnetic resonance spectroscopy at 7T. World J Radiol 2011;3(4):105-113.

126. Träber F, Block W, Freymann N, et al. A multicenter reproducibility study of single-voxel 1H-MRS of the medial temporal lobe. Eur Radiol 2006;16(5):1096-1103.

127. Pradhan S, Bonekamp S, Gillen JS, et al. Comparison of single voxel brain MRS AT 3T and 7T using 32-channel head coils. Magn Reson Imaging 2015;33(8):1013-1018.

128. Bednařík P, Moheet A, Deelchand DK, et al. Feasibility and reproducibility of neurochemical profile quantification in the human hippocampus at 3 T. NMR Biomed 2015;28(6):685-693.

129. Near J, Andersson J, Maron E, et al. Unedited in vivo detection and quantification of gamma-aminobutyric acid in the occipital cortex using short-TE MRS at 3 T. NMR Biomed 2013;26(11):1353-1362.

130. Wijtenburg SA, Gaston FE, Spieker EA, et al. Reproducibility of phase rotation STEAM at 3T: focus on glutathione. Magn Reson Med 2014;72(3):603-609.

131. Bednařík P, Tkáč I, Giove F, et al. Neurochemical and BOLD responses during neuronal activation measured in the human visual cortex at 7 Tesla. J Cereb Blood Flow Metab 2015;35(4):601-610.

132. Boer VO, Siero JC, Hoogduin H, van Gorp JS, Luijten PR, Klomp DW. High-field MRS of the human brain at short TE and TR. NMR Biomed 2011;24(9):1081-1088.

133. Emir UE, Auerbach EJ, Van De Moortele PF, et al. Regional neurochemical profiles in the human brain measured by (1)H MRS at 7 T using local B(1) shimming. NMR Biomed 2012;25(1):152-160.

134. Marjańska M, Auerbach EJ, Valabregue R, Van de Moortele PF, Adriany G, Garwood M. Localized 1H NMR spectroscopy in different regions of human brain in vivo at 7 T: T2 relaxation times and concentrations of cerebral metabolites. NMR Biomed 2012;25(2):332-339.

135. van de Bank BL, Emir UE, Boer VO, et al. Multi-center reproducibility of neurochemical profiles in the human brain at 7 T. NMR Biomed 2015;28(3):306-316.

136. Leech R, Sharp DJ. The role of the posterior cingulate cortex in cognition and disease. Brain 2014;137(Pt 1):12-32.

137. Broyd SJ, Demanuele C, Debener S, Helps SK, James CJ, Sonuga-Barke EJ. Default-mode brain dysfunction in mental disorders: a systematic review. Neurosci Biobehav Rev 2009;33(3):279-296.

138. Murray ME, Przybelski SA, Lesnick TG, et al. Early Alzheimer's disease neuropathology detected by proton MR spectroscopy. J Neurosci 2014;34(49):16247-16255.

139. Öz G. MR Spectroscopy in Health and Disease. In: Handbook of the Cerebellum and Cerebellar Disorders. Volume 1., ed. G.D. Manto M, Schmahmann JD, Koibuchi N, Rossi F. 2013; Dordrecht: Springer. p. 713-733.

140. Adriany G, Van de Moortele PF, Ritter J, et al. A geometrically adjustable 16-channel transmit/receive transmission line array for improved RF efficiency and parallel imaging performance at 7 Tesla. Magn Reson Med 2008;59(3):590-597.

141. Gruetter R, Tkac I. Field mapping without reference scan using asymmetric echo-planar techniques. Magn Reson Med 2000;43(2):319-323.

142. Ernst TK, R.; Ross, B. D. Absolute quantitation of water and metabolites in the human brain. I. Compartments and water. . J Magn Reson 1993;(102):1-8.

143. Deelchand DK, Henry PG, Uğurbil K, Marjańska M. Measurement of transverse relaxation times of J-coupled metabolites in the human visual cortex at 4 T. Magn Reson Med 2012;67(4):891-897.

144. Tkáč I. Refinement of simulated basis set for LCModel analysis. 16th Scientific Meeting of the ISMRM 2008; Toronto, Canada. p.1624.

145. Snoussi K, Gillen JS, Horska A, et al. Comparison of brain gray and white matter macromolecule resonances at 3 and 7 Tesla. Magn Reson Med 2015;74(3):607-613.

146. Siegel GJ. Basic Neurochemistry: Molecular, Cellular, and Medical Aspects. 6th ed. 1999; Philadelphia: Lippincott-Raven Publishers. p.

147. Provencher SW. LCModel & LCMgui User's Manual. 2001.

148. Vangel MG. Confidence intervals for a normal coefficient of variation. Am Stat 1996;50(1):21-26.

149. Hoult DI. Rotating frame zeugmatography. Philos Trans R Soc Lond B Biol Sci 1980;289(1037):543-547.

150. Kreis R. The trouble with quality filtering based on relative Cramer-Rao lower bounds. Magn Reson Med 2016;75(1):15-18.

151. Wijtenburg SA, Rowland LM, Edden RA, Barker PB. Reproducibility of brain spectroscopy at 7T using conventional localization and spectral editing techniques. J Magn Reson Imaging 2013;38(2):460-467.

152. Marjańska M, Emir UE, Deelchand DK, Terpstra M. Faster metabolite (1)H transverse relaxation in the elder human brain. PLoS One 2013;8(10):e77572.

153. Öngür D, Prescot AP, Jensen JE, et al. T2 relaxation time abnormalities in bipolar disorder and schizophrenia. Magn Reson Med 2010;63(1):1-8.

154. Emir UE, Deelchand D, Henry PG, Terpstra M. Noninvasive quantification of T2 and concentrations of ascorbate and glutathione in the human brain from the same double-edited spectra. NMR Biomed 2011;24(3):263-269.

155. Zaaraoui W, Fleysher L, Fleysher R, Liu S, Soher BJ, Gonen O. Human brain-structure resolved T(2) relaxation times of proton metabolites at 3 Tesla. Magn Reson Med 2007;57(6):983-989.

156. Park YW, Deelchand DK, Joers JM, et al. AutoVOI: real-time automatic prescription of volume-of-interest for single voxel spectroscopy. Magn Reson Med 2018.

157. Cheong I, Marjańska M, Deelchand DK, Eberly LE, Walk D, Öz G. Ultra-High Field Proton MR Spectroscopy in Early-Stage Amyotrophic Lateral Sclerosis. Neurochem Res 2017;42(6):1833-1844.

158. Kiernan MC, Vucic S, Cheah BC, et al. Amyotrophic lateral sclerosis. Lancet 2011;377(9769):942-955.

159. Bensimon G, Lacomblez L, Meininger V. A controlled trial of riluzole in amyotrophic lateral sclerosis. ALS/Riluzole Study Group. N Engl J Med 1994;330(9):585-591.

160. Turner MR, Kiernan MC, Leigh PN, Talbot K. Biomarkers in amyotrophic lateral sclerosis. Lancet Neurol 2009;8(1):94-109.

161. Turner MR, Verstraete E. What does imaging reveal about the pathology of amyotrophic lateral sclerosis? Curr Neurol Neurosci Rep 2015;15(7):45.

162. Barber SC, Shaw PJ. Oxidative stress in ALS: key role in motor neuron injury and therapeutic target. Free Radic Biol Med 2010;48(5):629-641.

163. Brooks BR, Miller RG, Swash M, Munsat TL, World Federation of Neurology Research Group on Motor Neuron D. El Escorial revisited: revised criteria for the diagnosis of amyotrophic lateral sclerosis. Amyotroph Lateral Scler Other Motor Neuron Disord 2000;1(5):293-299.

164. Woo JH, Wang S, Melhem ER, et al. Linear associations between clinically assessed upper motor neuron disease and diffusion tensor imaging metrics in amyotrophic lateral sclerosis. PLoS One 2014;9(8):e105753.

165. Mescher M, Merkle H, Kirsch J, Garwood M, Gruetter R. Simultaneous in vivo spectral editing and water suppression. NMR Biomed 1998;11(6):266-272.

166. Marjanska M, Lehericy S, Valabregue R, et al. Brain dynamic neurochemical changes in dystonic patients: a magnetic resonance spectroscopy study. Mov Disord 2013;28(2):201-209.

167. Deelchand DK, Adanyeguh IM, Emir UE, et al. Two-site reproducibility of cerebellar and brainstem neurochemical profiles with short-echo, single-voxel MRS at 3T. Magn Reson Med 2014.

168. Tkac I. Refinement of Simulated Basis Set for LCModel Analysis. In Proceedings of the 16th Annual Meeting of ISMRM, Toronto, Ontario, Canada, 2008, p. 1624.

169. Rooney WD, Johnson G, Li X, et al. Magnetic field and tissue dependencies of human brain longitudinal 1H2O relaxation in vivo. Magn Reson Med 2007;57(2):308-318.

170. Wansapura JP, Holland SK, Dunn RS, Ball WS, Jr. NMR relaxation times in the human brain at 3.0 tesla. J Magn Reson Imaging 1999;9(4):531-538.

171. Holm S. A Simple Sequentially Rejective Bonferroni Test Procedure. Scandinavian Journal of Statistics 1979;6:65-70.

172. Atassi N, Triantanfyllou C, Keil B, et al. Ultra High-Field (7T) Magnetic Resonance Spectroscopy (MRS) in People with Amyotrophic Lateral Sclerosis (ALS). Proceedings of the International Society of Magnetic Resonance in Medicine 2013.

173. Emir UE, Tuite PJ, Oz G. Elevated pontine and putamenal GABA levels in mild-moderate Parkinson disease detected by 7 tesla proton MRS. PLoS One 2012;7(1):e30918.

174. Ratai E, Kok T, Wiggins C, et al. Seven-Tesla proton magnetic resonance spectroscopic imaging in adult X-linked adrenoleukodystrophy. Arch Neurol 2008;65(11):1488-1494.

175. Unschuld PG, Edden RA, Carass A, et al. Brain metabolite alterations and cognitive dysfunction in early Huntington's disease. Mov Disord 2012;27(7):895-902.

176. Brandt AS, Unschuld PG, Pradhan S, et al. Age-related changes in anterior cingulate cortex glutamate in schizophrenia: A (1)H MRS Study at 7 Tesla. Schizophr Res 2016;172(1-3):101-105.

177. van den Bogaard SJ, Dumas EM, Teeuwisse WM, et al. Longitudinal metabolite changes in Huntington's disease during disease onset. J Huntingtons Dis 2014;3(4):377-386.

178. Atassi N, Xu M, Triantanfyllou C, et al. Biochemical Characteristics in Amyotrophic Lateral Sclerosis Detected by 7T MR Spectroscopy. Proceedings of the International Society of Magnetic Resonance in Medicine 2016.

179. Voevodskaya O, Sundgren PC, Strandberg O, et al. Myo-inositol changes precede amyloid pathology and relate to APOE genotype in Alzheimer disease. Neurology 2016;86(19):1754-1761.

180. Sturrock A, Laule C, Wyper K, et al. A longitudinal study of magnetic resonance spectroscopy Huntington's disease biomarkers. Mov Disord 2015;30(3):393-401.

181. Iltis I, Hutter D, Bushara KO, et al. (1)H MR spectroscopy in Friedreich's ataxia and ataxia with oculomotor apraxia type 2. Brain Res 2010;1358:200-210.

182. Oz G, Hutter D, Tkac I, et al. Neurochemical alterations in spinocerebellar ataxia type 1 and their correlations with clinical status. Mov Disord 2010;25(9):1253-1261.

183. Alshikho MJ, Zurcher NR, Loggia ML, et al. Glial activation colocalizes with structural abnormalities in amyotrophic lateral sclerosis. Neurology 2016;87(24):2554-2561.

184. Lavisse S, Guillermier M, Herard AS, et al. Reactive astrocytes overexpress TSPO and are detected by TSPO positron emission tomography imaging. J Neurosci 2012;32(32):10809-10818.

185. Zurcher NR, Loggia ML, Lawson R, et al. Increased in vivo glial activation in patients with amyotrophic lateral sclerosis: assessed with [(11)C]-PBR28. Neuroimage Clin 2015;7:409-414.

186. Ratai E, Alshikho M, Zurcher N, et al. Glial Activation Measured by [11C]-PBR28 PET Correlates with 1H-MRS Brain Metabolites in Amyotrophic Lateral Sclerosis. 27th International Symposium on ALS/MND 2016.

187. Usman U, Choi C, Camicioli R, et al. Mesial prefrontal cortex degeneration in amyotrophic lateral sclerosis: a high-field proton MR spectroscopy study. AJNR Am J Neuroradiol 2011;32(9):1677-1680.

188. Schott JM, Frost C, MacManus DG, Ibrahim F, Waldman AD, Fox NC. Short echo time proton magnetic resonance spectroscopy in Alzheimer's disease: a longitudinal multiple time point study. Brain 2010;133(11):3315-3322.

189. Sturrock A, Laule C, Decolongon J, et al. Magnetic resonance spectroscopy biomarkers in premanifest and early Huntington disease. Neurology 2010;75(19):1702-1710.

190. Foerster BR, Carlos RC, Dwamena BA, et al. Multimodal MRI as a diagnostic biomarker for amyotrophic lateral sclerosis. Ann Clin Transl Neurol 2014;1(2):107-114.

191. Simon NG, Turner MR, Vucic S, et al. Quantifying disease progression in amyotrophic lateral sclerosis. Ann Neurol 2014;76(5):643-657.

192. Kimura F, Fujimura C, Ishida S, et al. Progression rate of ALSFRS-R at time of diagnosis predicts survival time in ALS. Neurology 2006;66(2):265-267.

193. Verstraete E, Foerster BR. Neuroimaging as a New Diagnostic Modality in Amyotrophic Lateral Sclerosis. Neurotherapeutics 2015;12(2):403-416.

194. Radford RA, Morsch M, Rayner SL, Cole NJ, Pountney DL, Chung RS. The established and emerging roles of astrocytes and microglia in amyotrophic lateral sclerosis and frontotemporal dementia. Front Cell Neurosci 2015;9:414.

195. Swash M. Why are upper motor neuron signs difficult to elicit in amyotrophic lateral sclerosis? J Neurol Neurosurg Psychiatry 2012;83(6):659-662.

196. Chio A, Logroscino G, Hardiman O, et al. Prognostic factors in ALS: A critical review. Amyotroph Lateral Scler 2009;10(5-6):310-323.

197. Kantarci K, Weigand SD, Przybelski SA, et al. MRI and MRS predictors of mild cognitive impairment in a population-based sample. Neurology 2013;81(2):126-133.

198. Waragai M, Moriya M, Nojo T. Decreased N-Acetyl Aspartate/Myo-Inositol Ratio in the Posterior Cingulate Cortex Shown by Magnetic Resonance Spectroscopy May Be

One of the Risk Markers of Preclinical Alzheimer's Disease: A 7-Year Follow-Up Study. J Alzheimers Dis 2017;60(4):1411-1427.

199. Van Den Bosch L, Van Damme P, Bogaert E, Robberecht W. The role of excitotoxicity in the pathogenesis of amyotrophic lateral sclerosis. Biochim Biophys Acta 2006;1762(11-12):1068-1082.

200. Danbolt NC. Glutamate uptake. Prog Neurobiol 2001;65(1):1-105.

201. Ramadan S, Lin A, Stanwell P. Glutamate and glutamine: a review of in vivo MRS in the human brain. NMR Biomed 2013;26(12):1630-1646.

202. Schluchter MD. Estimating correlation between alternative measures of disease progression in a longitudinal study. Modification of Diet in Renal Disease Study. Stat Med 1990;9(10):1175-1188.

203. Qureshi M, Schoenfeld DA, Paliwal Y, Shui A, Cudkowicz ME. The natural history of ALS is changing: improved survival. Amyotroph Lateral Scler 2009;10(5-6):324-331.

204. Ong ML, Tan PF, Holbrook JD. Predicting functional decline and survival in amyotrophic lateral sclerosis. PLoS One 2017;12(4):e0174925.

205. Menke RA, Agosta F, Grosskreutz J, Filippi M, Turner MR. Neuroimaging Endpoints in Amyotrophic Lateral Sclerosis. Neurotherapeutics 2017;14(1):11-23.

206. Ding XQ, Maudsley AA, Sabati M, Sheriff S, Dellani PR, Lanfermann H. Reproducibility and reliability of short-TE whole-brain MR spectroscopic imaging of human brain at 3T. Magn Reson Med 2015;73(3):921-928.

207. Braak H, Brettschneider J, Ludolph AC, Lee VM, Trojanowski JQ, Del Tredici K. Amyotrophic lateral sclerosis--a model of corticofugal axonal spread. Nat Rev Neurol 2013;9(12):708-714.

208. Cardenas-Blanco A, Machts J, Acosta-Cabronero J, et al. Structural and diffusion imaging versus clinical assessment to monitor amyotrophic lateral sclerosis. Neuroimage Clin 2016;11:408-414.

APPENDICES

Appendix 1. ALS Functional Rating Scale-Revised Form [39]

1. Speech
   4 – Normal Speech processes
   3 – Detectable speech with disturbances
   2 – Intelligible with repeating
   1 – Speech combined with nonvocal communication
   0 – Loss of useful speech

2. Salivation
   4 – Normal
   3 – Slight but definite excess of saliva in mouth; may have nighttime drooling
   2 – Moderately excessive saliva; may have minimal drooling
   1 – Marked excess of saliva with some drooling
   0 – Marked drooling; requires constant tissue or handkerchief

3. Swallowing
   4 – Normal eating habits
   3 – Early eating problems – occasional choking
   2 – Dietary consistency changes
   1 – Needs supplemental tube feeding
   0 – NPO (exclusively parenteral or enteral feeding)

4. Handwriting
   4 – Normal
   3 – Slow or sloppy; all words are legible
   2 – Not all words are legible
   1 – Able to grip pen but unable to write
   0 – Unable to grip pen

5. Does subject have gastrostomy?
   No – Answer 5a
   Yes – Answer 5b

a. Cutting Food and Handling Utensils (patients without gastrostomy)
   4 – Normal
   3 – Somewhat slow and clumsy, but no help needed
   2 – Can cut most foods, although clumsy and slow; some help needed
   1 – Food must be cut by someone, but can still feed slowly
   0 – Needs to be fed

b. Cutting Food and Handling Utensils (alternate scale for patients with gastrostomy)
   4 – Normal
   3 – Clumsy but able to perform all manipulations independently
   2 – Some help needed with closures and fasteners
   1 – Provides minimal assistance to caregivers
   0 – Unable to perform any aspect of task

6. Dressing and Hygiene
   4 – Normal function

3 – Independent and complete self-care with effort or decreased efficiency
2 – Intermittent assistance or substitute methods
1 – Needs attendant for self-care
0 – Total dependence

7. Turning in bed and adjusting bed clothes
4 – Normal
3 – Somewhat slow and clumsy, but no help needed
2 – Can turn alone or adjust sheets, but with great difficulty
1 – Can initiate, but not turn or adjust sheets alone
0 – Helpless

8. Walking
4 – Normal
3 – Early ambulation difficulties
2 – Walks with assistance
1 – Nonambulatory functional movement only
0 – No purposeful leg movement

9. Climbing Stairs
4 – Normal
3 – Slow
2 – Mild unsteadiness or fatigue
1 – Needs assistance
0 – Cannot do

10. Dyspnea
4 – None
3 – Occurs when walking
2 – Occurs with one or more of the following: eating, bathing, dressing
1 – Occurs at rest, difficulty breathing when either sitting or lying
0 – Significant difficulty, considering using mechanical respiratory support

11. Orthopnea
4 – None
3 – Some difficulty sleeping at night due to shortness of breath, does not routinely use more than two pillows
2 – Needs extra pillow in order to sleep (more than two)
1 – Can only sleep sitting up
0 – Unable to sleep

12. Respiratory Insufficiency
4 – None
3 – Intermittent use of NIPPV
2 – Continuous use of NIPPV during the night
1 – Continuous use of NIPPV during the night and day
0 – Invasive mechanical ventilation by intubation or tracheostomy

Total Score for ALSFRS-R (0-48):
Total Score for ALSFRS-R Bulbar Questions 1, 2, 3 (0-12):
Total Score for ALSFRS-R Upper Limb Questions 4, 5, 6 (0-12):

Appendix 2. In-house-developed UMN Burden Scale

Score 1 point each for hyperreflexia and spasticity in each spinal cord segment. Laterality of deficits are not accounted for.

1. Bulbar
   Pathological brisk jaw jerk reflex (0-1)
   Slow tongue coordination (0-1)

2. Cervical
   Pathologically brisk biceps, triceps, brachioradialis, or finger flexor reflexes (0-1)
   Spasticity (0-1)

3. Lumbosacral
   Pathologically brisk patellar or ankle jerk reflexes or Babinski sign (0-1)
   Spasticity (0-1)

Total UMN Burden Score (0-6):
Total UMN Burden Score for Bulbar Only (0-2):
Total UMN Burden Score for Cervical Only (0-2):
Total UMN Burden Score for Lumbosacral Only (0-2):

Appendix 3. Modified Penn UMN Burden Scale [164]

Modifications to this established scale include the following:

- Binary scoring of spasticity (0-1) instead of Ashworth grading
- Omission of clonus, pseudobulbar affect, and palmomental sign

1. Bulbar
   Jaw Jerk (0-1)
   Facial Reflex (0-1)

2. Right Cervical
   Spasticity (0-1)
   Triceps Reflex (0-1)
   Biceps Reflex (0-1)
   Finger Flexors (0-1)
   Hoffman's Sign (0-1)

3. Left Cervical
   Spasticity (0-1)
   Triceps Reflex (0-1)
   Biceps Reflex (0-1)
   Finger Flexors (0-1)
   Hoffman's Sign (0-1)

4. Thoracic
   Abdominal Reflex (0-1)

5. Right Lumbosacral
   Spasticity (0-1)
   Patellar Reflex (0-1)
   Crossed Adduction (0-1)
   Ankle Reflex (0-1)
   Babinski Sign (0-1)

6. Left Lumbosacral
   Spasticity (0-1)
   Patellar Reflex (0-1)
   Crossed Adduction (0-1)
   Ankle Reflex (0-1)
   Babinski Sign (0-1)

Total UMN Burden Score (0-23):
Total UMN Burden Score for Bulbar Only (0-2):
Total UMN Burden Score for Single Limb Only (0-5):

Appendix 4. CReATe UMN and LMN Burden Scoring

UMN

1. Bulbar

Speed of Tongue Movements
Normal 0
Slow 1
Minimal or no movement 2

Jaw Jerk
Present or Absent 0
Brisk 1

Total Bulbar UMN (0-3):

2. Cervical (single limb)

Hyperactive Reflexes
Biceps 0.5
Brachioradialis 0.5
Triceps 0.5
Hoffman 0.5
Subtotal (0-2):

Tone
Tone normal or reduced 0
Spastic 2
Subtotal (0-2):

Strength
Assigns new point values to the Medical Research Council's 5-point strength scale:

MRC	0	1	2	3	4-	4	4+	5-	5
new point	10	9	8	7	6	4	2	1	0

Shoulder abduction (0-10)
Elbow extension (0-10)
Wrist extension (0-10)
Finger extension (0-10)
Subtotal divided by 20 (0-2):

Total Cervical UMN (0-6):

3. Lumbosacral (single limb)

Hyperactive Reflexes
Patellar 0.667
Ankle 0.667
Babinski 0.667
Subtotal (0-2):

Tone
Tone normal or reduced 0

Spastic 2

Subtotal (0-2):

Strength

MRC	0	1	2	3	4-	4	4+	5-	5
new point	10	9	8	7	6	4	2	1	0

Hip flexion (0-10)
Knee flexion (0-10)
Ankle dorsiflexion (0-10)

Subtotal divided by 15 (0-2):

Total Lumbosacral UMN (0-6):

LMN

1. Bulbar

Tongue Atrophy
Absent 0
Present 2

Fasciculations
Upper Face 0.25
Lower Face 0.25
Tongue 0.5

Total Bulbar LMN (0-3):

2. Cervical (single limb)

Hypoactive Reflexes
Biceps 0.667
Brachioradialis 0.667
Triceps 0.667

Subtotal (0-2):

Tone
Tone normal or increased 0
Flaccid 2

Subtotal (0-2):

Bulk
Normal muscle bulk 0
Atrophy 2

Subtotal (0-2):

Strength

MRC	0	1	2	3	4-	4	4+	5-	5
new point	10	9	8	7	6	4	2	1	0

Proximal:
Shoulder abduction (0-10)

Elbow flexion (0-10)
Elbow extension (0-10)

Subtotal divided by 7.5 (0-4):

Distal:
Wrist flexion (0-10)
Wrist extension (0-10)
Finger flexion (0-10)
Finger extension (0-10)
First dorsal interosseous (0-10)
Abductor pollicis brevis (0-10)

Subtotal divided by 15 (0-4):

Total Cervical LMN (0-8):

3. Lumbosacral (single limb)

Hypoactive Reflexes
Patellar 1
Ankle 1

Subtotal (0-2):

Tone
Tone normal or increased 0
Flaccid 2

Subtotal (0-2):

Bulk
Normal muscle bulk 0
Atrophy 2

Subtotal (0-2):

Strength

MRC	0	1	2	3	4-	4	4+	5-	5
new point	10	9	8	7	6	4	2	1	0

Hip flexion (0-10)
Knee flexion (0-10)
Knee extension (0-10)
Ankle dorsiflexion (0-10)
Ankle plantarflexion (0-10)
Ankle inversion (0-10)
Ankle eversion (0-10)
Toe flexion (0-10)
Toe extension (0-10)

Subtotal divided by 22.5 (0-4):

Total Lumbosacral LMN (0-8):